UNIVERSITY OF CALIFORNIA SAN DIEGO

Effects of sub-perceptual vagus nerve stimulation on brain activity measured intra-cranially in humans

A Thesis submitted in partial satisfaction of the requirements for the degree Master of Science

in

Bioengineering

by

Yihan Zi

Committee in charge:

Professor Eric Halgren, Chair
Professor Gert Cauwenberghs, Co-Chair
Professor Tzyy-Ping Jung

2020

The Thesis of Yihan Zi is approved, and it is acceptable in quality and form for publication on microfilm and electronically:

_____

_____
Co-Chair

_____
Chair

University of California San Diego

2020

DEDICATION

To two.

TABLE OF CONTENTS

LIST OF FIGURES

LIST OF TABLES

ACKNOWLEDGEMENTS

I would first like to thank my thesis advisor Prof. Eric Halgren of the Neuroscience Department at University of California San Diego (UCSD). His expertise and passion in research keeps inspiring me and makes me fall in love with our project everyday and I'm more dedicated to further study of neuroscience. He trusted in me leading an exploratory project, tutored my research and writing skills with endless patience and upfront advice, most importantly supported me strongly during my hardest time through warm conversations. I am well guided and protected to keep learning and become better and stronger.

I would also like to acknowledge my lab mates Burke Rosen and Charles Dickey, PhD Candidates of the Neuroscience Program at UCSD as the mentors of this project, I am gratefully indebted to their very patient and valuable assistance during this project. I would also like to thank Dr. John Hermiz, data scientist of Vorso Corp. for his kind contribution to this collaboration project with Vorso Corp.

I would also like to thank the my program advisor Vanessa Hollingsworth of the Bioengineering Department of UCSD, she is always there for me whenever I needed, I wouldn't be able to focus on my research and successfully finished without her.

Finally, I must express my very profound gratitude to my parents and to my husband for providing me with unfailing support and continuous encouragement throughout my years of study and through the process of researching and writing this thesis. This accomplishment would not have been possible without them. Thank you.

Chapter 2 is coauthored with Jerry Shih, Sharona Ben-Haim, Burke Rosen, Charles Dickey. Chapter 3 is coauthored with Charles Dickey. The thesis author was the primary author of these two chapters.

ABSTRACT OF THE THESIS

Effects of sub-perceptual vagus nerve stimulation on brain activity measured intra-cranially in humans

by

Yihan Zi

Master of Science in Bioengineering

University of California San Diego, 2020

Professor Eric Halgren, Chair
Professor Gert Cauwenberghs, Co-Chair

The general state of the human organism is modulated by the Autonomic Nervous System (ANS) comprised of two balancing influences: sympathetic and parasympathetic. The basal forebrain (BF) cholinergic and the locus coeruleus (LC) noradrenergic system within the brain innervates the cerebral cortex and regulates cognitive functions such as arousal, attention, learning, and sleep. The peripheral autonomic nervous system is linked with the cortical projection systems and modulates cortical activity levels in the human brain, which has been shown in various studies of vagus nerve stimulation (VNS) effect on cognitive functions, but its mechanism still

remains unclear. The purpose of this study is to determine if sub-perception stimulation on the auricular branch of the vagus nerve will produce mild event-related cortical modulation. Our study provided a detailed view of local neuron population activity through depth electrodes implanted in 5 epileptic subjects, and analyzed the acute effect of VNS on intracranial EEG in post-stimulation period versus baseline in the time and frequency domains. We have found rare but significant ($p < .001$) small-amplitude modulations: 1) 2 out of 487 channels contain event-related changes in local field potentials activity (0.1-40Hz) located in insula and postcentral gyrus; 2) 4 out of 487 channels contain high gamma (70-190Hz) analytic amplitude decrease located in lateral temporal and frontal cortex, amplitude increase located in cingulate gyrus; and 3) 7 out of 71 channels contain α & β band power reduction located in insula, prefrontal cortex and cingulate gyrus. These results suggest that sub-perception non-invasive VNS may be able to modulate cortical activity in widely distributed regions, which provides a potential method for a variety of illness treatment such as Parkinson disease and Alzheimer's disease.

Chapter 1

Introduction

1.1 Autonomic Nervous System

The Autonomic Nervous System (ANS) innervates our internal organs and modulates their activities, generally not under direct voluntary control. The functions of the ANS are to keep the internal homeostasis or adjust it as required by changing circumstances [26].

ANS is composed of 2 anatomically and functionally distinct divisions, the sympathetic system and the parasympathetic system. The parasympathetic nervous system is often considered the ”rest and digest” or ”feed and breed” system, while the sympathetic nervous system is often considered the ”fight or flight” system [39]. Both systems provide some degree of nervous input to a given tissue at all times and either increase/enhances or decrease/inhibits the activity of the innervated structure. Parasympathetic fibres are sent to various viscera to ensure different involuntary functions, such as Cranial Nerve X (Vagus nerve) originates from the medulla of the central nervous system (CNS), interfacing with the parasympathetic control of organs in the neck, thorax, abdomen and reaching to the colon [45].

Parasympathetic Nervous System presynaptic neuron cell bodies are located in medulla and the sacral segment of the spinal cord within the central nervous system (CNS). The medulla

receives information from the hypothalamus, which acts as an integrator for autonomic functions, receives autonomic regulatory input from the limbic system and cortex. In summary, ANS activities are modulated by the hypothalamus and the brainstem, also influenced by the cerebral cortex and the limbic system. Direct outputs to autonomic preganglionic neurons arise from the paraventricular and lateral hypothalamus, the parabrachial nucleus (PB), the nucleus tractus solitarius (NTS), certain monoamine groups such as the A5 noradrenergic neurons, serotonergic raphe neurons, and adrenergic neurons in the ventrolateral medulla. Less direct outputs from the cerebral cortex, amygdala, and periaquaductal gray matter are relayed into the cell groups with direct input to the preganglionic inputs [25].

Beyond anatomical structure providing a link between the central and autonomic nervous system, there are lots of experiments revealed cortical regulation on ANS in humans. A great number of functional imaging studies have revealed the correlation between cortical regions and autonomic functions [3]. For lesion data, a study on stroke patients indicated that the cardiac arrhythmias is very common after acute cerebrovascular events, even in the absence of structural heart disease. Patients (right-handed) from the studied groups presented higher sympathetic activation in right hemisphere stroke. These data are according to other results of similar studies, where it was proved that the right insular cortex seems to modulate the sympathetic tone and left insular cortex modulates the parasympathetic activity in these patients [16]. In a study applying a counting Stroop task to probe dorsal (dACC) and ventral (vACC), fMRI data analysis revealed a cluster of activation in the left vACC which was correlated significantly with high-frequency heart rate variability and represented the parasympathetic modulatory role of the vACC [38]. There are also electroencephalographic (EEG) studies have shown that greater right frontal activation was associated with increases in HR or blood pressure during unpleasant emotional stimuli [48][55]. The cortical neural firing was found co-varying with cardiac-cycle duration from depth electrodes recordings on epilepsy patients [29]. Theta band activities in the frontal area were correlated negatively with sympathetic activation based on heart rate variability during the performance of

an attention-demanding meditation procedure [31].

1.2 Vagus Nerve Stimulation

Due to vagus nerve's important role in ANS, Vagus Nerve Stimulation (VNS) is widely studied in clinics to modulate systemic inflammatory responses to endotoxin [7], becoming a new promising therapeutic tool inflammatory bowel disease [6], and a potential beneficial therapy in heart failure, cardiac arrhythmias, and other cardiac diseases [49][59]. Besides the descending regulation of autonomic functions, the vagus nerve comprises more than 80% of afferent nerves mostly conveying sensory information about the state of the body's organs to the CNS. Vagal afferents primarily project to the nucleus tractus solitarius (NTS), which in turn sends fibers to other brainstem nuclei important in modulating the activity of subcortical and cortical circuitry as shown in Figure 1.1[22].

Vagus nerve afferent network provides the condition for VNS modulation on the cortical activity. In implanted VNS therapy on depression patients, blood oxygenation level dependent (BOLD) signal revealed that over time VNS therapy was associated with ventro-medial prefrontal cortex deactivation, and acute VNS produced greater right insula activation [41]. Assessed by questionnaire and clinical evaluation, VNS is also found being able to enhance emotion recognition ability [15], recognition memory and memory storage [14] in humans. VNS has shown significant improvement on seizure control by many authors with an overall mean seizure reduction of 28% to 85%. However, the mechanism of how it works still remains unclear. VNS induced changes in EEG has long been studied in animal models. VNS at a frequency of 24–50 Hz induced rapid desynchronized activity in the orbitofrontal cortex and cerebellum in cats [9], and suppressed sleep spindling whereas it attenuates synchronized activities [58][12]. Synaptic plasticity in the pathway between the infralimbic (IL) medial prefrontal cortex and the basolateral complex of the amygdala was also found modulated by VNS [13]. But there is still a lack of

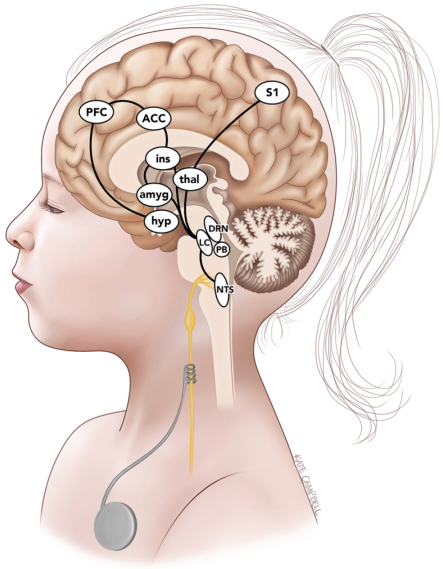

Figure 1.1: **The vagus afferent network.** Schematic diagram showing the important brainstem centers and subcortical and cortical structures that likely underlie VNS treatment effect. ACC = anterior cingulate cortex; amyg = amygdala; hyp = hypothalamus; ins = insula; PB = parabrachial nucleus; PFC = prefrontal cortex; S1 = primary somatosensory cortex; thal = thalamus. Copyright Kate Campbell, Medical & Scientific Visualizations. Published with permission.

direct evidence of cortical activity level changes from VNS shown for human subjects. An early cervical VNS study by Hammond et al. [24] brought up a concern that VNS evoked potential was myogenic in the region of the stimulation, based on amplitude scalp distribution and verified through chemically induced muscle paralysis. Another study by Salinski and Burchiel [47] failed to find any acute effect on awake scalp EEG following pre- and post- periods of stimulation activation, which was 30 to 60s train of square wave pulses at 5 to 10min interval with a total of 24 epochs. Despite of those two cases, what's often seen was cognitive functions evaluations by means of auditory or visual ERP measured from cap EEG, such as visual N2/P3 amplitude was found affected by VNS [8]. Post VNS treatment, P3 of auditory ERP from mid-line cap EEG electrodes is found significantly increased and correlated with Hamilton depression score [42]. EEG-desynchronization is another mainly investigated effect of VNS, which is considered the major mechanism of anti-epileptic action of VNS in patients with intractable seizures [27].

Chronic VNS on epileptic subjects was found to increase the power spectrum as well as the intra- and interhemispheric synchronization of EEG frequencies between 20-50 Hz (gamma frequencies) [35]. Chronic VNS also affects EEG desynchronization through the entire sleep-waking cycle by increasing the proportion of rapid eye movements (REM) sleep and decreasing daytime sleepiness [34][20].

Various medical devices were approved by FDA for treatments like epilepsy, anxiety and depression, and under investigation as a possible treatment for asthma and Alzheimer's disease. Though VNS therapy systems efficacy benefits were more common to be seen in an implantable device on adjunctive, long-term treatment of chronic or recurrent diseases in patients. Stimulation-related adverse events, cost and accessibility led to the development of non-invasive VNS modulators. There is NEMOS & NSS-2 Bridge VNS devices providing stimulation with electrodes placed on the auricular branch of the vagus nerve for the treatment of epilepsy and opoid withdrawal, or cervical VNS like gammaCore device for the treatment of migraine and cluster headache. Stimuli amplitude was commonly adjusted above the detection threshold and below the pain threshold at the stimulation site. In very few sub-perception stimulation preliminary findings, one study found that sub-perception threshold auricular trans-dermal vagal stimulation improved supine cardio-vagal function in POTS patients with low vagal modulation [17].

Despite numerous preclinical and clinical studies and its widespread applications for patients, the precise mechanism that enables those clinical benefits still remains unknown. The effect of VNS on different EEG phenomena is now increasingly investigated in order to understand mechanisms of VNS at a neurophysiological level. In this thesis, we looked for biomarkers from human Intracranial EEG recordings with depth electrodes, which provide neuronal information from relatively local population and temporal resolution at the millisecond scale. Therefore our study has the potential to track the link between cortical activities and autonomic modulation, and thus potentially treat a variety of illnesses through a non-invasive method with mild VNS

stimulation.

Chapter 2

Materials

2.1 Recording

2.1.1 Subjects

Intracranial-encephalography (iEEG) was obtained in 5 epilepsy patients undergoing depth electrode implantation to localize seizure onset for surgical treatment at Thornton Hospital, La Jolla, CA. For detailed patient demographics and clinical information, see Table 2.1.

Table 2.1: Patients characteristics

Patient no.	Gender	Age	Regions w/ interictal discharges	Day of stim
15	F	55	left hippocampus	4
16	M	26	left hippocampal head	11
17	M	21	(posterior) hippocampus	8
19	M	21	left & right hippocampal formation	2
21	F	33	frontal pole & middle frontal sulcus & anterior cingulate	2

'Days of stim' is relative to implant day.

Patients were from 21 to 55 years old, with no previous excision of brain tissue. All patients gave fully informed consent for data usage as monitored by the local Institutional Review Board, in accordance with clinical guidelines and regulations at Thornton hospital.

2.1.2 Electrode localization

Each electrode was 1.27 mm in diameter and 1.5 mm long. Each iEEG shaft had 10 to 16 electrodes (2mm or 4 mm or 4.25 mm spacing). Electrode contacts were localized using postimplant CT superimposed on the preoperative 3T structural MRI after alignment with the skull.(See two example shafts in Figure 2.1) This allows visualization of individual contacts with respect to anatomy, which was interpreted in reference to published atlases [18].

Channels from contacts that are located in white matter or regions with interictal discharges as addressed in Table 2.1 were excluded in further analysis, the same as the epileptogenic zone right hippocampus of subject 15. Channels were also rejected if they contained frequent interictal spikes in further abnormal artifact detection. There were in total 487 clean channels accepted for further analysis, and the recordings were sampled at 512 or 1024 Hz.

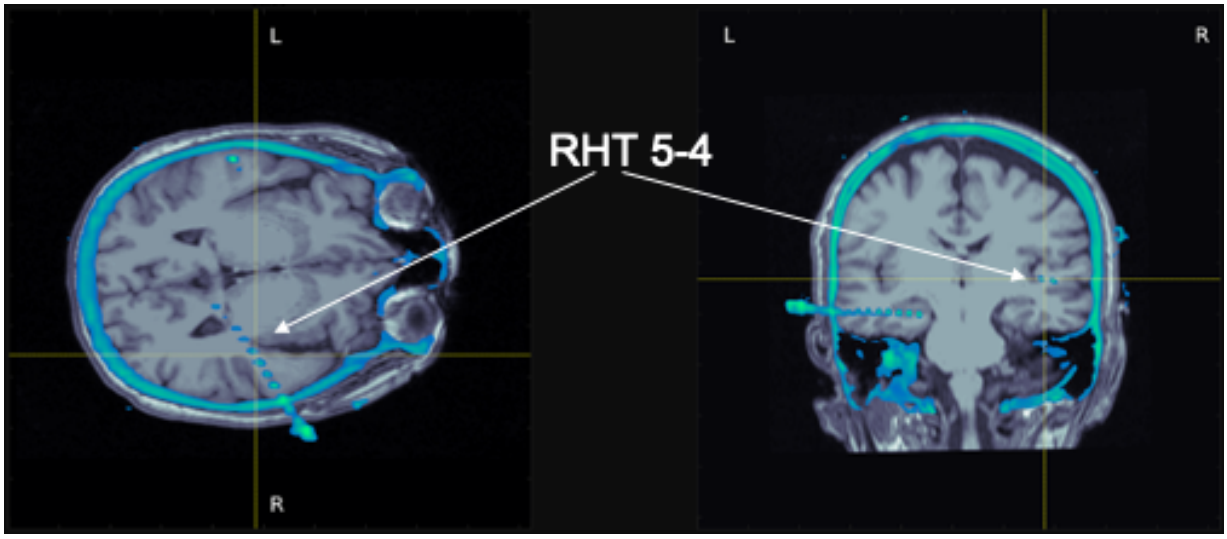

(a) Channel RHT 5-4 from subject #15

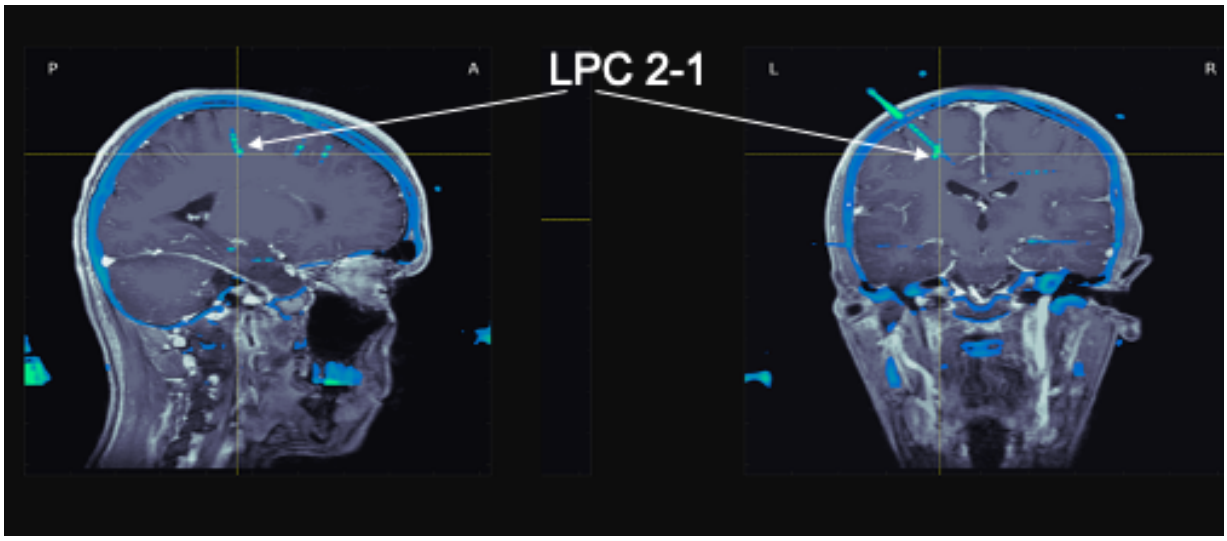

(b) Channel LPC 2-1 from subject #19

Figure 2.1: Electrode localization

Electrode final coverage distribution of each subject within the same six regions is shown in the brain surface reconstruction Figure 2.2.

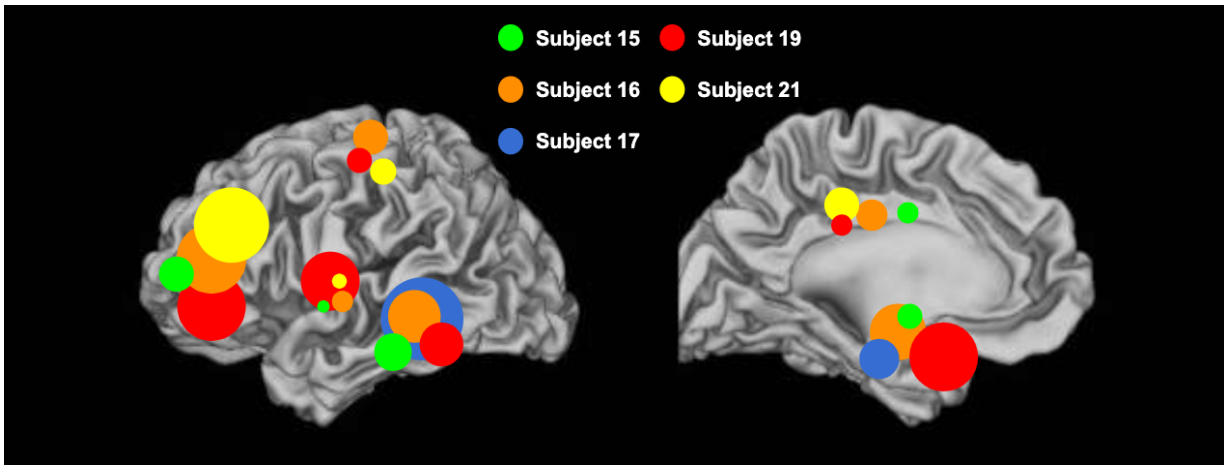

Figure 2.2: Electrodes distribution of each subject. The radius of the circles represents the number of channels grouped in the corresponding brain region.

We can discretize the contacts across all subjects into six regions, recordings were obtained from: 143 prefrontal cortex channels, 45 cingulate cortex channels, 96 amygdala & hippocampus channels, 44 insula operculum channels, 37 rolandic cortex & supra-marginal gyrus channels, and 115 temporal lobe channels.

2.2 Experiment design

2.2.1 Device

We used auricular nerve stimulation techniques [52] designed by Vorso Corp., which mainly consists of two parts: an earpiece and a signal generator. The earpiece was manufactured in our lab using the design of Vorso STIM100 Earpiece, which allows us to customize ear mold having a contoured outer surface shaped to fit against the skin of each subject's external ear in order to provide stable and comfortable usability. One of the left or right ear was used for stimuli application, the picked side was dependent on the contralateral side of the cerebral hemispheres

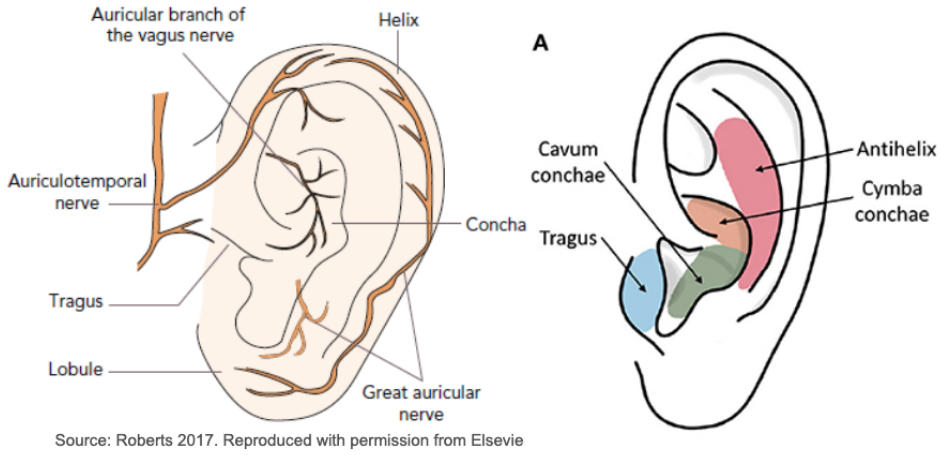

(a) Vagus nerve branch on external ear

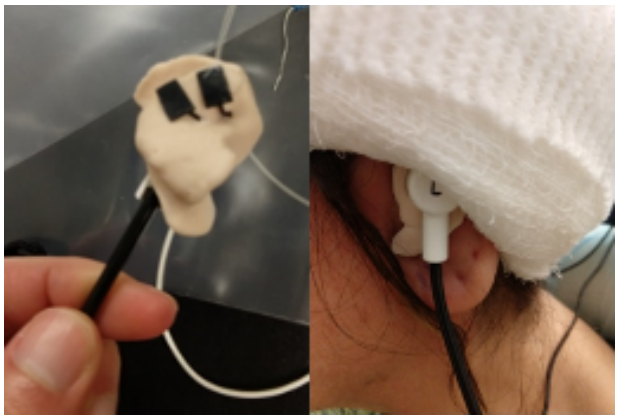

(b) VNS earpiece

Figure 2.3: Auricular VNS device

electrodes mainly distributed in each subject. Stimuli were delivered through two hydro gel electrodes attached to the ear mold shown in Figure 2.3b, whose location was specifically designed to place on the cymba conchae area when wearing the earpiece. The auricular area was chosen based on the vagus nerve branch location as shown in Figure 2.3a [56], it's the only place on the surface of the human body where there is afferent vagus nerve distribution.

The signal generator is connected to a Xbee trigger box who outputs trigger pulses for the purpose of synchronizing events with data acquisition. Vorso program runs on an Arduino Funnel I/O board which is connected to a computer through Bluetooth, to control the Inter-stimulus

Interval (ISI) of the stimulus current applied between two electrodes.

2.2.2 Stimulation

The signal generator generates the electrical therapy signal with 20 kHz bi-phasic rectangular current pulse in a pulse width 20 microseconds, the amplitude can range from about 0.1 mA to about 10 mA. The stimulation intensity was set individually to 70 or 80 percent of each subject's threshold of the current perception.

We tested subjects' threshold of perception through the stair case method. After the stimulation electrodes were applied to the ear, subjects received increasing and decreasing series of 10s stimulation trials, and rated the subjective sensation of the stimulation on an 11-point scale, ranging from nothing (0), light tingling (3), strong tingling (6), to painful (10). The increasing series of trials started from an intensity of 0.1 mA and increased 0.1 mA on a trial by trial basis until participants reported a "tingling" sensation of 9. Before starting the decreasing series, the same intensity was repeated and then reduced trial by trial in 0.1 mA steps until a subjective sensation of 6 or below was experienced. This procedure was repeated a second time. The final stimulation intensity used for the experimental procedure was calculated based on the average of the four intensities rated as 8 (i.e., 2 from increasing and 2 from decreasing series). Details of each subject see Table 2.2.

Table 2.2: Stimulation parameters

Patient	State	Ear of stim	Duration	Amplitude	Trials
15	Awake	Left	1.5h	2.6mA	3k
16	Napping	Right	2h	1.7mA	1.5k
17	Awake	Left	2.5h	2.3mA	5k
19	Sleep	Left	7h	2.3mA	6.7k
21	Sleep	Left	4h	1.7mA	3k

2.2.3 Inter-stimulus Interval (ISI)

Stimulation was designed to be applied continuously for 100ms, following by different ISI in each subject. Detailed diagram see Figure 2.4.

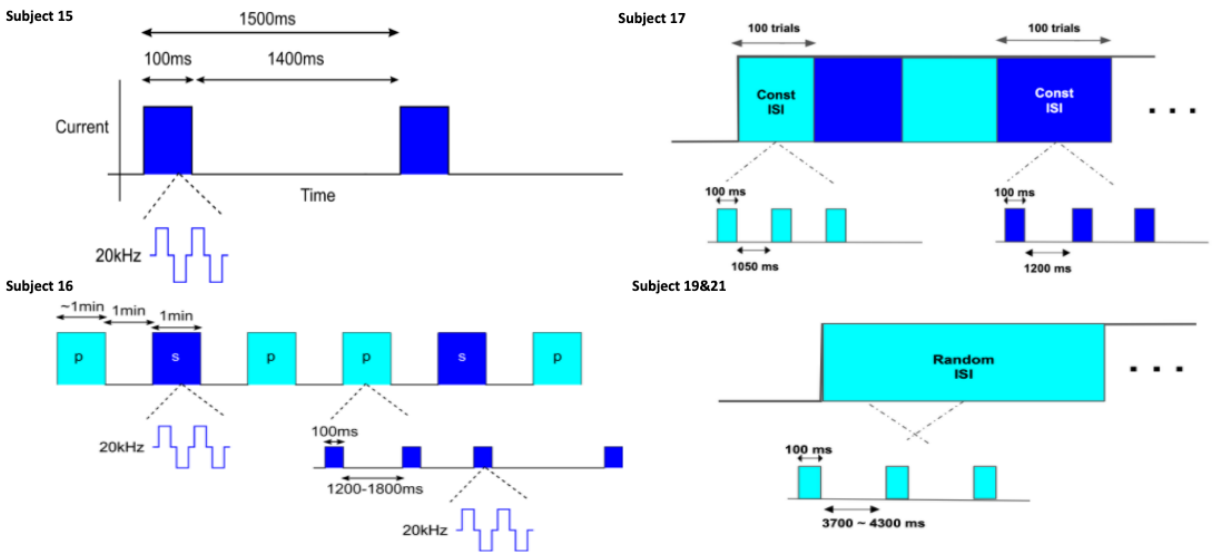

Figure 2.4: Stimulation and ISI in each subject

In subject 15, ISI was fixed to 1400ms. In subject 16, we varied ISI length randomly

ranging from 1200 to 1800ms in the original phasic trial type (indicated as a block with a letter ”P” in the diagram). In addition, we tested continuous stimulation application for 1min (indicated as a block with a letter ”S” in the diagram). We alternated these two types of stimulation with 1min resting time window in between. The 1min continuous stimulation failed to show any response and was excluded in further analysis. In subject 17, for the purpose of testing if brainwave entrainment could be induced by our stimulation, we used a constant ISI in every 100 consecutive trials and varied ISI randomly ranging from 1050 to 1450ms. Trial average temporal response at each fixed ISI was examined separately, as well as the comparison between the first trial and the last trial where every ISI transition happened. No brainwave entrainment effect was observed. In subject 19 & 21, we used random ISI between trials throughout the whole experiment session, and extended the ISI length range to 3700 to 4300ms, due to low frequency sleep-grapho elements (slow oscillation 0.1-4Hz, spindles 10-16Hz) exploration need.

Chapter 2 is coauthored with Jerry Shih, Sharona Ben-Haim, Burke Rosen, Charles Dickey. The thesis author was the primary author of this chapter.

Chapter 3

Method

3.1 Preprocessing

Intracranial-EEG (iEEG) recordings were bi-polarized between adjacent contacts to provide relatively focal measurements of the local field potentials. Bipolar iEEG signals went through the preprocessing pipeline as per Figure 3.1 before further stimulation evoked response analysis.

Explanation for each block is below. *Line noise* was first cleaned by applying a notch filter at 60, 120 and 180 Hz. Next, extracted features would be either the desired frequency band or short transients such as Slow Oscillation (SO) or sleep spindles.

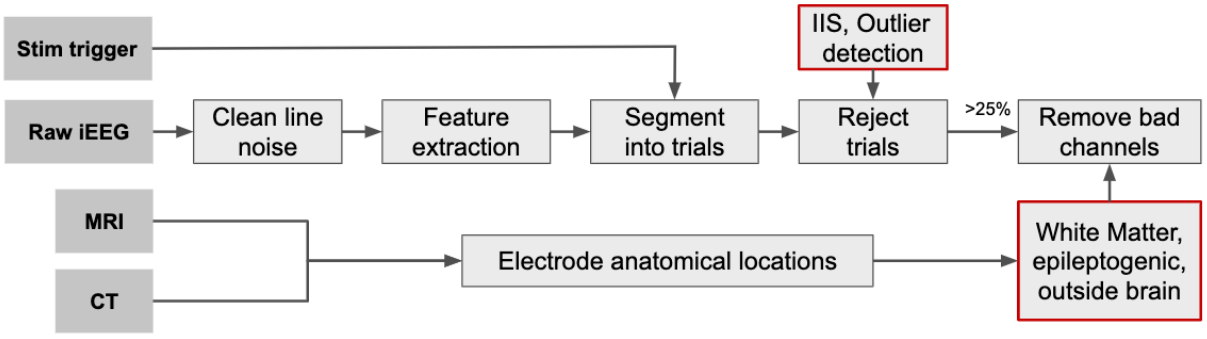

Figure 3.1: Block Diagram of Preprocessing

Segmentation. Continuous channels were segmented into trials afterwards, where time 0 corresponds to the onset of stimulation recorded through the trigger channel. Each trial was constructed with three types of time windows: pre-stimulation baseline, stimulation, and post-stimulation resting (or responsive) window, window length varies according to the ISI of the stimulation on different subjects.

Artifact detection mainly targeted two types of artifacts: Inter-Ictal Spike (IIS) and amplitude outliers, in order to exclude trials that contain a pathological signal or large amplitude artifacts. Stimulation artifacts that occurred during the stimulation window were always excluded. IIS detection is elaborated further in the epileptic background Section 3.1.1.

Outlier detection. We detected outliers through amplitude threshold. The threshold was decided based on the distribution of maximum neuronal potentials in each trial. For each subject and each type of feature, the threshold was manually selected from the superimposed distributions across all channels. Trials that contained detected outliers were discarded before later analysis. Examples will be shown in specific feature analysis Sections 3.1.1 3.2.1.

Channel Rejection. Lastly, a channel was excluded if its electrode contact location was in (1) White Matter (WM), (2) outside of the brain, (3) a clinically diagnosed epileptogenic zone. Noisy channels were also rejected, if they met the condition of more than 25 percentage of trials were rejected due to significant epileptiform discharges or large amplitude outliers.

3.1.1 Abnormal epileptic background

An epileptic brain can be characterized by interictal state (between seizures), ictal state (during a seizure), and post-ictal states (after the seizure). Between seizures, the EEG recordings usually contain interictal epileptiform discharges (IEDS), which are distinctive waves or complexes, distinguished from background activity. IEDs may be divided morphologically into sharp waves, spikes, spike-wave complexes and polyspike-wave complexes, which have pointed peaks and last for 20-70 ms (spike) and 70-200 ms (wave). Each of these will be referred to as spikes

for simplicity.

Since epileptiform discharges are known to correspond to the frequency band of 4-32 Hz with a large amplitude and sharp edges associated with high-frequency field oscillations [21], the detection and rejection of these spikes is important for reconstructing a high Signal Noise Ratio (SNR) recording in Event Revoked Potential (ERP) analysis. We have designed an auto-spike pattern recognition algorithm as follows:

Inter-Ictal Spike rejection. (1) apply a zero-phase sixth-order Butterworth band-pass filter from 4 to 40 Hz, with MATLAB function filtfilt() (process signal in both the forward and reverse directions which reduce edge effect and avoid phase distortion);

Frequency band 4 to 40 Hz was selected by taking the low cut-off of IEDs (4-32Hz) and high cut-off of Local Field Potential (0.1-40Hz), the frequency band of interest in the following analysis. This step works as flattening the background of EEG because spike detection was based on relative amplitude. Setting the high pass cut-off frequency to 4Hz also prevented physiological large amplitude transients like slow oscillation from being captured.

(2) apply a zero-phase sixth-order Butterworth high-pass filter with cut-off frequency at 200 Hz, using MATLAB function filtfilt(). Then we segmented continuous recording to stimulation trials, converted each trial to z-score, and thresholded it with Standard Deviation (SD). We rejected trials that had spike amplitude $>$ 10 SD. See Figure 3.2 for the histogram used for estimating threshold.

Applying a high-pass filter at 200Hz to the IIS frequency band signal, was able to capture the large and sharp edge of the spikes. According to [30], representing a sharp vertical edge requires many high frequency sinusoidal components. The cut-off frequency of 200Hz was selected to exclude any possible physiological ripples. Those regularly occur in normal tissue and are thought to reflect population spike bursts from 100 to 200 Hz paced and synchronised by recurrent inhibition, while fast ripples' frequency range exceeds the maximal firing frequency of most neurons and may appear as pathological activity under epileptic conditions.[32]

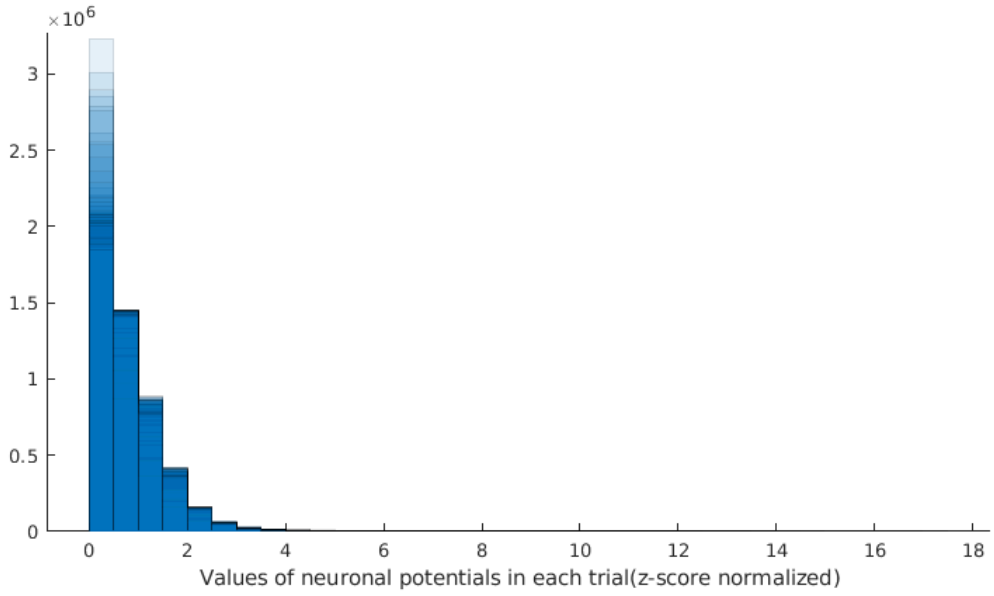

Figure 3.2: **Amplitude histogram in IIS frequency band**. Histograms for every channel are superimposed together creating the shades of color, each histogram represents the distribution of maximum amplitudes (z-score normalized) in each trial. The dark shade of color suggests shared distribution across all channels.

3.2 Temporal analysis

3.2.1 Local Field Potential

We got the trial average plot in Local Field Potential(LFP) frequency band through the following procedure: (1) apply a zero-phase sixth-order Butterworth band-pass filter from 0.1 to 40 Hz, with MATLAB function filtfilt() (process signal in both the forward and reverse directions which reduce edge effect and avoid phase distortion); (2) Segment continuous bipolar channel signals into stimulation trials (length is around 2s or 4s dependent on the subject); (3) Detect outliers by converting amplitudes of each trial to z-score, generating the histogram of maximum Standard Deviation (SD) of each trial, and superimposing the histogram across all channels. (Figure 3.3 is an example from subject #15 with 99 channels in 0.1 to 40Hz local field potential frequency band, from which threshold was picked at 4.5 SD); (4) Reject trials that contain outliers or IIS, and average clean trials.

To decide the threshold for amplitude based outlier detection, we converted each trial to z-score, generated one histogram containing the absolute value of z-score values of all trials from one channel, and superimposed histograms from all channels together.

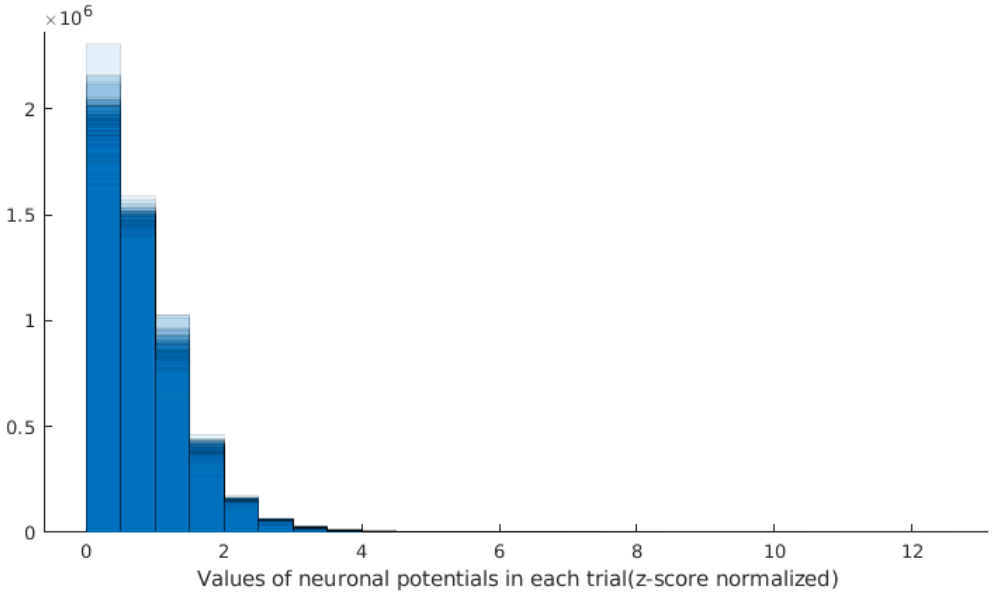

Figure 3.3: **Amplitude histogram in LFP frequency band**. Histograms for every channel are superimposed together creating the shades of color, each histogram represents the distribution of maximum amplitudes (z-score normalized) in each trial. The dark shade of color suggests shared distribution across all channels.

3.2.2 High Gamma

We generated trial average plot in High Gamma frequency band through the following procedure: (1) apply a zero-phase sixth-order Butterworth band-pass filter from 70 to 190 Hz, with MATLAB function filtfilt() (process signal in both the forward and reverse directions which reduce edge effect and avoid phase distortion); (2) Compute upper Hillbert envelope of the continuous signal using a Hillbert filter with length 500 and take the magnitude; (3) Smooth the HG envelope by applying a zero-phase sixth-order Butterworth low-pass filter with cut-off frequency at 20Hz, down-sample to 125Hz to improve computation speed; (4) Segment continuous envelope into stimulation trials (length is around 2s or 4s dependent on the subject); (5) Detect outliers by

converting amplitudes of each trial to z-score, generating the histogram of maximum Standard Deviation (SD) of each trial, and superimposing the histogram across all channels. (The same method as detecting LFP outliers); (6) Reject trials that contain outliers or IIS, and average clean trials.

3.2.3 Statistics

Student's t-test One-sample, two-tailed student's t-test was performed on both of the responses (Local Field Potential and High Gamma frequency Hilbert envelope) to evaluate the difference between the post stimulation and pre-stimulation resting neuron activity. Assuming LFP and HG envelope amplitude values at any time point follow a normal distribution, the mean amplitude value across all trials at each time point in the time window [50ms 1050ms], was compared to the average amplitude value across the time window [-250ms -50ms]. Using MATLAB function ttest(), we got a p-value for each time point, which represents the probability that each time point's amplitude is the same as the pre-stimulation amplitude. We chose two-tailed type test because the polarity of each channel is not consistent and activation or suppression modulation are both accepted. Given a p-value threshold of alpha = 0.05, we discovered the responsive time range resutling from stimulation.

FDR Correction Since we performed roughly 1000 tests simultaneously (when sample rate is 1024 Hz)independently, with a critical value of 0.05, we are accepting the risk of 50 ms of false positive response. For solving the multiple comparison problem, we used the MATLAB function mafdr(p, 'BHFDR', alpha) to correct p-value threshold. 'BHFDR' represents the Benjamini–Hochberg step-up procedure False Discovery Rate correction[4].

Due to limited sample size, some visible amplitude modification after stimulation in the average trial plot didn't appear significant after correction, although it was consistent on odd and even average trial plot. To test if the observations are meaningful, we reduced the number of multiple comparisons by testing only the average value over a short time window. Instead of

running the t-test on every single sample point, we broke the post stimulation time window [50ms 1050ms] into 10 sub-windows with lengths 50, 50, 50, 50, 100, 100, 100, 100, 200, and 200 ms (sequentially) and ran FDR correction only among 10 tests. For further analysis, we mainly used significant report from epoch method and sample points reports for supplementary potential responses.

Effect Size Beyond the usage of the statistical significance test, we also used effect size to quantify the effectiveness of stimulation. The effect size, the standardized mean difference between pre-stimulation and post stimulation EEG recordings, uses Equation 3.1.

$$Effect\ Size = \frac{[Mean\ of\ experimental\ group] - [Mean\ of\ control\ group]}{Standard\ Deviation\ of\ experimental\ group} \tag{3.1}$$

With the assumption that LFP and HG envelope amplitude values at any time point follow normal distribution, we used the MATLAB function fitdist() to estimate μ and σ, two parameters needed to describe normal distribution, in Equation 3.2.

$$Effect\ Size_t = \frac{\mu_{pre}\mu_{t,post}}{\sigma_{t,post}} \tag{3.2}$$

Within each channel, we took the baseline window [-250ms -50ms] amplitude values across all trials to construct a control group distribution getting μ_{pre}. For every time point in the post stimulation response window [50ms 1050ms], we constructed an amplitude value distribution getting $\mu_{t,post}$ and $\sigma_{t,post}$. Therefore, we were able to keep an accurate record of stimulation effectiveness varying at different latencies post stimulation.

3.2.4 Time-Frequency analysis

After seeing the amplitude modulation over time from LFP and HG frequency band, we were interested in taking a closer look across a broader frequency band. We used the EEGLAB function newtimef() to detect transient event-related spectral perturbation (ERSP). In our case, the

system is non-stationary, meaning the spectrum characteristic changes at different post stimulation latencies. In addition, we would like to see from low frequency theta band (4-7 Hz) to HG band (70-190Hz) power change at the same time. For these two reasons, we picked Wavelet Transform (WT) method for its temporal and spectral resolution trade-off property. The wavelet cycle's range we used was [2 10], because the default lowest frequency window is about 0.5 seconds long, two cycles in 0.5 seconds sets the lowest frequency analyzed to about 4 Hz. With $\alpha = 0.05$, newtimef() was also able to perform two-tailed permutation significance test through shuffling times. Function fdr() from EEGLAB was used for multiple comparison correction, which is based on Benjamini & Yekutieli implementation of FDR control [5] for the case when the test statistics have positive regression dependency on each of the test statistics corresponding to the true null hypotheses like including multivariate *t*. Number of permutation replications to accumulate was set to 1000 to maintain more observations.

3.3 Sleep grapho-elements

Sleep recordings from subjects #16, #19 and #21 were used for studying sleep grapho-elements like spindles and Slow Oscillation activity modulation that result from stimulation. While sleep stage transitions can be a latent factor that results in spindles and SO activity variation, analysis was only performed in the N2 period.

In order to distinguish sleep stages throughout EEG recording for each subject, we created histograms of superimposed detected spindles and SO peak locations across all channels (see Figure 3.4 for example). N2 sleep stage was estimated to be time period when spindles distributed evenly and SO activity is not bursting.

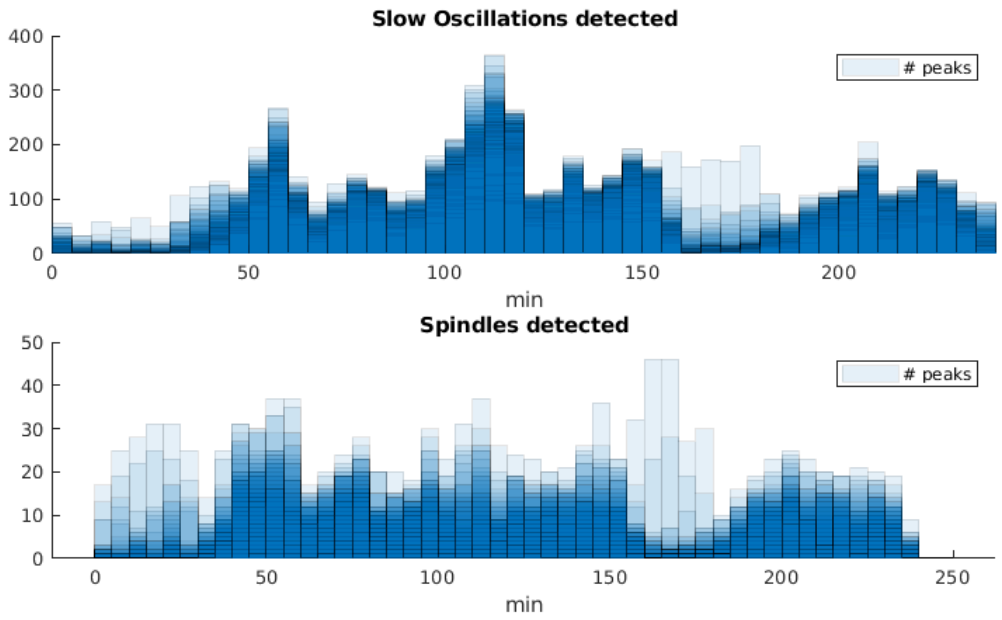

Figure 3.4: **SO & spindles counts distribution through sleep cycles of subject #21**. Histograms for every channel are superimposed together creating the shades of color, each histogram represents the distribution of detected peaks of SO or spindles in time. The dark shade of color suggests shared distribution across all channels.

3.3.1 Slow Oscillation

SOs were detected on each channel-based algorithm as follows: (1) apply a zero-phase eighth-order Butterworth bandpass filter from 0.1 to 4 Hz[36]; (2) reject large amplitude ($>$ 15 standard deviation above mean) events; (3) identify consecutive zero crossings within 0.25-3 s; (4) calculate amplitude peak between zero crossings and retain only the top 20% of peaks for intracranial recordings. For each channel, every Slow Oscillation's time location and amplitude of peak/trough was saved in a matrix.

Peaks and troughs were corrected to align with upstate and downstate of SO. Through looking at HG band power, polarity of bipolar channel was inverted if necessary to ensure both upstate involves an up-regulation in high gamma and downstate involves a down-regulation in high gamma.

3.3.2 Spindles

Spindles were detected on each channel-based algorithm as follows: (1) apply a zero-phase eighth-order Butterworth bandpass filter from 10 to 16 Hz[23]; (2) take the Hilbert envelope of spindle-band signal, smooth the envelope using 300ms win-length Gaussian kernel and 30ms sigma; (3) peaks in the envelope were detected using a mean + 3 standard deviation threshold, merge peaks within 1 sec of each other, the peak with greatest amplitude is taken as the true peak; (4) onset and offset times were determined based on a mean + 1 standard deviation threshold; (5) putative sleep spindles that were shorter than 0.5 s or longer than 2 s were rejected, as well as those with large amplitude broadband increases in power. For every spindle in each channel, time location of [onset, peak, offset], and amplitude of peak were saved in a matrix.

To study stimulation event revoked SO and spindle activity modulation, we re-referenced peak location of each transient relative to each trial's stimulation onset time 0. Then we were able to create peri-stimulus time histograms, in which each bar's width represent 100ms time window, height(y-axis) represents number of transients occurred in total across all trials within 100ms, and each bar's location(x-axis) represent latency relative to stimulation onset.

Chapter 3 is coauthored with Charles Dickey. The thesis author was the primary author of this chapter.

Chapter 4

Results

VNS responses were observed under five types of analysis methods: Local Field Potential (LFP), High Gamma (HG) envelope, Event-Related Spectral Perturbation (ERSP) , Slow Oscillation (SO) and spindles during sleep in different subjects.

4.1 Temporal Response

We first looked for temporal response in the LFP and HG frequency band, which suggests brain regions where VNS evoked time-locked neuron activities.

4.1.1 Local Field Potential

The following set of figures is presenting local field potential responses grouped by subjects, from which we are able to spot different kinds of response due to the individual differences and stimulus differences. Meanings and data used to calculate each element presented in the figures are explained as follow:

The blue trace represents the mean of all trials within one bipolar channel, shaded with Standard Error Mean. Solid and dotted vertical lines at 0s and 0.1s indicate stimulation onset

and offset, respectively. The red horizontal line indicates the baseline (average value) across the channel. Sample points masked in red represent significant changes relative to the individual trial baseline with p-value $< .05$, after point to point multiple comparison correction but without Bonferroni correction for the number of channels tested. Colored bars located at the bottom of each figure highlight a significant change in amplitude relative to baseline. Red, green and cyan colored bars represent p-values smaller than 0.05, 0.01, and 0.001 respectively after window to window multiple comparison correction but without Bonferroni correction for the number of channels tested. Yellow star labeled channels are the ones that also passed at $p < .05$ after Bonferroni correction for the number of channels in that subject. Figures are grouped by subjects. Responses' consistency were validated through comparing the average trace of odd and even trials. Figures with red and orange traces show odd and even trials' mean from the channels with significant responses reported by t-test. In addition to significant test for responses, we also used effect size to describe the effectiveness of stimulation on different locations.

Subject 15

Figure 4.1 and 4.2 are both LFP results from subject 15, whose time domain responses are observed in the following brain regions: prefrontal cortex, cingulate, amygdala, hippocampus, insula, and temporal lobe.

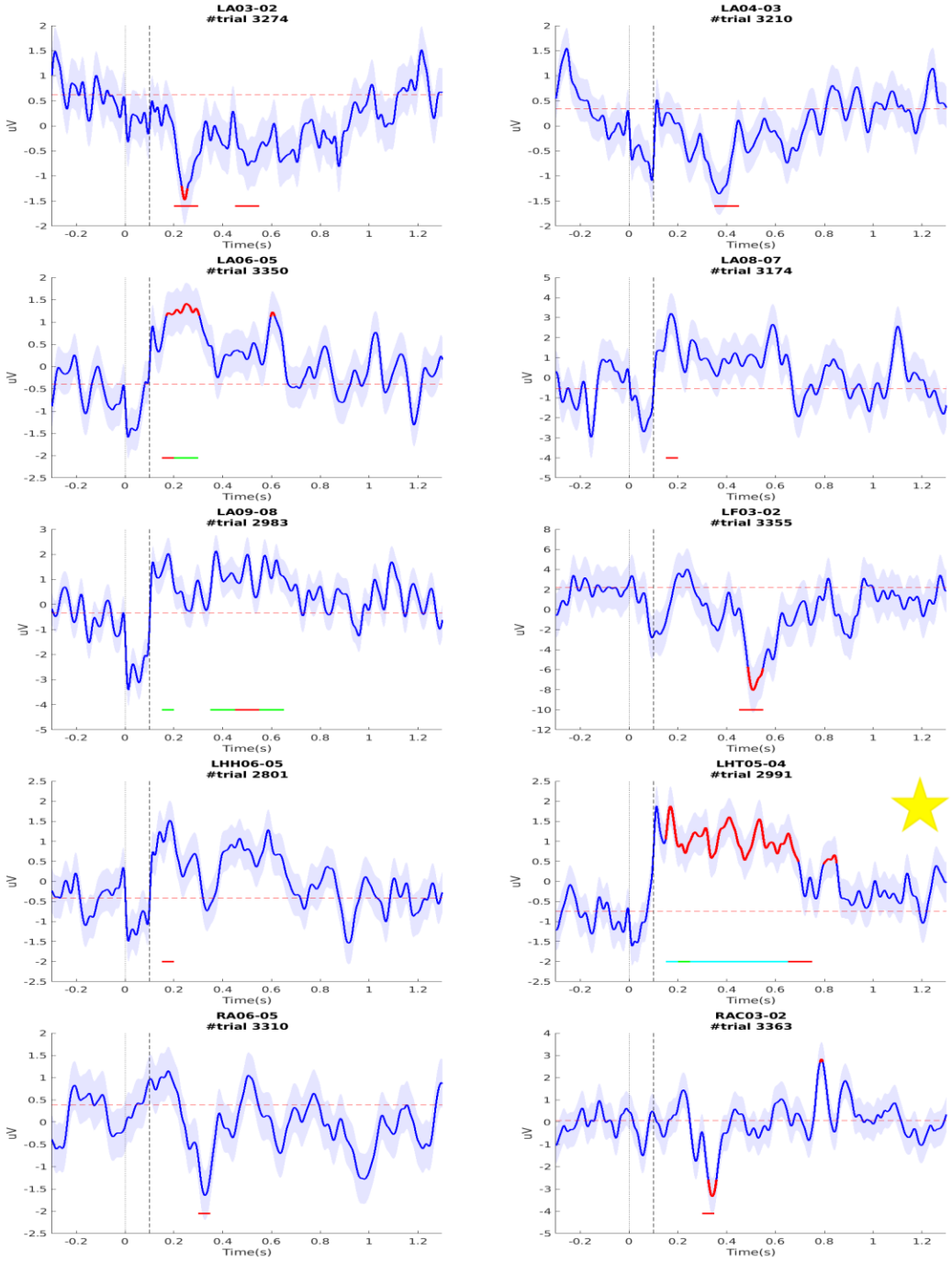

Figure 4.1: **Subject 15 LFP Response Part I** Each sub-figure shows LFP of a bipolar channel varying along time , with the y-axis indicates the amplitude in micro-volts and the x-axis indicates the time in seconds. Channel notations and anatomical locations: LA 03-02: amygdala, LA 06-05: fundus of collateral sulcus, LA 04-03: amygdala, LA 08-07: superior temporal sulcus, LA 09-08: middle temporal gyrus, LF 03-02: anterior superior frontal gyrus, LHH 06-05: fundus of collateral sulcus, RA 06-05: temporal stem, LHT 05-04: temporal stem, RAC 07-06: middle frontal sulcus

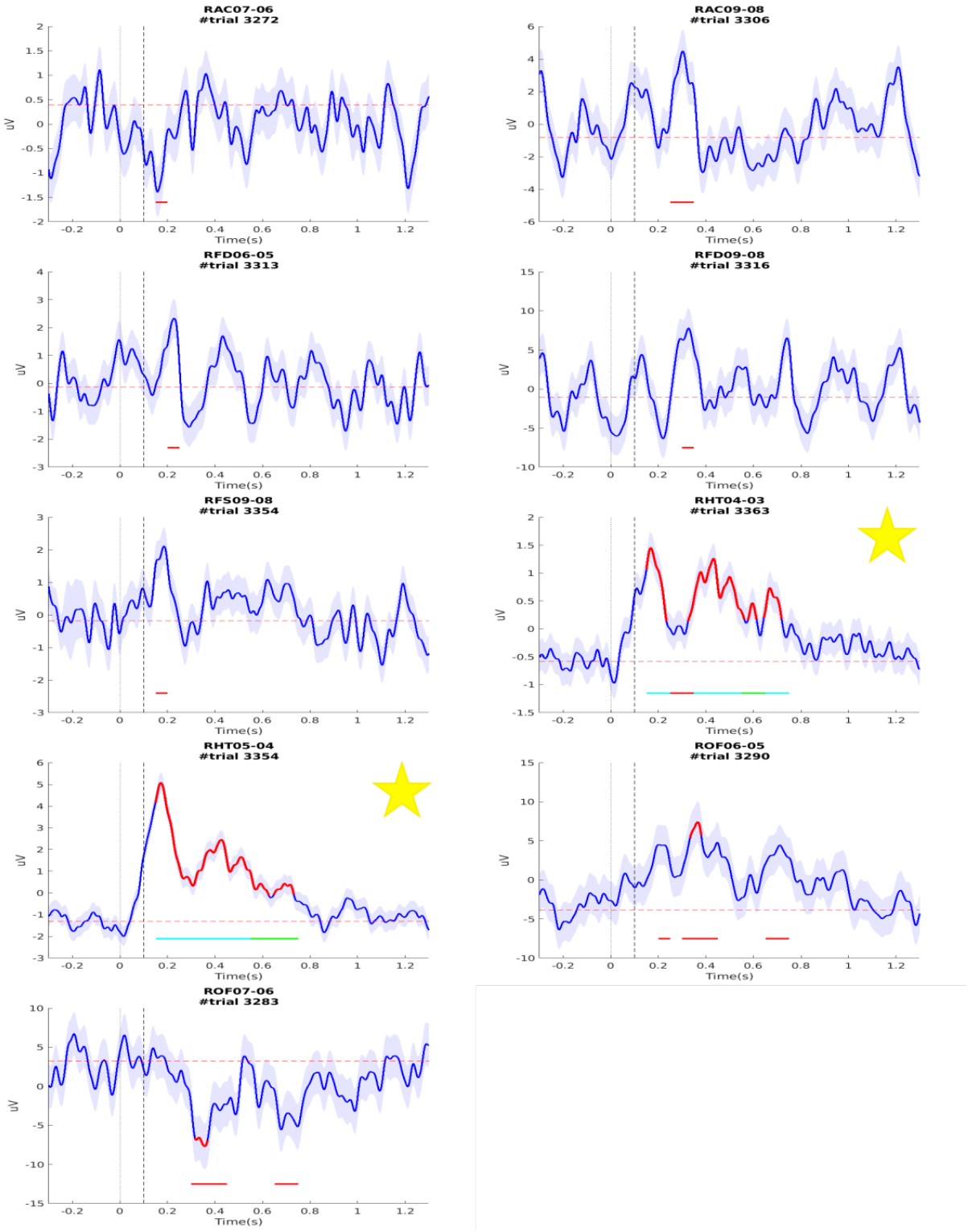

Figure 4.2: **Subject 15 LFP Response Part II** Channel notations and anatomical locations: RAC 03-02: anterior cingulate gyrus, RAC 09-08: middle frontal sulcus, RFD 06-05 & 09-08: frontal sulcus, RFS 09-08: frontal grey matter, RHT 04-03: posterior hippocampus, RHT 05-04: insula, ROF 06-05 & 07-06: anterior middle frontal sulcus

Out of 85 clean channels in subject 15, significant responses are observed in 19 channels, when expecting 4 channels by chance with FDR control level $\alpha = .05$. Most of the responses occurred in the range around 200 to 400ms post-stimulation onset. In channels ROF 7-6 and 6-5 (located in prefrontal cortex), we also observed non-continuous late responses in the time range of 600ms - 800ms post-stimulation onset.

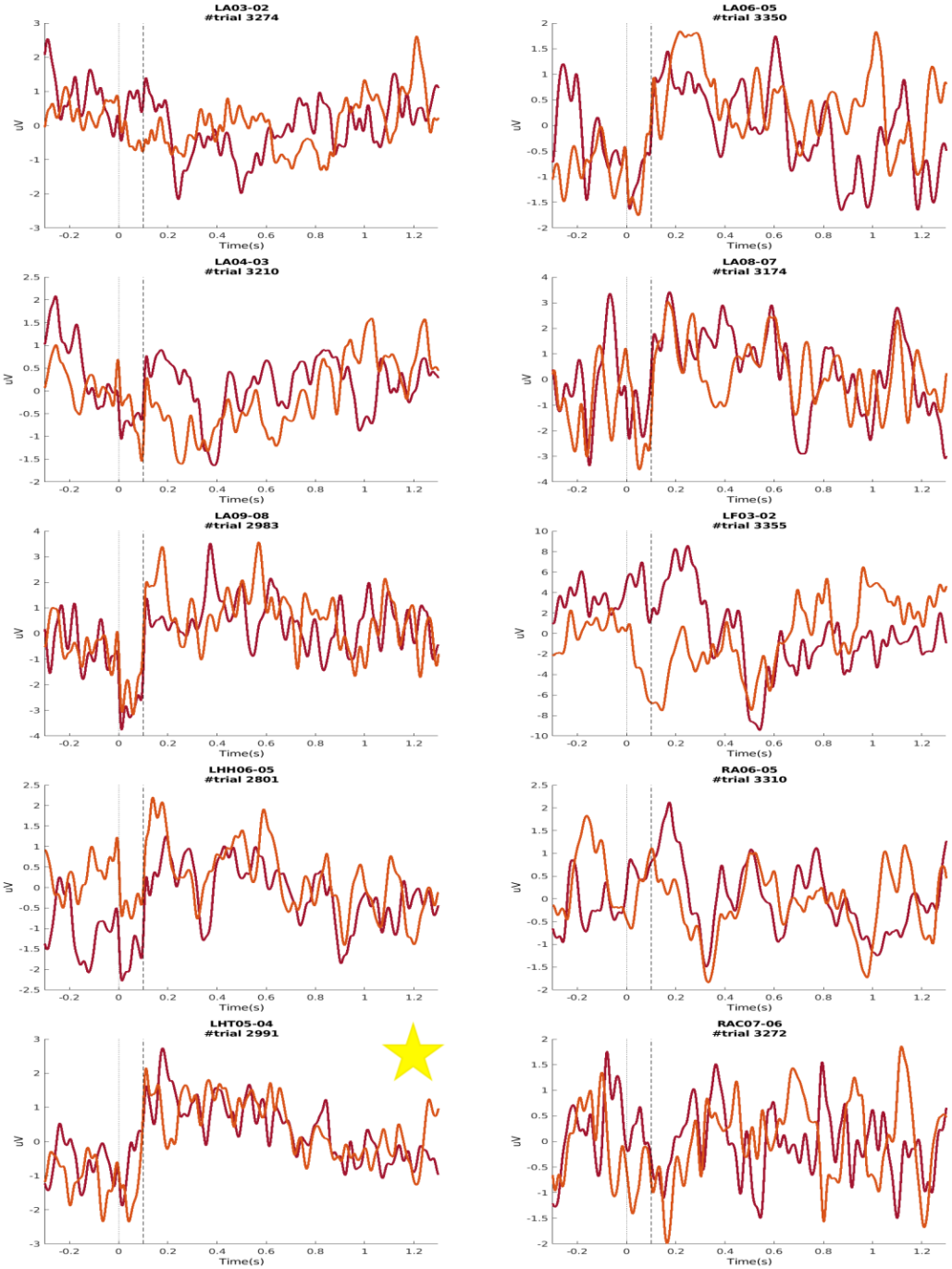

Figure 4.3: **Subject 15 LFP Response in Odd/ Even Validation Part I** Each sub-figure shows LFP of a bipolar channel split into odd and even trials, with the y-axis indicates the amplitude in micro-volts and the x-axis indicates the time in seconds. Channel notations and anatomical locations: LA 03-02: amygdala, LA 06-05: fundus of collateral sulcus, LA 04-03: amygdala, LA 08-07: superior temporal sulcus, LA 09-08: middle temporal gyrus, LF 03-02: anterior superior frontal gyrus, LHH 06-05: fundus of collateral sulcus, RA 06-05: temporal stem, LHT 05-04: temporal stem, RAC 07-06: middle frontal sulcus

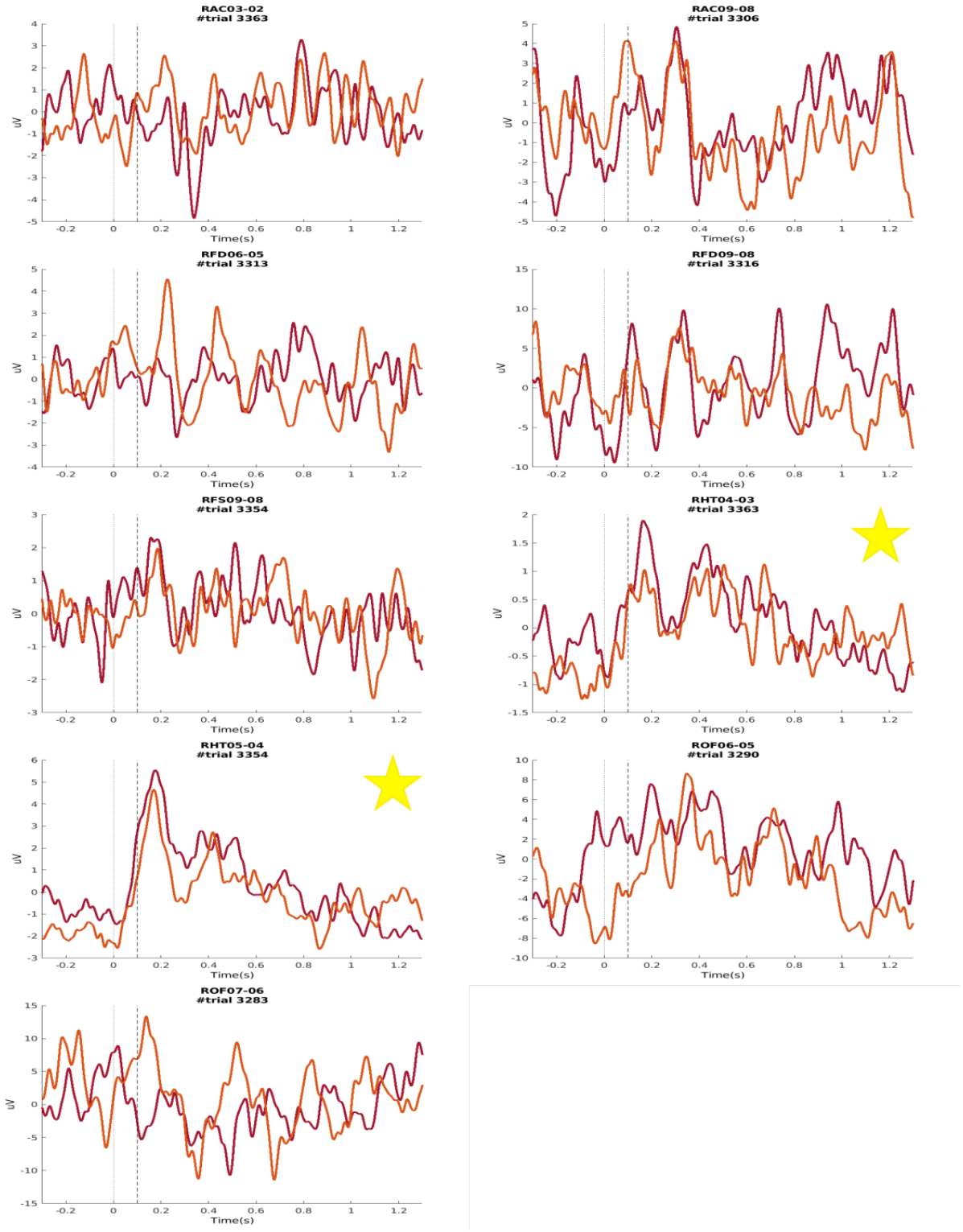

Figure 4.4: **Subject 15 LFP Response Odd/ Even Validation Part II** Channel notations and anatomical locations: RAC 03-02: anterior cingulate gyrus, RAC 09-08: middle frontal sulcus, RFD 06-05 & 09-08: superior frontal sulcus, RFS 09-08: frontal grey matter, RHT 04-03: posterior hippocampus, RHT 05-04: insula, ROF 06-05 & 07-06: anterior middle frontal sulcus

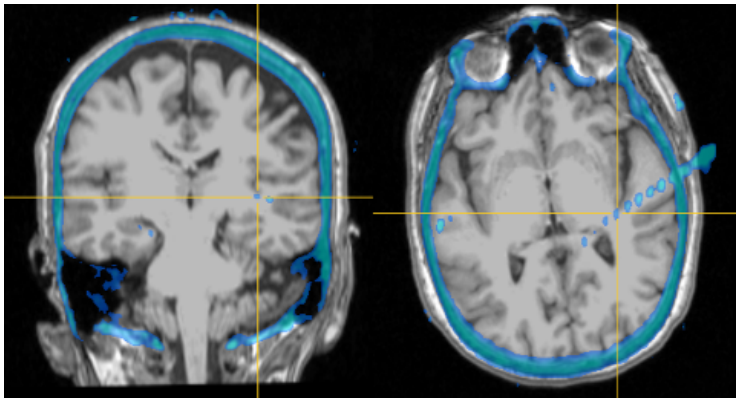

(a) Channel RHT 5-4 & 4-3

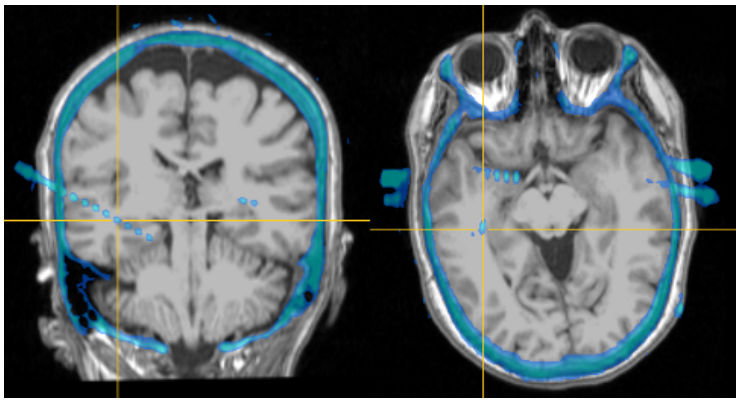

(b) Channel LHT 5-4

Figure 4.5: Starred channel electrodes localization in MRI image

According to Figure 4.3 and 4.4, the responses not replicating in mean amplitude of odd and even trials reveals that in most channels the significant difference between pre- and post-stimulation is not from physiological response. In channel LA 6-5 & 8-7, LHH 6-5, RAC 7-6 the amplitude difference size is not bigger than baseline variation. After consistency validation, only responses in channel LHT 5-4 (located in temporal stem), RHT 5-4 and 4-3 (located around insula) were accepted (see their anatomical locations in MRI image in Figure 4.5a4.5b), electrodes mainly located in white matter explain the small amplitude responses. Those accepted three channels all contain continuous upregulation of the amplitude starting from 50ms post-stimulation onset.

Channel LHT 5-4 reached to the peak first at around stimulation offset and gradually fell

back to baseline at around 800ms post stimulation onset; channel RHT 5-4 & 4-3 share similar trend reaching peak at around 180ms post-stimulation and back to baseline at around 800ms post stimulation onset too. The largest response happened in channel RHT5-4 reaching 5 microvolts at peak.

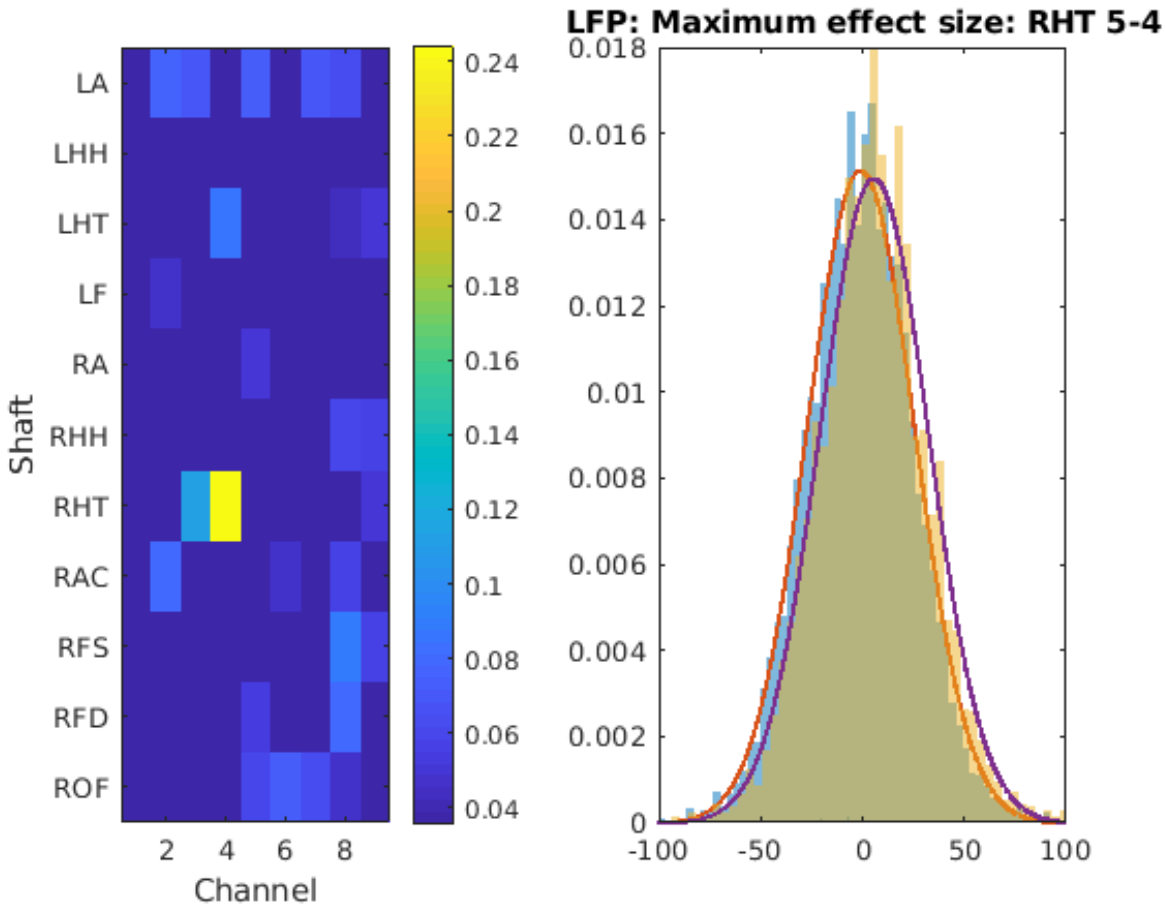

Figure 4.6: **Subject 15 Effect Size Map and Distribution Example of LFP** The left panel shows the biggest effect size in each channel across the response time window. The color scale represents the effect size. The right panel shows the distribution, where the x-axis is micro-volts and y-axis is the probability density. The distribution of LFP amplitude values during the baseline window across all trials is plotted in blue, and the distribution of those during responsive window is plotted in yellow bar. The orange and purple Gaussian curves are calculated from blue and yellow distributions respectively.

The effect sizes are small among all the channels, but channel RHT 5-4 (located in insula) has the distinguished largest effect size of around 0.24. Shown in the distribution on the right

panel of Figure 4.6, the stimulation increases the mean of LFP amplitude by 6.441 microvolts when post-stimulation LFP variance is around 26.64.

Subject 16

Figure 4.7 shows the LFP results from subject 16, in which time domain responses are found in the following areas: prefrontal cortex, insula and primary somatosensory cortex.

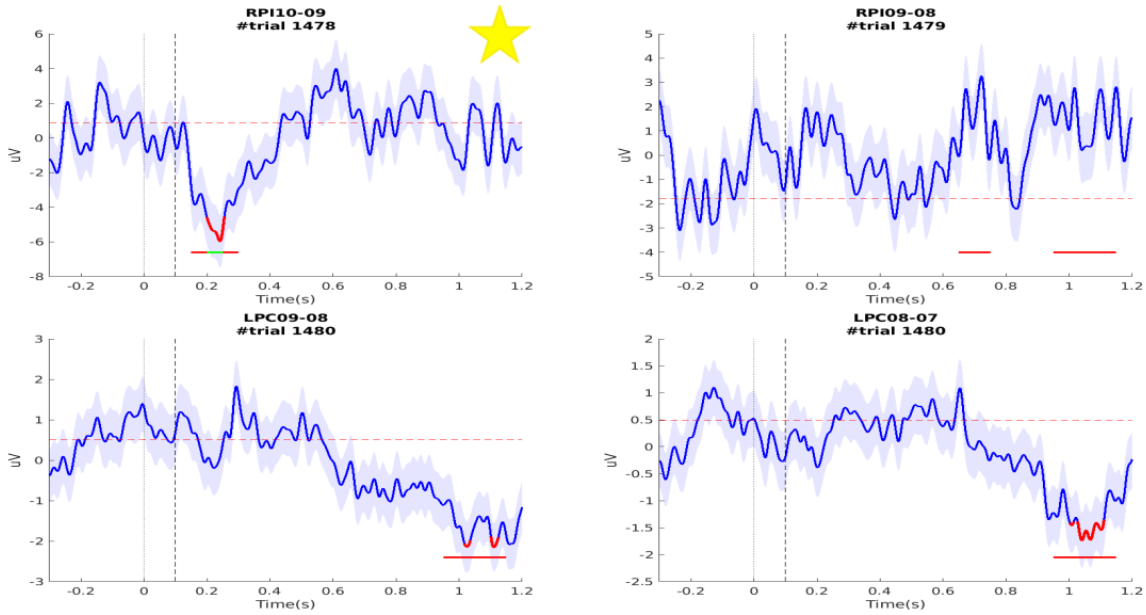

Figure 4.7: **Subject 16 LFP responses** Channel notations and anatomical locations: RPI 10-09 & 09-08: postcentral gyrus, LPC 09-08 & 08-07: rolandic

Out of 145 clean channels in subject 16, significant responses are observed in 4 channels when expecting 7 channels by chance with FDR control level $\alpha = .05$. One response in channel RPI 10-9 (located in postcentral gyrus) occurs in the range around 200ms - 400ms post-stimulation onset. Then, in channel RPI 9-8 (located in postcentral gyrus), a response occurs at 600ms and 1s post-stimulation. The remaining two channels LPC 9-8 and 8-7 (located in rolandic) contain downregulation on LFP amplitude after 1s post-stimulation onset, which is unlikely physiological response in brain.

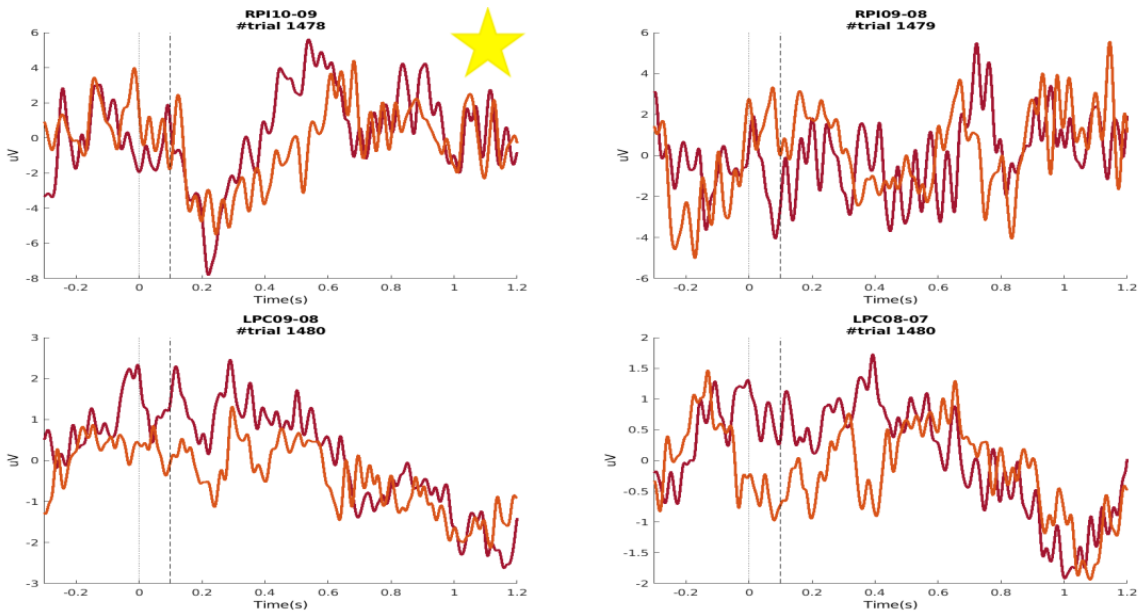

Figure 4.8: **Subject 16 LFP Response Odd/ Even Validation** Channel notations and anatomical locations: RPI 10-09 & 09-08: postcentral gyrus, LPC 09-08 & 08-07: rolandic

In Figure 4.8, we can see the two traces of channel RPI 9-8 don't share a similar trend during the statistically reported significant time and the amplitude increase is not bigger than background variation. After consistency validation only response in channel RPI 10-9 was accepted, which started from stimulation offset and reached to the peak at around 210ms post-stimulation offset and gradually raised back to baseline at around 500ms post stimulation onset with peak amplitude reaching 6 microvolts. We can see from Figure 4.9 that the electrode is mainly located in white matter and outside, which explains the small amplitude response.

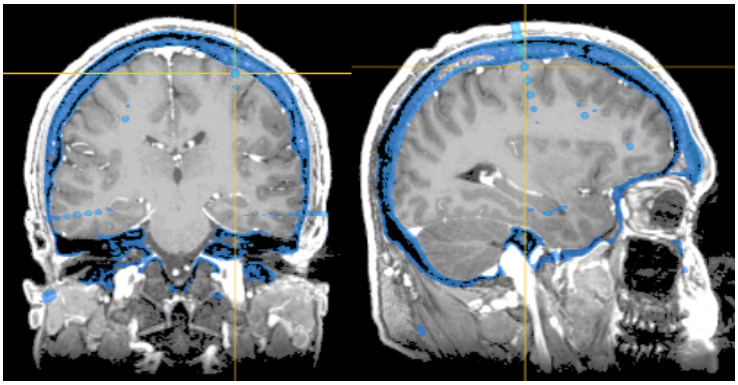

Figure 4.9: Starred channel RPI 10-9 electrodes localization in MRI image

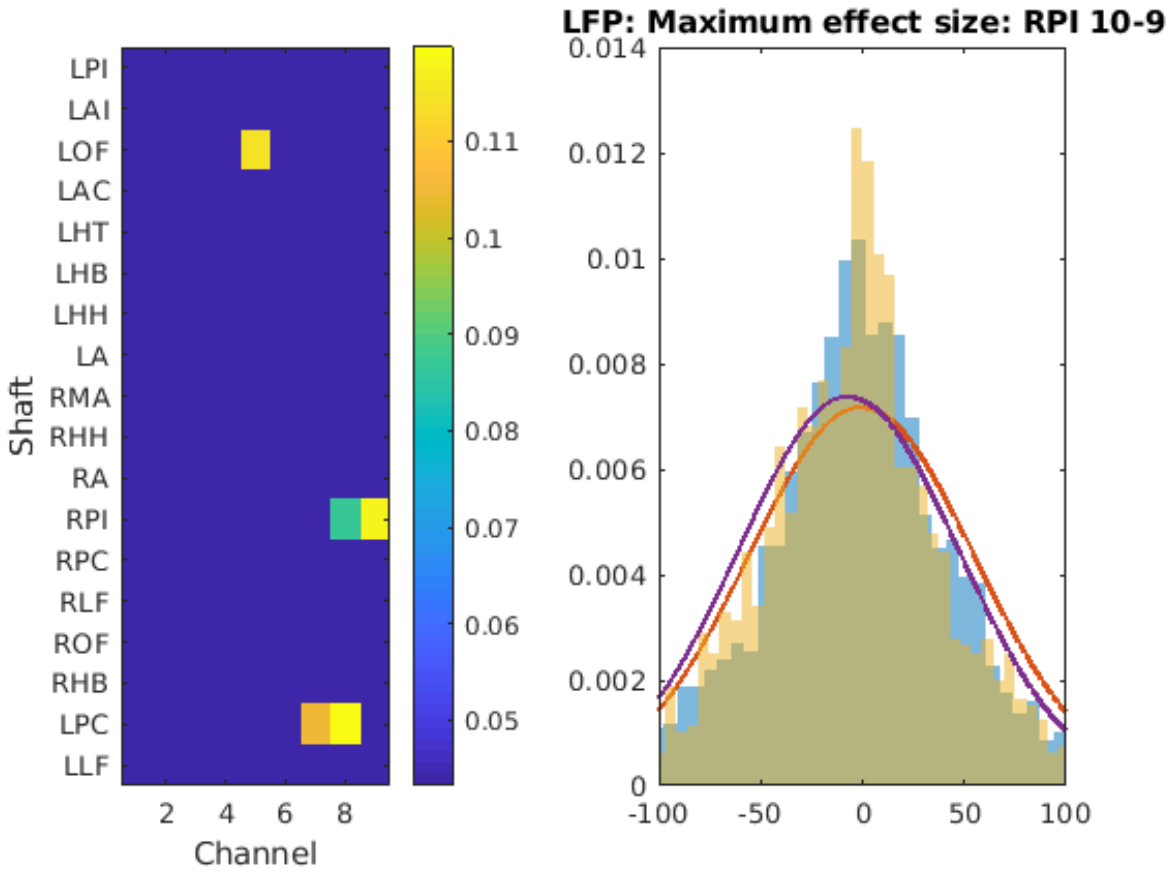

Figure 4.10: **Subject 16 Effect Size Map and Distribution Example of LFP** The left panel shows the biggest effect size in each channel across the response time window. The color scale represents the effect size. The right panel shows the distribution, where the x-axis is micro-volts and y-axis is the probability density. The distribution of LFP amplitude values during the baseline window across all trials is plotted in blue, and the distribution of those during responsive window is plotted in yellow bar. The orange and purple Gaussian curves are calculated from blue and yellow distributions respectively.

Only very few channels in subject #16 contain significant responses, whose effect sizes are shown in the color-map. The reported biggest effect size around 0.12 in channel LPC 9-8 (located in rolandic) has already been rejected through odd & even trial average validation. For channel RPI 10-9 with classic waveform, the mean of LFP was downregulated for about 6.389 microvolts, when the post stimulation variance is about 54, together the effect size is about 0.12.

Subject 17

Figure 4.11 is from subject 17, in which time domain responses are found in the following areas: amygdala, hippocampus, lingual gyrus and fusiform gyrus.

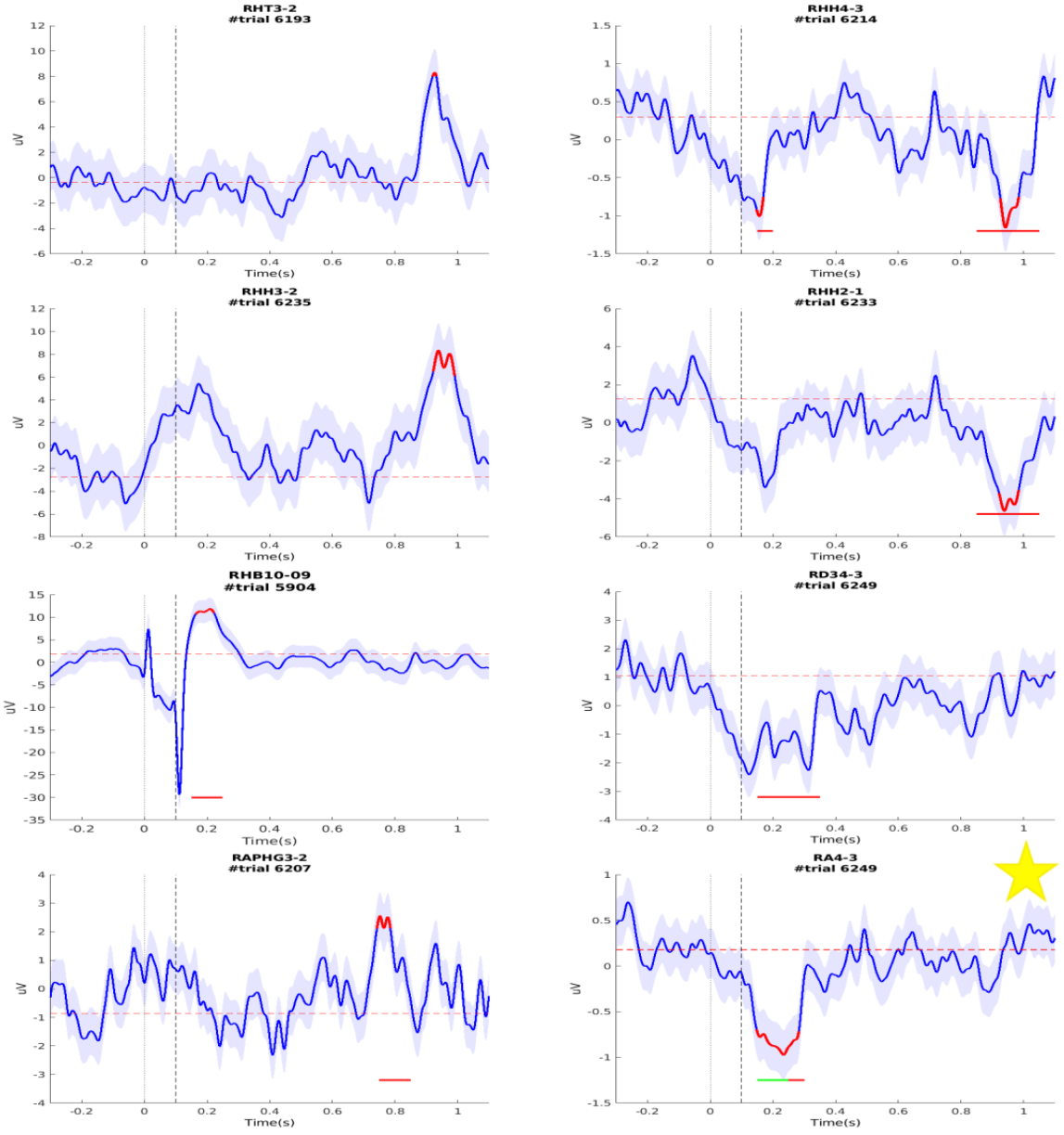

Figure 4.11: **Subject 17 LFP responses** Channel notations & anatomical locations: RHT 3-2: posterior hippocampus, RHH 4-3: hippocampus, RHH 3-2: subiculum, RHH 2-1: entorhinal, RHB 10-9: medial temporal gyrus, RD3 4-3: fusiform gyrus/lingual gyrus, RAPHG 3-2: hippocampus, RA 4-3: amygdala

Out of 77 clean channels in subject 17, significant responses are observed in 8 channels when expecting 3 channels by chance with FDR control level $\alpha = .05$ Three channels located in amygdala and temporal lobe area have responses occurring in the range of 200ms to 400ms post-stimulation onset. Five channels RHH4-3-2-1, RHT3-2, RAPHG3-2 (located near hippocampus) have responses occur in the range around 800ms - 1s post-stimulation onset, which is unlikely physiological response in brain.

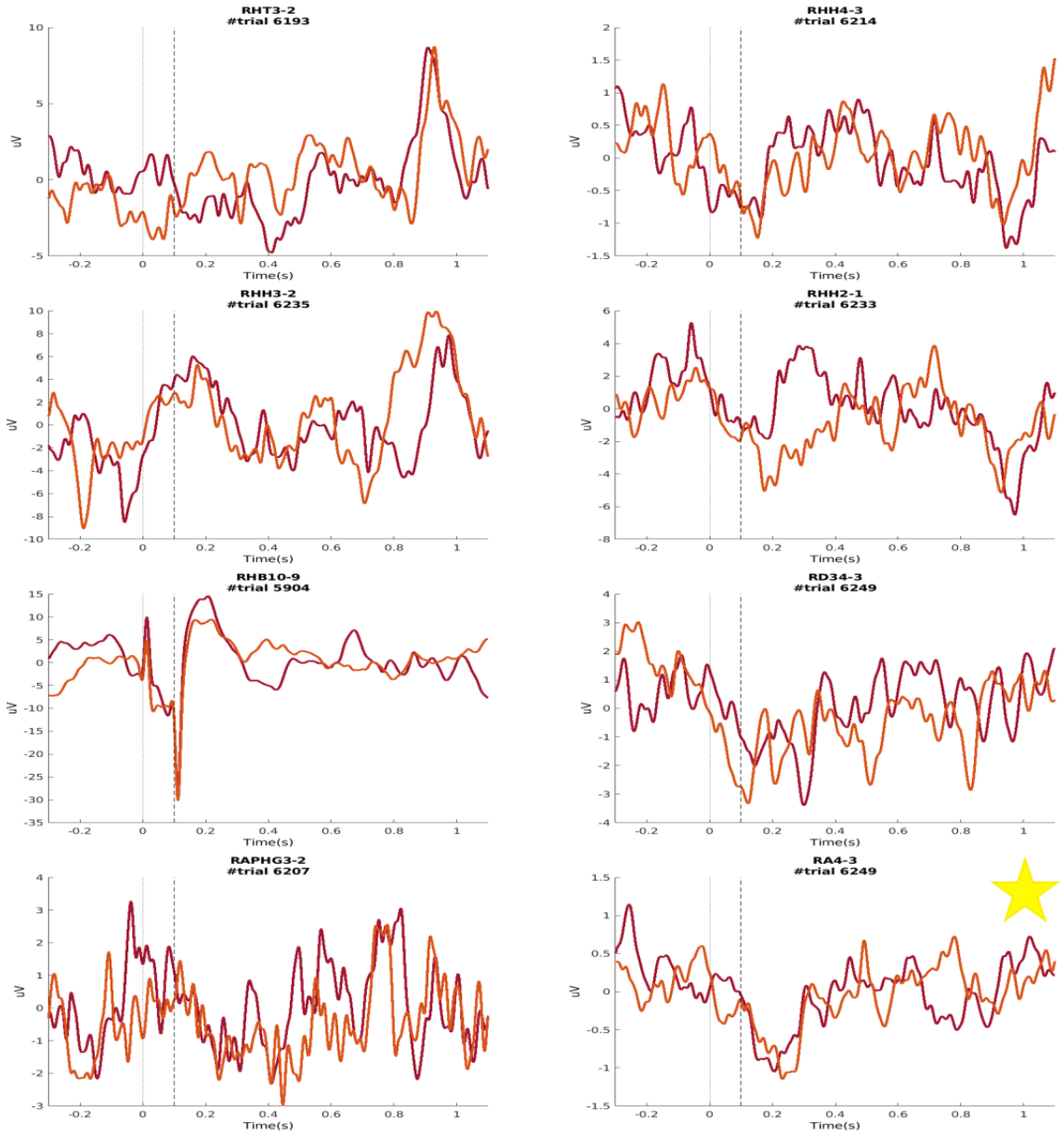

Figure 4.12: **Subject 17 LFP Response Odd/ Even Validation** Channel notations & anatomical locations: RHT 3-2: posterior hippocampus, RHH 4-3: hippocampus, RHH 3-2: subiculum, RHH 2-1: entorhinal, RHB 10-9: medial temporal gyrus, RD3 4-3: fusiform gyrus/lingual gyrus, RAPHG 3-2: hippocampus, RA 4-3: amygdala

In Figure 4.12, response in channel RHB 10-9 may result from large stimulation artifact. In channel RD3 4-3, the two traces share a similar trend during the statistically reported significant time but it's problematic that the downregulation seems start before stimulation onset, plus it

didn't pass the Bonferroni correction. Response in channel RHT 3-2 and channel RA 4-3 are highly replicated in both odd and even trial averages. But response in channel RHT 3-2 has already been ruled out due to the latency. After consistency validation, the only accepted significant response was in channel RA 4-3, which started from stimulation offset, reached peak 1 microvolts at around 210ms post-stimulation onset, abruptly ends at around 300ms post-stimulation onset. We can see from Figure 4.13 that the electrode #4 is mainly located in temporal stem (white matter), electrode #3 is located in amygdala.

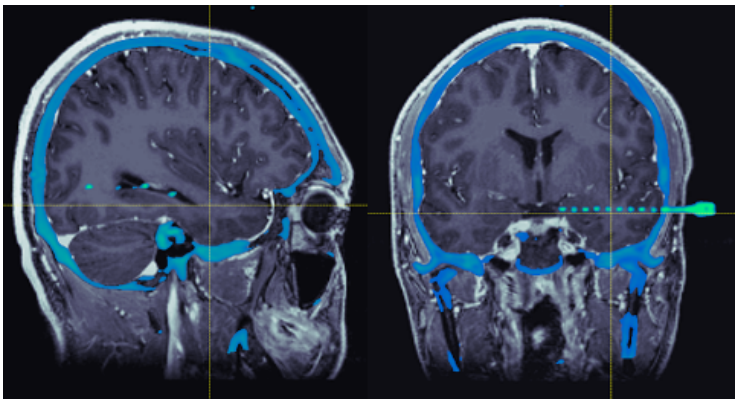

Figure 4.13: Starred channel RA 4-3 electrodes localization in MRI image

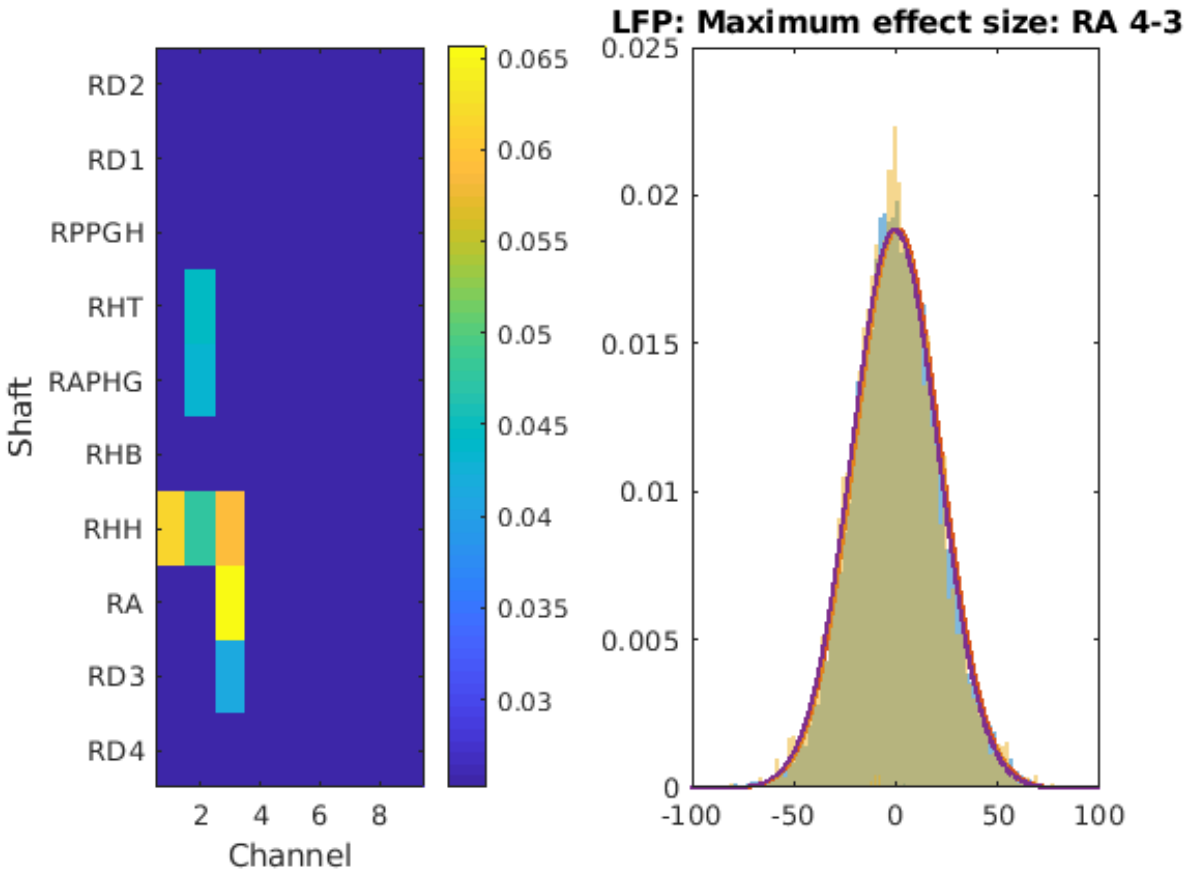

Figure 4.14: **Subject 17 Effect Size Map and Distribution Example of LFP** The left panel shows the biggest effect size in each channel across the response time window. The color scale represents the effect size. The right panel shows the distribution, where the x-axis is micro-volts and y-axis is the probability density. The distribution of LFP amplitude values during the baseline window across all trials is plotted in blue, and the distribution of those during responsive window is plotted in yellow bar. The orange and purple Gaussian curves are calculated from blue and yellow distributions respectively.

All effect sizes in subject 17 are very small, among all channels which reported significant responses, channel RA 4-3 located in amygdala has the biggest effect size. Shown in the distribution on right panel, stimulation downregulates the mean of LFP amplitude by 1.39 microvolts when post-stimulation LFP variance is around 21.16, together the effect size is about 0.065, which is minuscule.

Subject 19

Figure 4.15 is from subject 19, in which time domain responses are mainly found in the following areas: prefrontal cortex, cingulate cortex, amygdala & hippocampus.

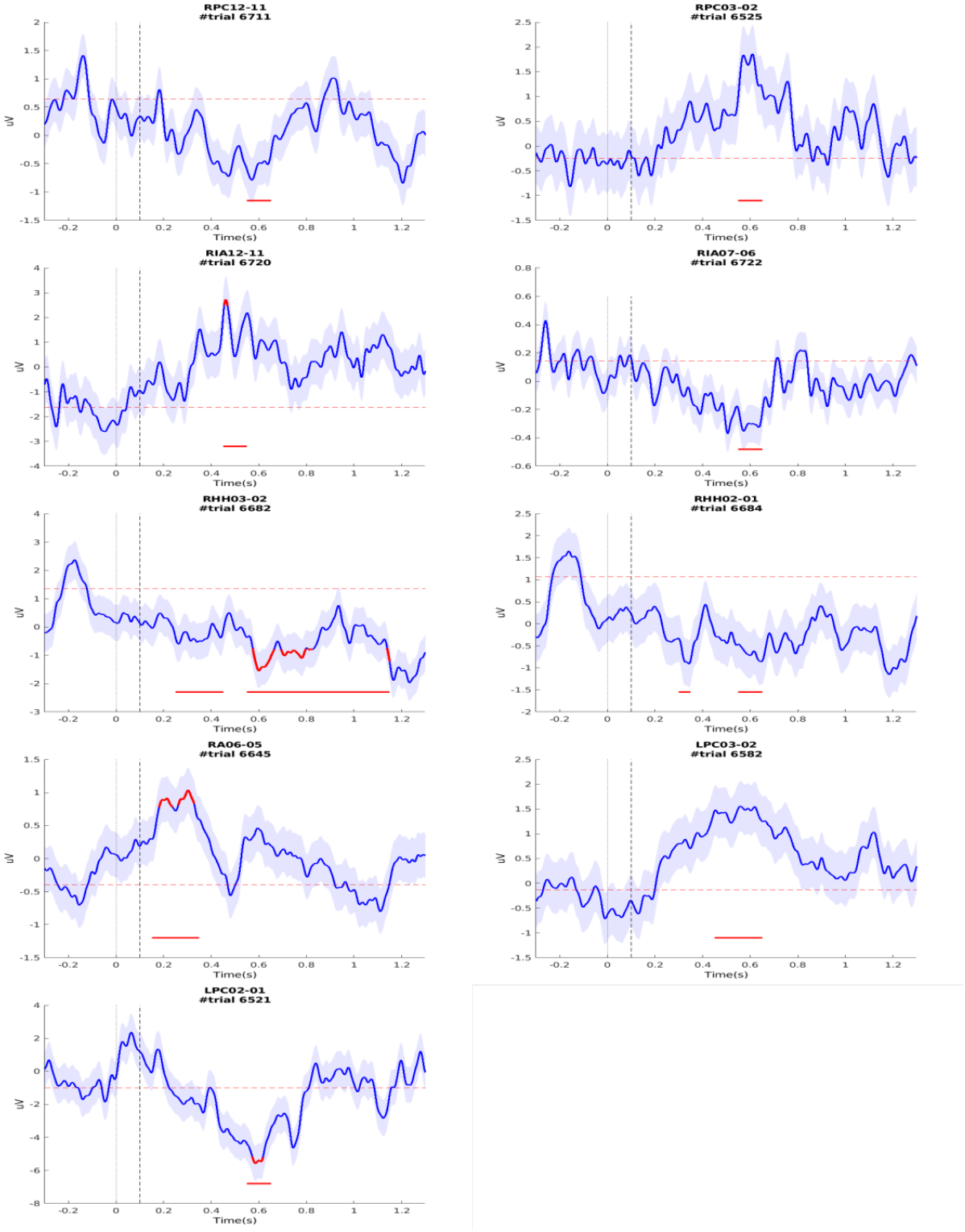

Figure 4.15: **Subject 19 LFP responses** Channel notations & anatomical locations: RPC 12-11:fundus of posterior sulcus, RPC 03-02:, RIA 12-11: superior frontal gyrus, RIA 07-06: insula, RHH 03-02: entorhinal, RHH 02-01: cisterna ambiens, RA 06-05: amygdala, LPC 03-02 & 02-01: cingulate cortex

Out of 162 clean channels in subject 19, significant responses are observed in 9 channels when expecting 8 channels by chance with FDR control level $\alpha = .05$. Channel RA 6-5 (located in amygdala) has the LFP modified earliest occurring around the range of 200ms to 400ms post-stimulation onset. Following by channel RIA 12-11 & 7-6 & 3-2 and channel LPC 3-2 & 2-1 (located in cingulate cortex) have LFP modified at around 600 ms post-stimulation onset. The rest channels have problematic waveforms.

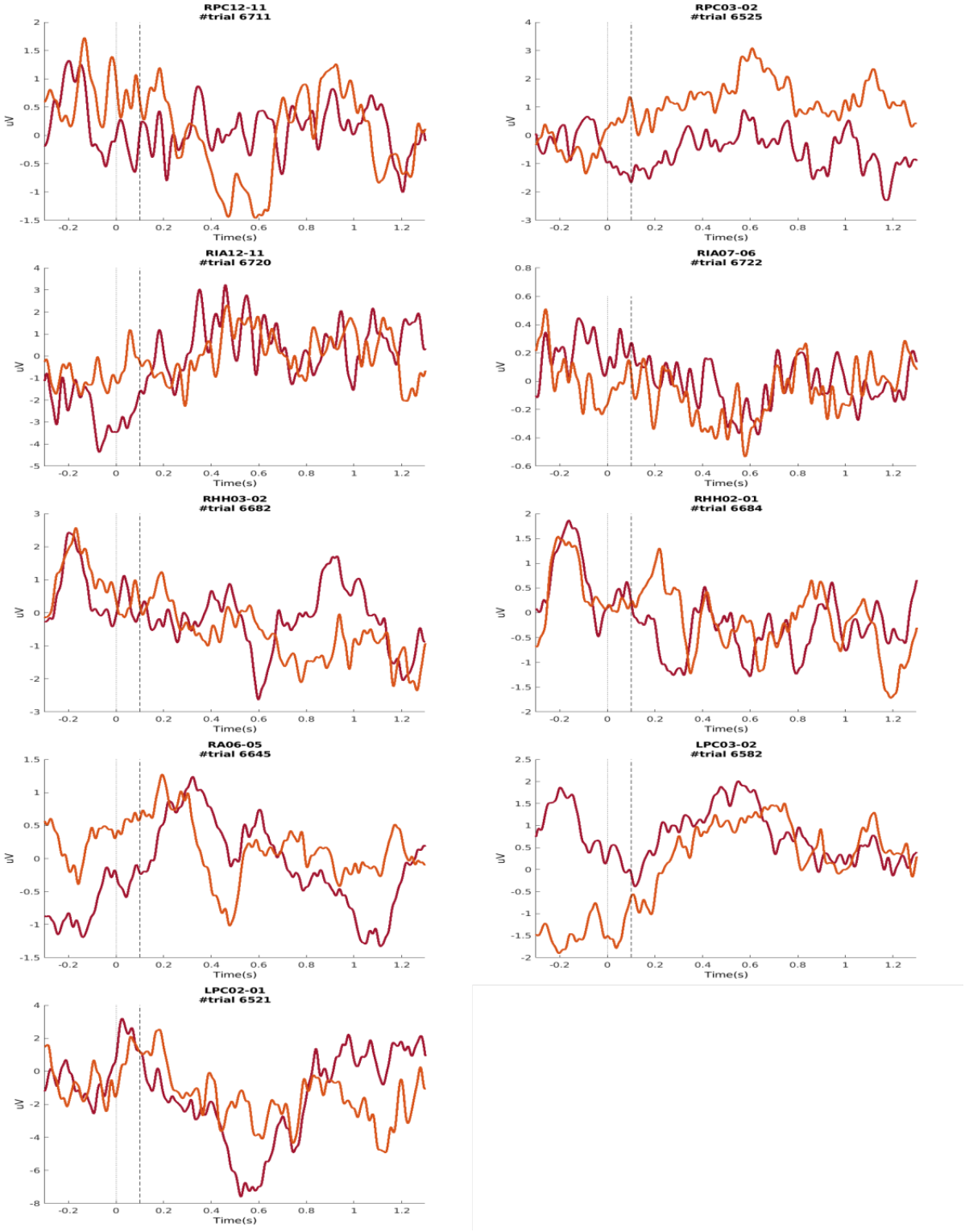

Figure 4.16: **Subject 19 LFP Response Odd/ Even Validation** Channel notations & anatomical locations: RPC 12-11:fundus of posterior sulcus, RPC 03-02:, RIA 12-11: superior frontal gyrus, RIA 07-06: insula, RHH 03-02: entorhinal, RHH 02-01: cisterna ambiens, RA 06-05: amygdala, LPC 03-02 & 02-01: posterior cingulate

Figure 4.16 shows that only channel RIA 12-11 & 7-6 exhibit a aligned regulation between odd and even average trial traces where were reported as significant in Figure 4.15. But response in RIA 12-11 has problematic waveform and the size is not larger than the variance in baseline. After consistency validation, no responses were accepted from subject 19 which aligns with the result that no channels passed Bonferroni correction.

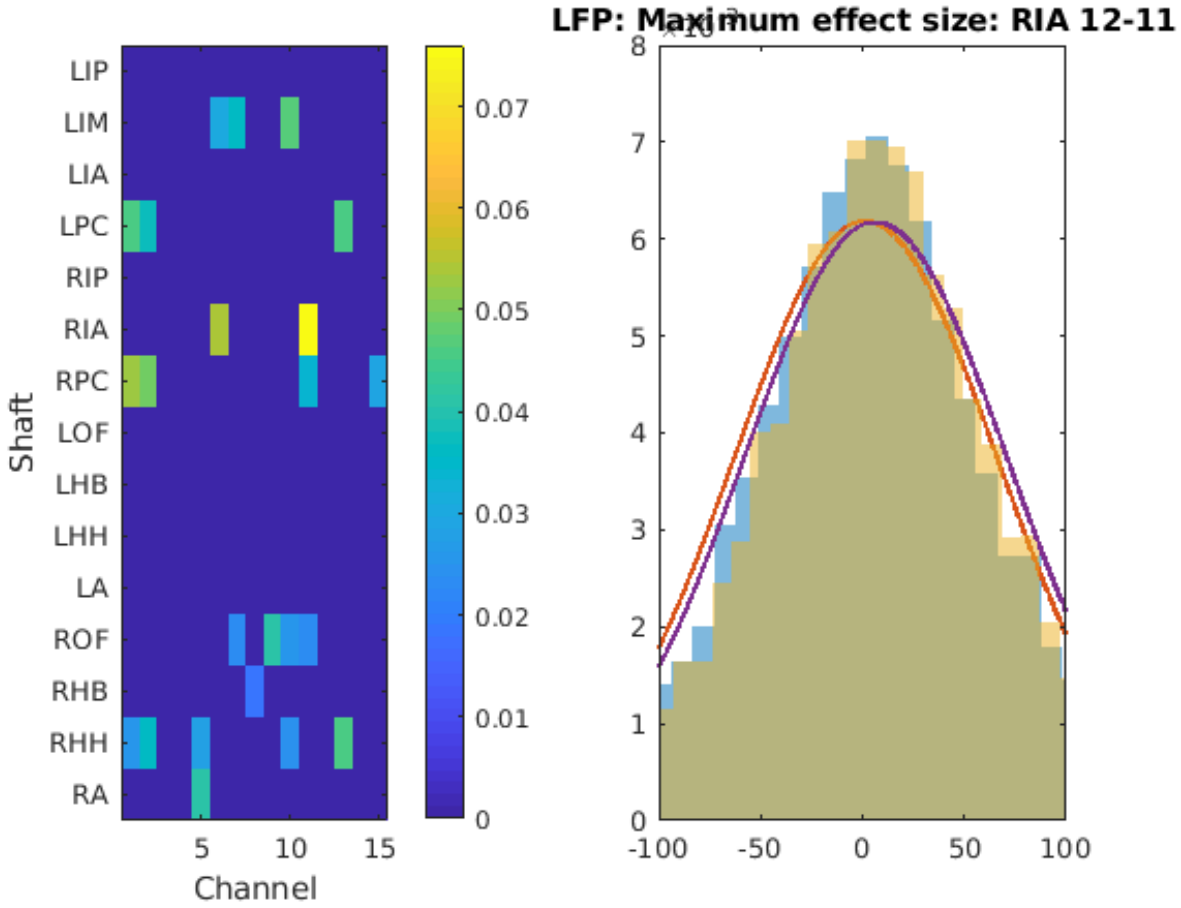

Figure 4.17: **Subject 19 Effect Size Map and Distribution Example of LFP** The left panel shows the biggest effect size in each channel across the response time window. The color scale represents the effect size. The right panel shows the distribution, where the x-axis is micro-volts and y-axis is the probability density. The distribution of LFP amplitude values during the baseline window across all trials is plotted in blue, and the distribution of those during responsive window is plotted in yellow bar. The orange and purple Gaussian curves are calculated from blue and yellow distributions respectively.

Effect sizes in Subject 19 are all very small and evenly spread out with the biggest effect

size only about 0.075 and happens in channel RIA 12-11, which is located in superior frontal sulcus. From the distribution on right panel, we can see that stimulation up regulates the mean of LFP amplitude by 4.9 microvolts when post-stimulation LFP variance is around 64 which aligns with the observation in Figure 4.16. The effect size in channel RIA 7-6 is about 0.05 read off the color map, the reason why we couldn't accepted it is its minuscule LFP amplitude change by 0.5 microvolts, plus it couldn't pass the Bonferroni correction.

Subject 21

Figure 4.18 is from subject 21, in which time domain responses are mainly found in the following areas: prefrontal cortex and cingulate.

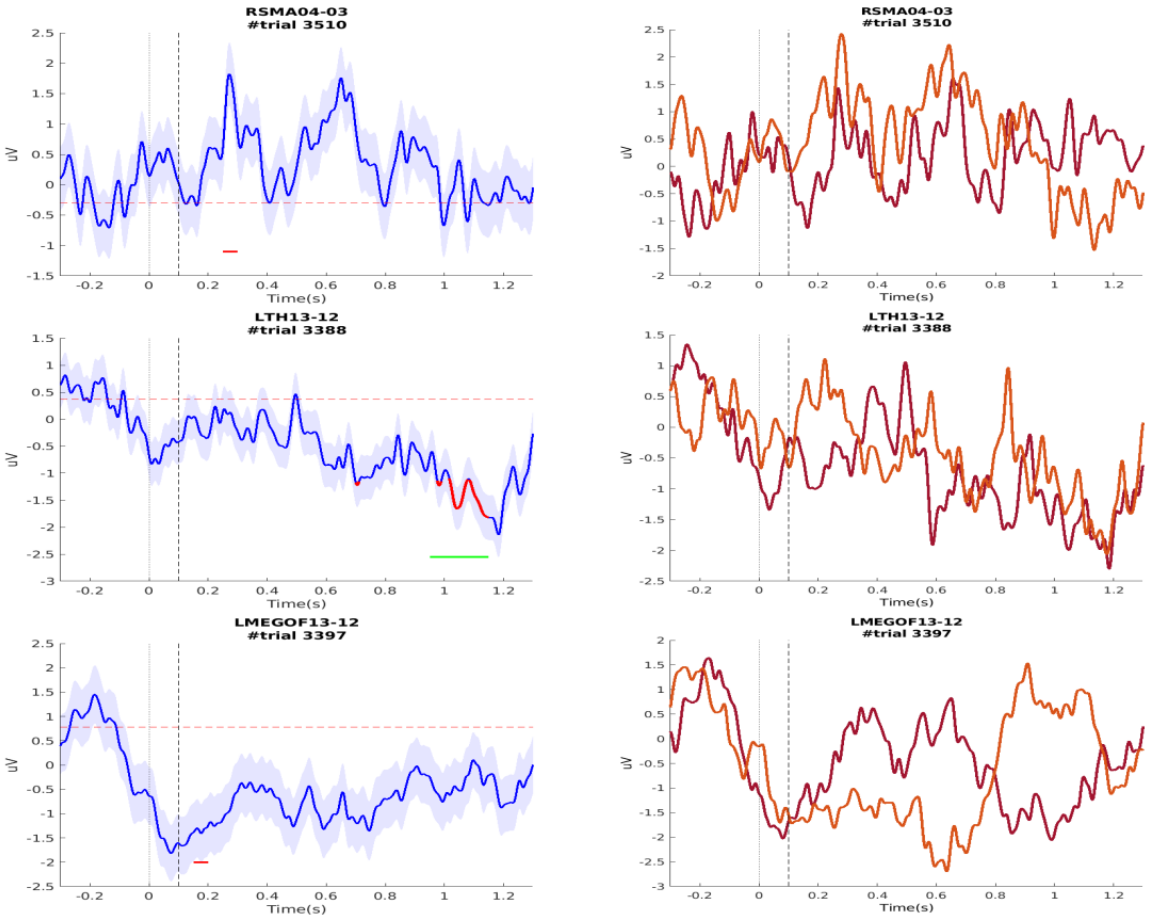

Figure 4.18: **Subject 21 LFP Response** Channel notations & anatomical locations: RSMA 04-03: middle cingulate, LTH 13-12: inferior frontal gyrus, LMEGOF 13-12: inferior frontal gyrus

Out of 108 clean channels in subject 21, no channel was accepted for significant response due to no response is replicated in odd and even trial averages and problematic waveforms.

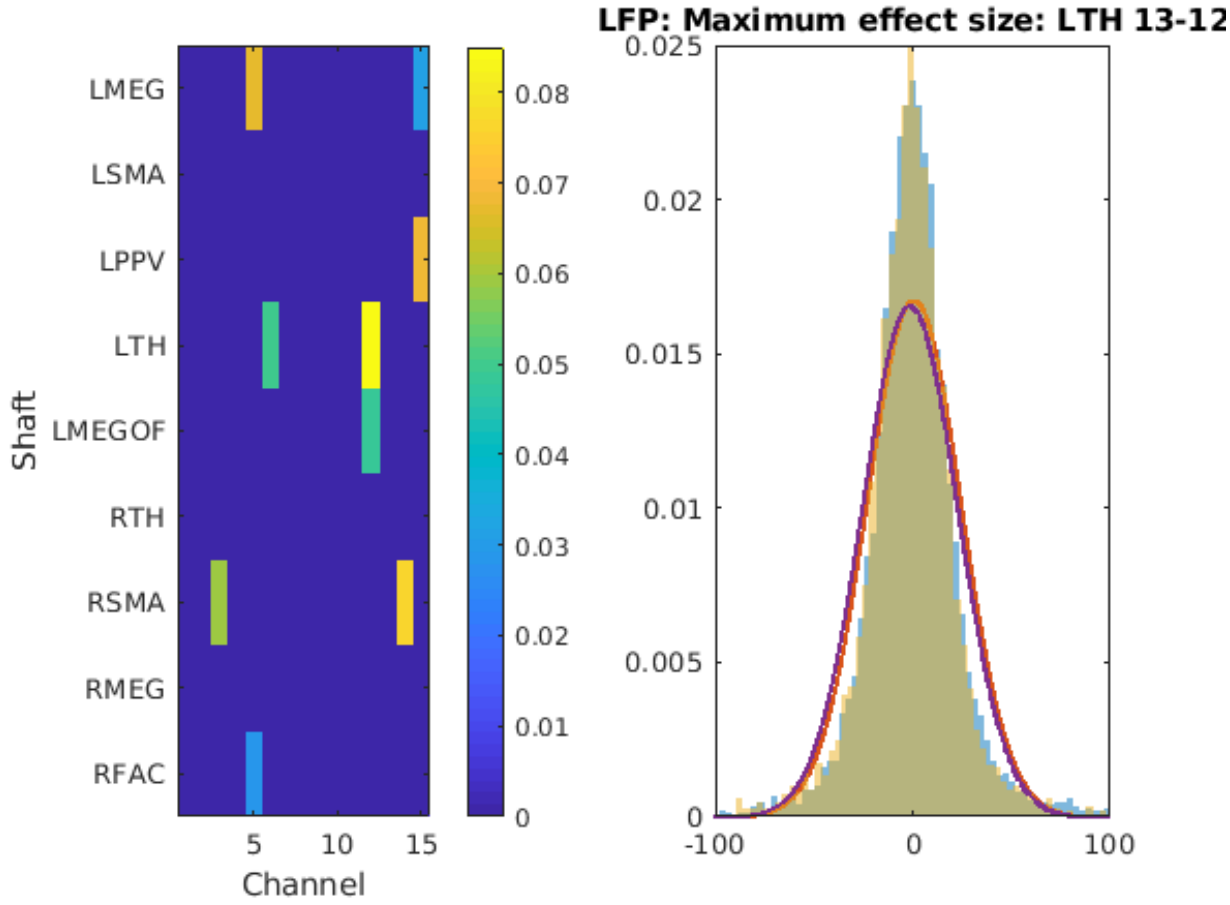

Figure 4.19: **Subject 21 Effect Size Map and Distribution Example of LFP** The left panel shows the biggest effect size in each channel across the response time window. The color scale represents the effect size. The right panel shows the distribution, where the x-axis is micro-volts and y-axis is the probability density. The distribution of LFP amplitude values during the baseline window across all trials is plotted in blue, and the distribution of those during responsive window is plotted in yellow bar. The orange and purple Gaussian curves are calculated from blue and yellow distributions respectively.

Effect sizes in Subject 21 are also all very small with the biggest effect size is lower than .1 and happens in channel LTH13-12, which is located in inferior frontal gyrus. But this channel has been ruled out due to problematic latency.

4.1.2 High Gamma Frequency Band Responses

The next set of figures presents Hilbert transform of High Gamma frequency band responses (y-axis: analytical amplitude in micro-volts; x-axis: time in second). The figures in this section use the same notation as the LFP figures in Section 4.1.1 but they are restated here. For each figure, the y-axis shows the amplitude in micro-volts and the x-axis the time in seconds. The blue trace represents the mean of all trials within one bipolar channel, shaded with Standard Error Mean. Solid and dotted vertical lines at 0s and 0.1s indicate stimulation onset and offset, respectively. The red horizontal line indicates the baseline (average value) across the channel. Sample points masked in red represent significant changes relative to the individual trial baseline with p-value $< .05$, after point to point multiple comparison correction but without Bonferroni correction for the number of channels tested. Colored bars located at the bottom of each figure highlight a significant change in amplitude relative to baseline. Red, green and cyan colored bars represent p-values smaller than 0.05, 0.01, and 0.001 respectively after window to window multiple comparison correction but without Bonferroni correction for the number of channels tested. Yellow star labeled channels are the ones that also passed at $p < .05$ after Bonferroni correction for the number of channels in that subject. Figures are grouped by subjects. Responses' consistency were validated through comparing the average trace of odd and even trials. Figures with red and orange traces show odd and even trials' mean from the channels with significant responses reported by t-test. In addition to significant test for responses, we also used effect size to describe the effectiveness of stimulation on different locations.

Subject 15

Figure 4.20 is from Subject 15, where the time domain responses are found in the following areas: prefrontal cortex, temporal lobe.

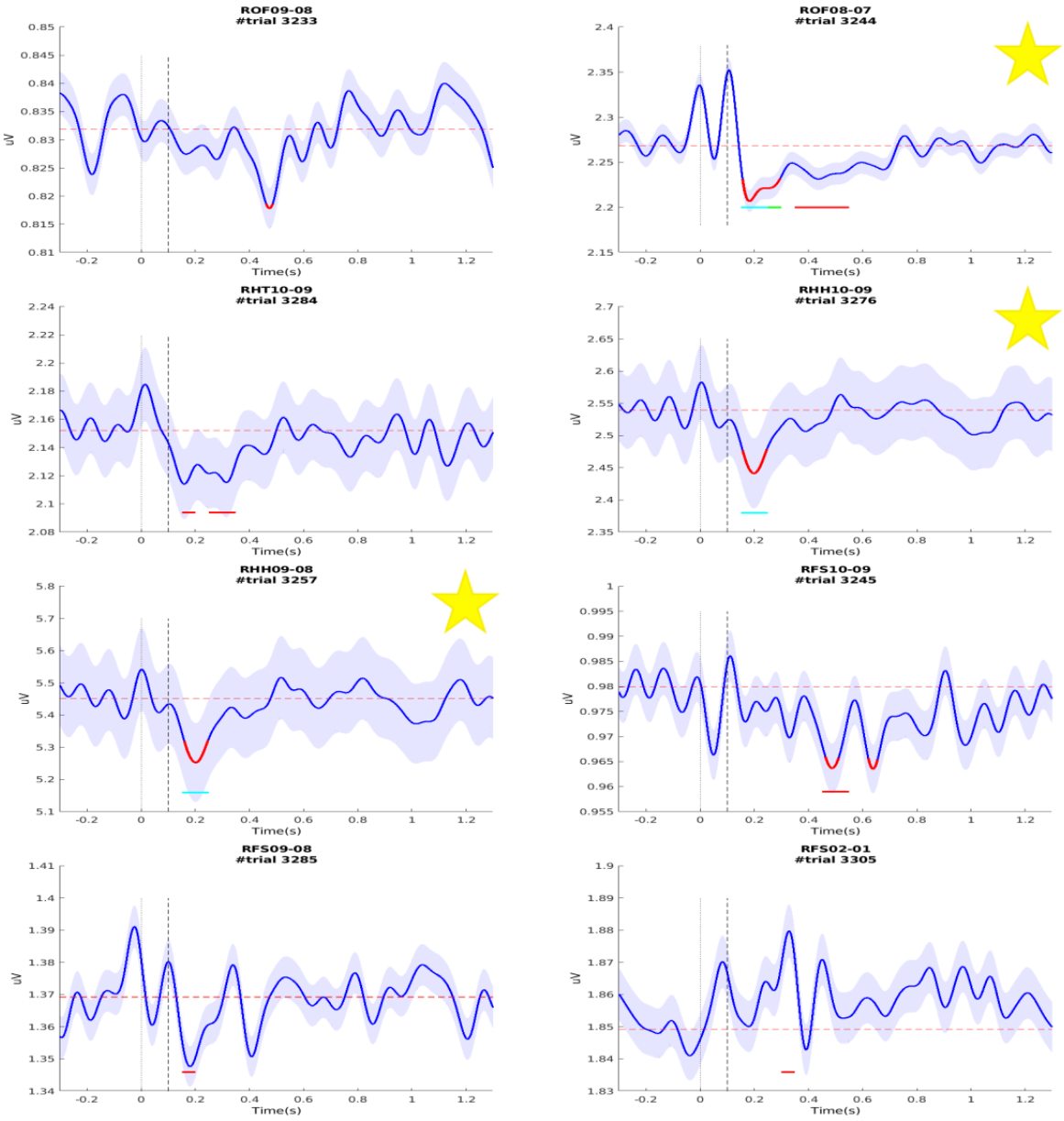

Figure 4.20: **Subject 15 HG responses** Channel notations & anatomical locations: ROF 09-08 & 08-07: middle frontal gyrus, RHT 10-09: superior temporal gyrus, RHH 10-09 & 09-08: middle temporal gyrus, RFS 10-09 & 09-08 & 02-01: frontal grey matter

Out of 79 clean channels in subject 15, the 8 channels presented above are detected to contain significant responses when expecting 3 channels by chance with $\alpha = .05$. Channels: ROF 8-7(middle frontal gyrus), RHT 10-9(superior temporal gyrus), RHH 10-9 & 9-8(middle temporal gyrus) share similar waveforms and have earliest responses starting at around 180ms

post-stimulation onset. Amplitude suppression ends first in channel RHH 10-9 & 9-8 at around 220ms post-stimulation onset. In channel ROF 8-7, the suppression of amplitude lasts until around 600ms post-stimulation onset. Overall HG analytical amplitude change is very small with the biggest one in channel RHH 9-8 reaching 0.17 microvolts at peak.

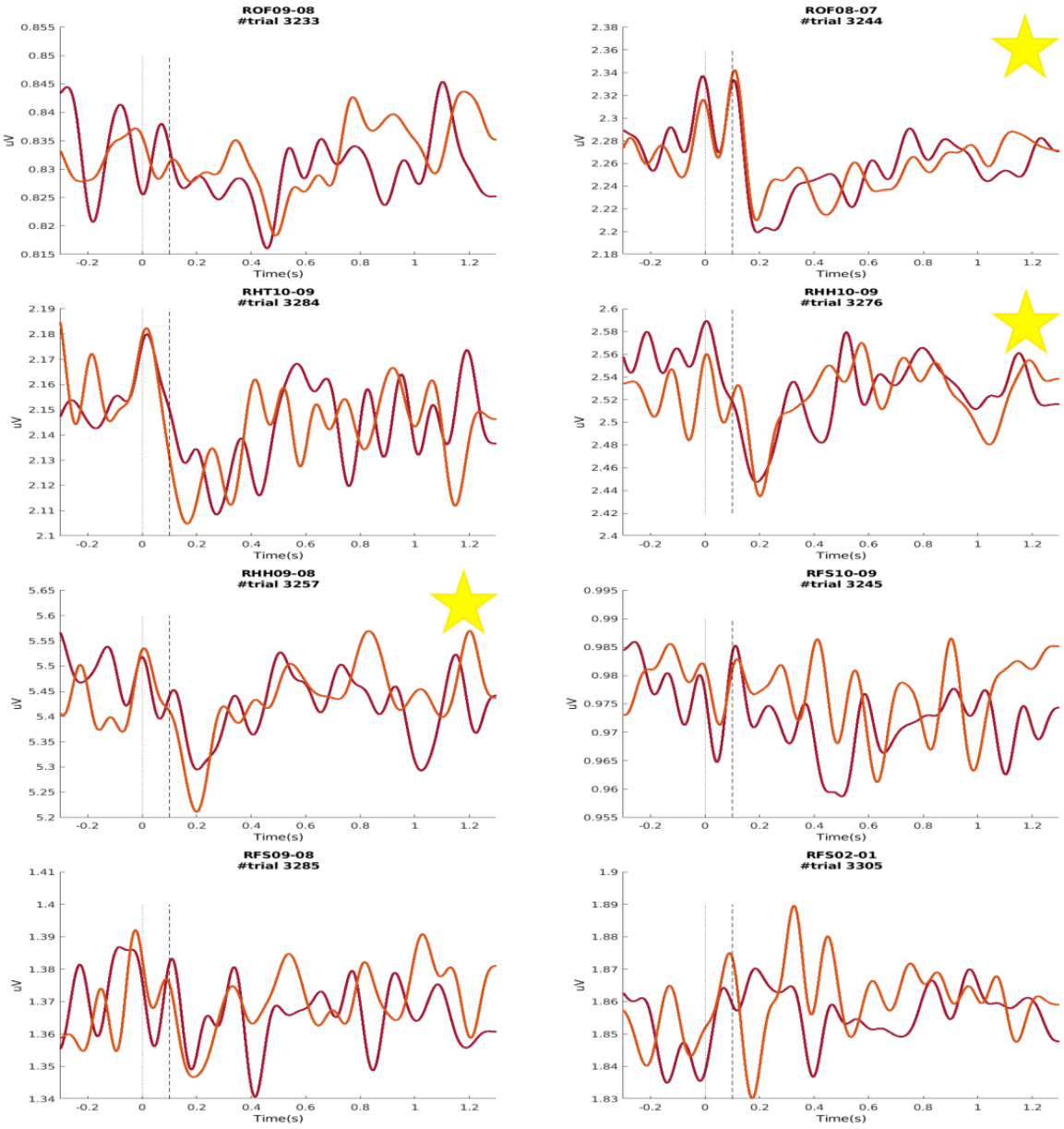

Figure 4.21: **Subject 15 HG Response Odd/ Even Validation** Channel notations & anatomical locations: ROF 09-08 & 08-07: middle frontal gyrus, RHT 10-09: superior temporal gyrus, RHH 10-09 & 09-08: middle temporal gyrus, RFS 10-09 & 09-08 & 02-01: frontal grey matter

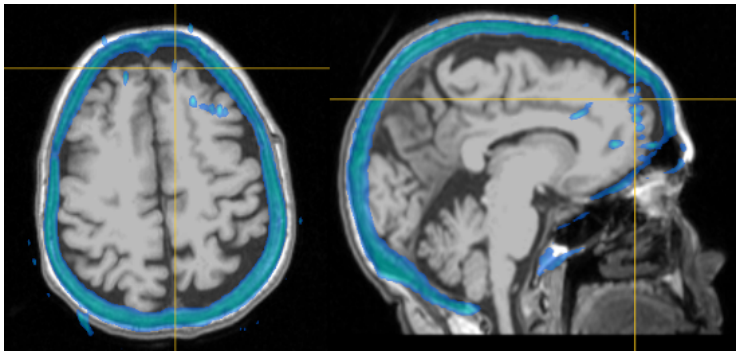

(a) Channel ROF 8-7

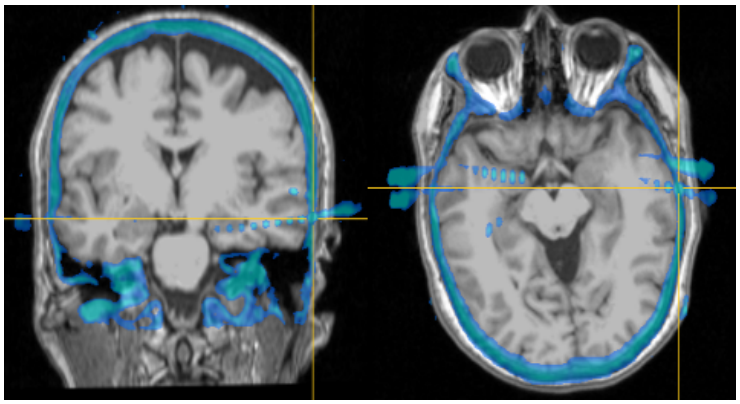

(b) Channel RHH 10-9& 9-8

Figure 4.22: Starred channel electrodes localization

From figures above, we find channel RFS 2-1 & 10-9 doesn't have consistent response in odd and even trial mean. Therefore after consistency validation, total number of significant responses is 6. But only channel ROF 8-7(middle frontal gyrus), and channel RHH 10-9 & 9-8 (middle temporal gyrus) passed Bonferroni correction for the number of tested channels in subject #15, see their anatomical location in MRI images in Figure 4.22a4.22b. Besides significant test for responses, we also used effect size to describe the effectiveness of stimulation on different locations.

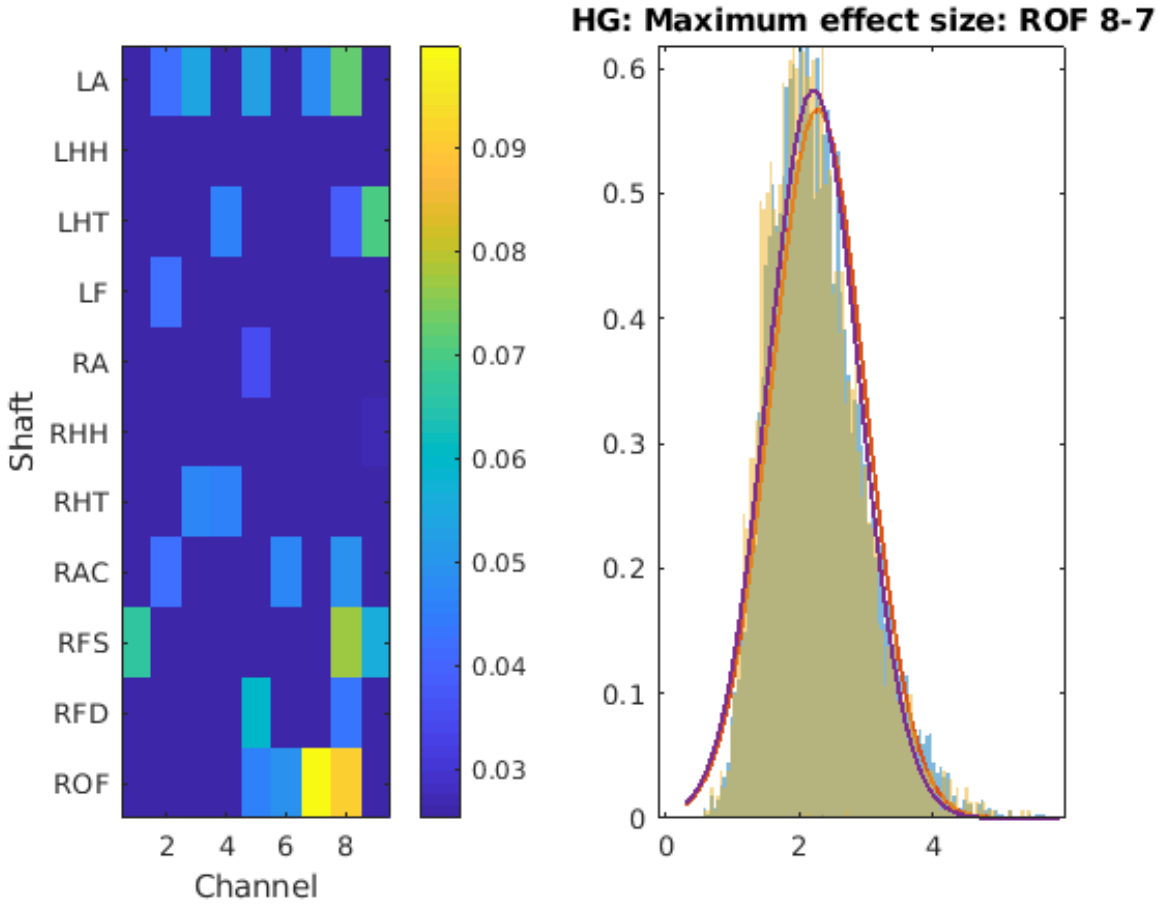

Figure 4.23: **Subject 15 Effect Size Map and Distribution Example of HG** The left panel of figure above shows biggest effect size in each channel across responsive time window. Right panel: distribution: x-axis unit micro-volts, y-axis probability density. the distribution of HG amplitude values during baseline window across all trials is plotted in blue bars, and the distribution of those during responsive window is plotted in yellow bars

The biggest effect size of HG envelope in Subject 15 is about 0.1 and happens in channel ROF 8-7, which is located in middle frontal gyrus. For channel RHT 10-9 that didn't pass the Bonferroni correction, we can see its effect size is minuscule (smaller than 0.03 reading off color-map). From the distribution on right panel, we can see stimulation downregulates the mean of HG envelope by 0.069 microvolts when variance of it in post-stimulation is around 0.684.

Subject 16

The following figure is from subject 16. In subject 16, time domain responses are found in the following areas: prefrontal cortex, parietal operculum, rolandic.

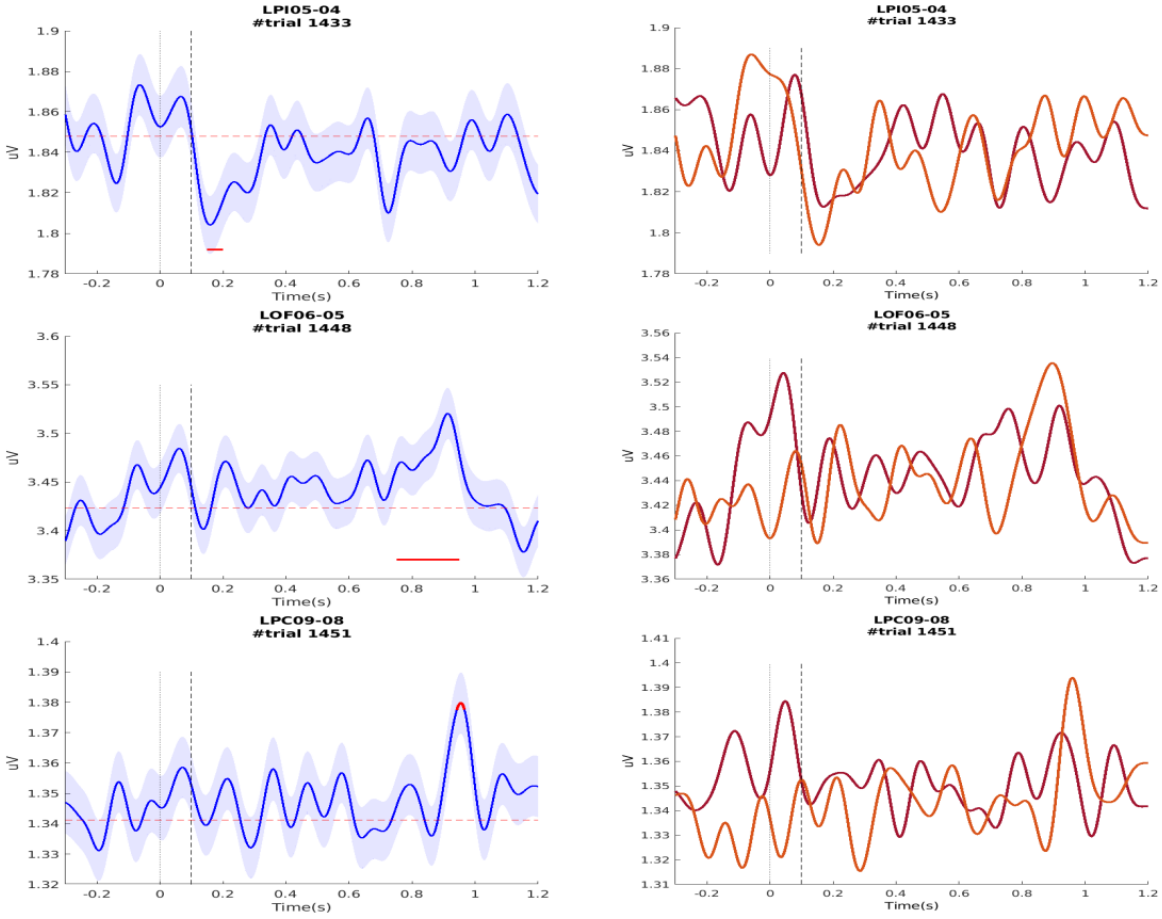

Figure 4.24: **Subject 16 HG responses** Channel notations & anatomical locations: LPI 05-04: parietal operculum, LPC 09-08: rolandic, LOF 06-05: obital frontal

Out of 145 clean channels in subject 16, 3 channels presented above are detected containing significant responses when expecting 7 channels by chance with $\alpha = .05$ Channels: LPI5-4 located in parietal operculum has the earliest response occurring at around 150ms post-stimulation onset, but it's problematic that the size of response is not larger than the variance in baseline. In channel LPC9-8 (located in rolandic) and LOF6-5 (located in orbital frontal), we observed late response in the time range of 800ms - 1s post-stimulation onset, which is problematic latency.

From odd and even trials plots above, we find channel LPC 9-8 and LOF 6-5 don't have aligned odd and even trial average traces. Therefore, the total number of channels with significant responses was corrected to 1.

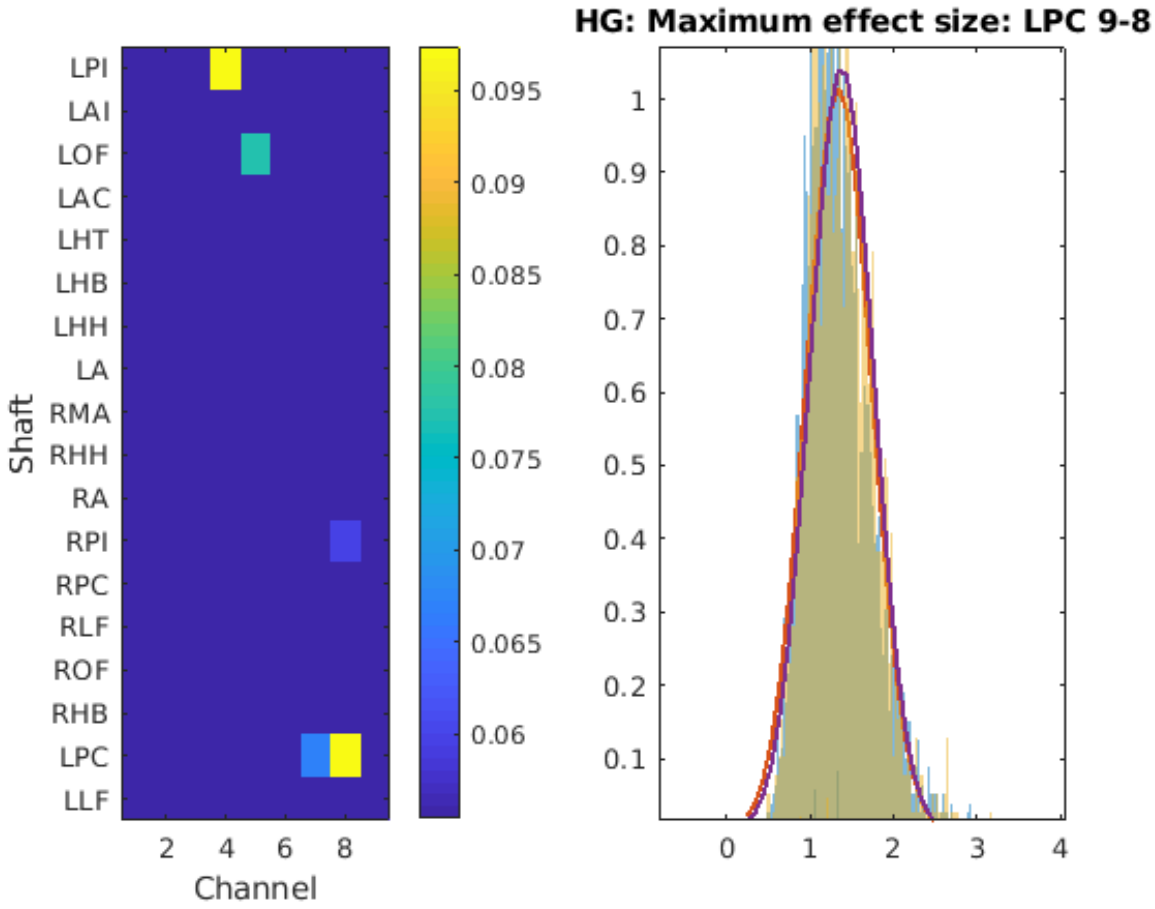

Figure 4.25: **Subject 16 Effect Size Map and Distribution Example of HG** The left panel of figure above shows biggest effect size in each channel across responsive time window. Right panel: distribution: x-axis unit micro-volts, y-axis probability density. the distribution of HG amplitude values during baseline window across all trials is plotted in blue bars, and the distribution of those during responsive window is plotted in yellow bars

The biggest effect size of HG envelope in Subject 16 is around 0.12, which happens in channel LPC 9-8, which is located in rolandic. But this channels has been ruled out due to problematic response latency.

Subject 17

The following figure is from subject 17. In subject 17, time domain responses are found only in temporal lobe.

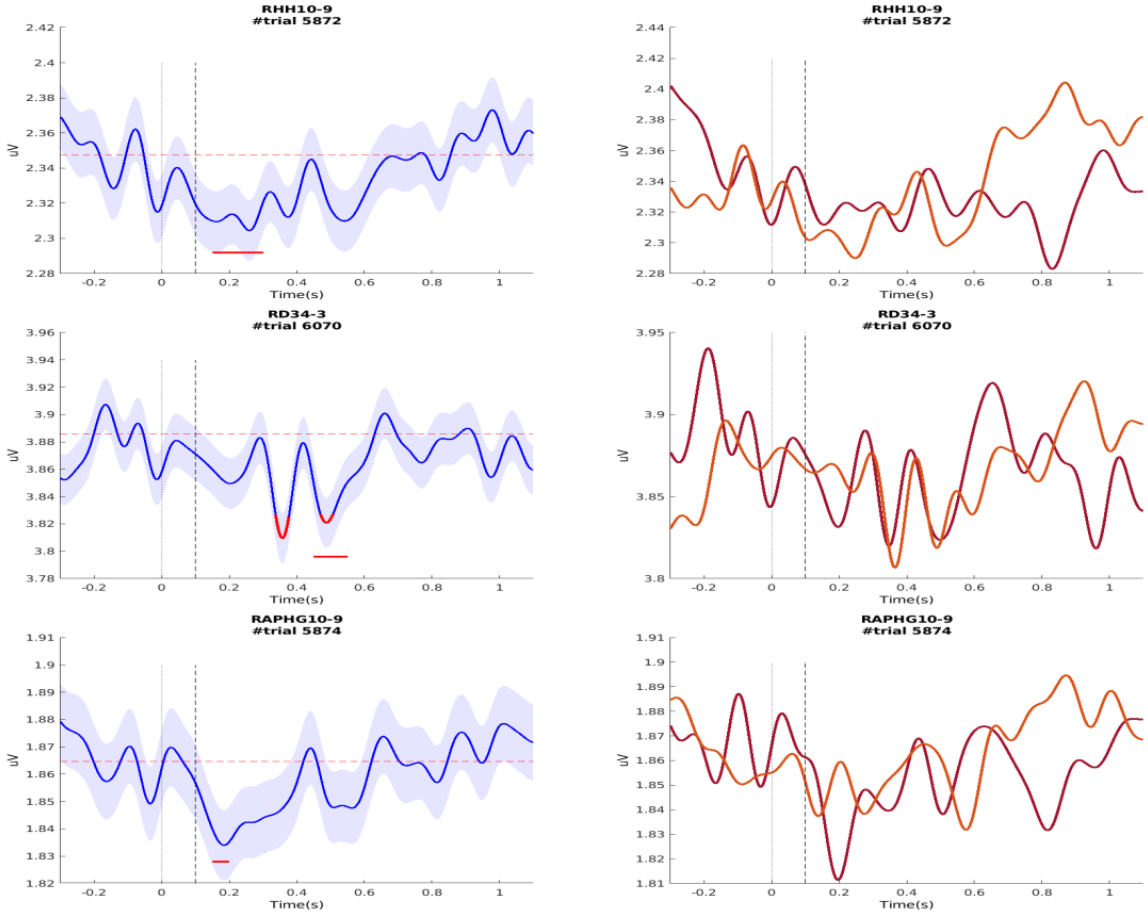

Figure 4.26: **Subject 17 HG responses** Channel notations & anatomical locations: RHH 10-9: medial temporal gyrus, RD3 4-3:fusiform gyrus/lingual gyrus, RAPHG 10-9: medial temporal gyrus

After odd and even trial mean consistency validation, out of 74 clean channels in subject 17, 3 channels presented above are detected containing significant responses when expecting 3 channels by chance with $\alpha = .05$. But channel RHH10-9 and RAPHG10-9 located in middle temporal gyrus don't have the aligned odd and even trial average traces. Only channel RD3 4-3 (located in fusiform gyrus/lingual gyrus) has a significant response occur at around 400ms

post-stimulation onset, but it's problematic that the size of response is not larger than the variance in baseline.

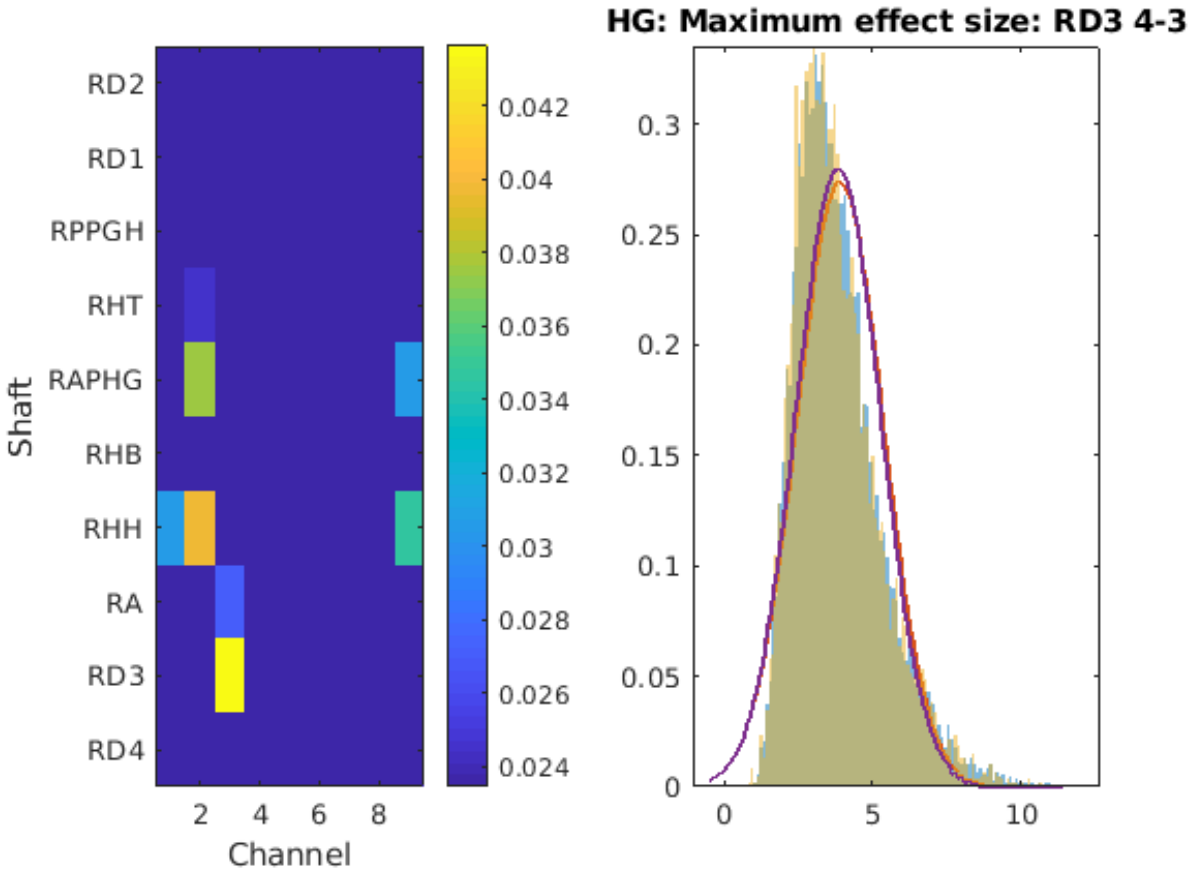

Figure 4.27: **Subject 17 Effect Size Map and Distribution Example of HG** sThe left panel of figure above shows biggest effect size in each channel across responsive time window. Right panel: distribution: x-axis unit micro-volts, y-axis probability density. the distribution of HG amplitude values during baseline window across all trials is plotted in blue bars, and the distribution of those during responsive window is plotted in yellow bars

Subject 17 shows the biggest effect sizes of HG envelope among all subjects in the color-map, but those are from refractory period of neuron firing from stimulation artifact in certain channels. For channels that have significant responses validated through former amplitude-time figures, channel RD3 4-3 located in fusiform gyrus/lingual gyrus has the biggest effect size at around 0.04. From the distribution on right panel, we can see stimulation downregulates the mean of LFP amplitude by 0.062 microvolts when post-stimulation LFP variance is around 1.424.

Subject 19

The following two figures are from subject 19. In subject 19, time domain responses are found in the following areas: prefrontal cortex, cingulate, amygdala & hippocampus, insula, somatosensory cortex & parietal lobe, temporal lobe.

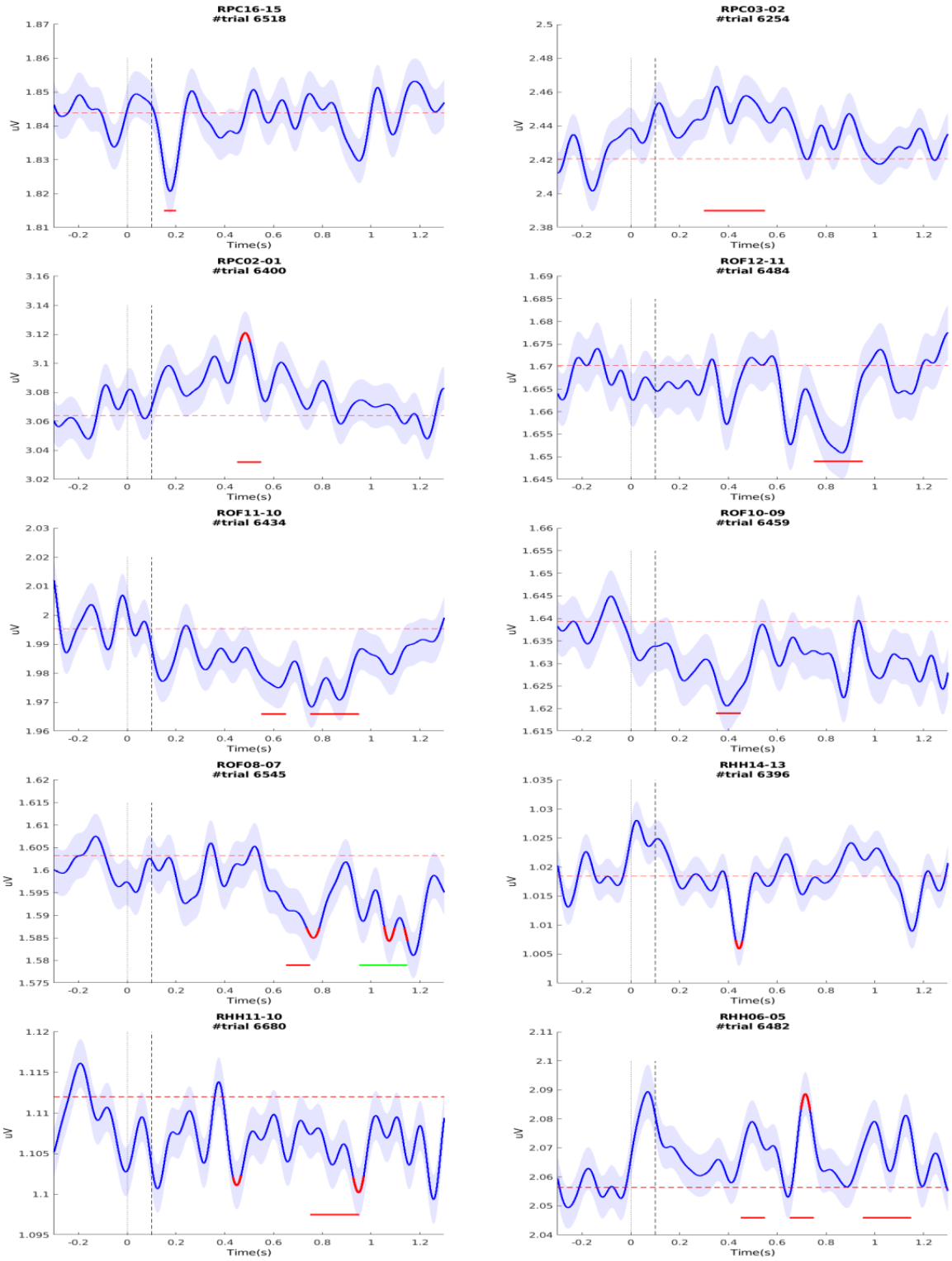

Figure 4.28: **Subject 19 HG responses Part I** Channel notations & anatomical locations: RPC 16-15: supramarginal gyrus, RPC 03-02: cingulate gyrus, RPC 02-01: cingulate gyrus, ROF 12-11 & 11-10 & 10-09 & 08-07: inferior frontal gyrus, RHH 14-13 & 11-10: inferior temporal sulcus, RHH 06-05: hippocampus

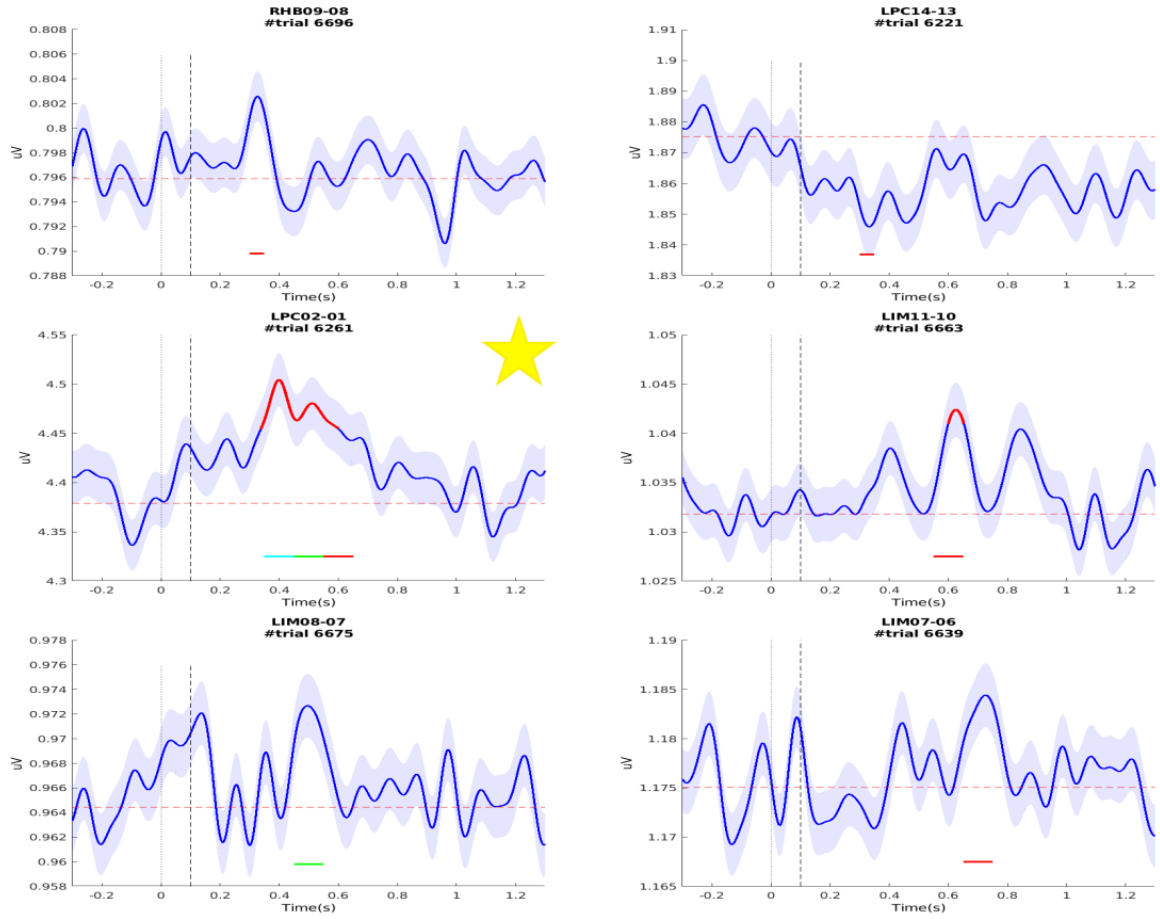

Figure 4.29: **Subject 19 HG responses Part II** Channel notations & anatomical locations: RHB 09-08: superior temporal sulcus, LPC 14-13: postcentral gyrus, LPC 02-01: posterior cingulate, LIM 11-10: fundus of superior frontal sulcus, LIM 08-07 & 07-06: insula

Out of 163 clean channels in subject 19, 17 channels presented above are detected containing significant responses when expecting 8 channels by chance with $\alpha = .05$ Except channel LPC 2-1(cingulate cortex) contains response reaching 0.07 microvolts and channel RPC 2-1 (cingulate gyrus) contains response reaching 0.06 microvolts at peak, the rest responses are either minuscule smaller than 0.05 microvolts or have problematic waveforms. Responses in channel ROF 12-11 & 8-7 (inferior frontal gyrus) occurred in the time range of 0.8s - 1.2s post-stimulation onset, which are problematic latency.

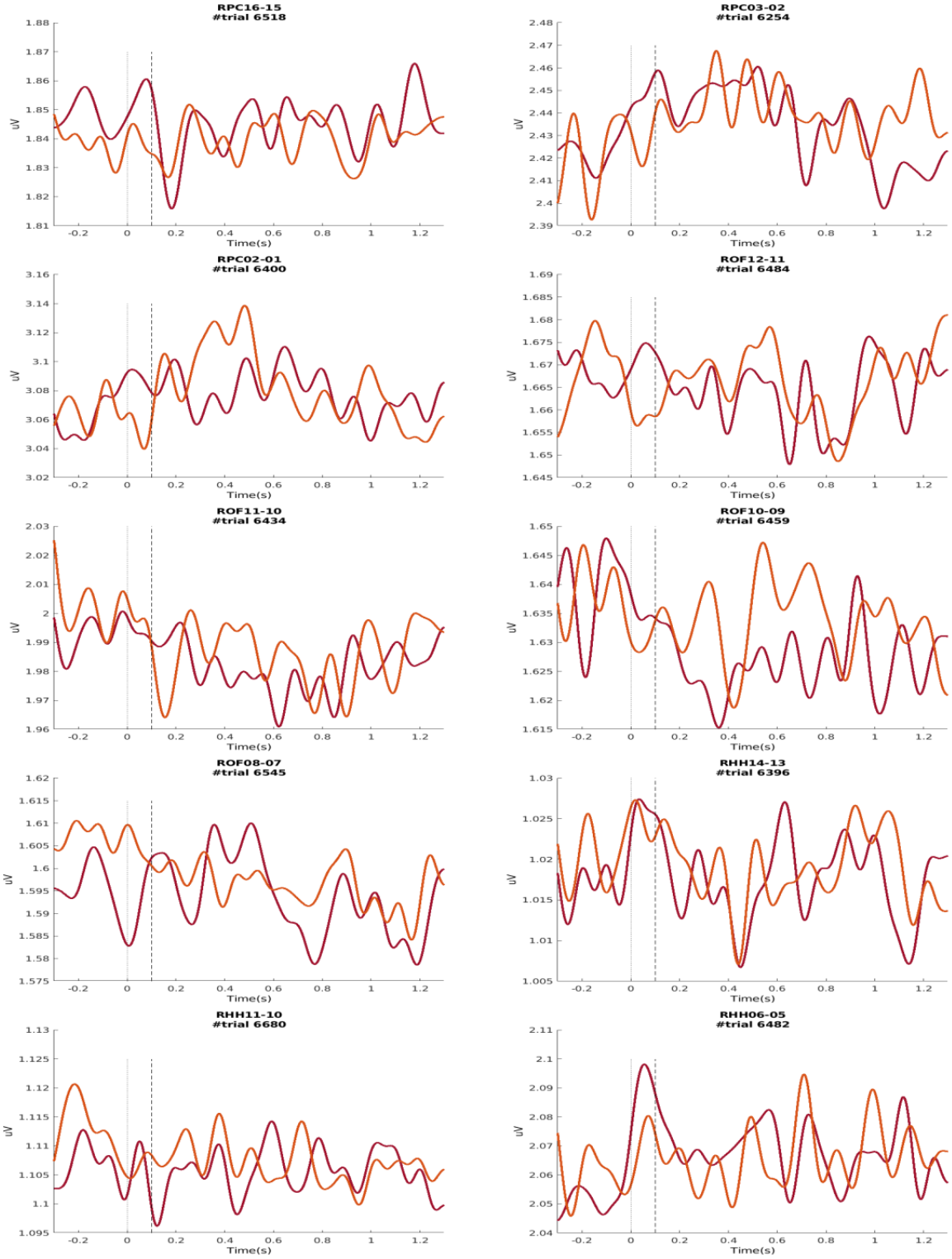

Figure 4.30: **Subject 19 HG Response Odd/ Even Validation Part I** Channel notations & anatomical locations: RPC 16-15: supramarginal gyrus, RPC 03-02: cingulate gyrus, RPC 02-01: cingulate gyrus, ROF 12-11 & 11-10 & 10-09 & 08-07: inferior frontal gyrus, RHH 14-13 & 11-10: inferior temporal sulcus, RHH 06-05: hippocampus

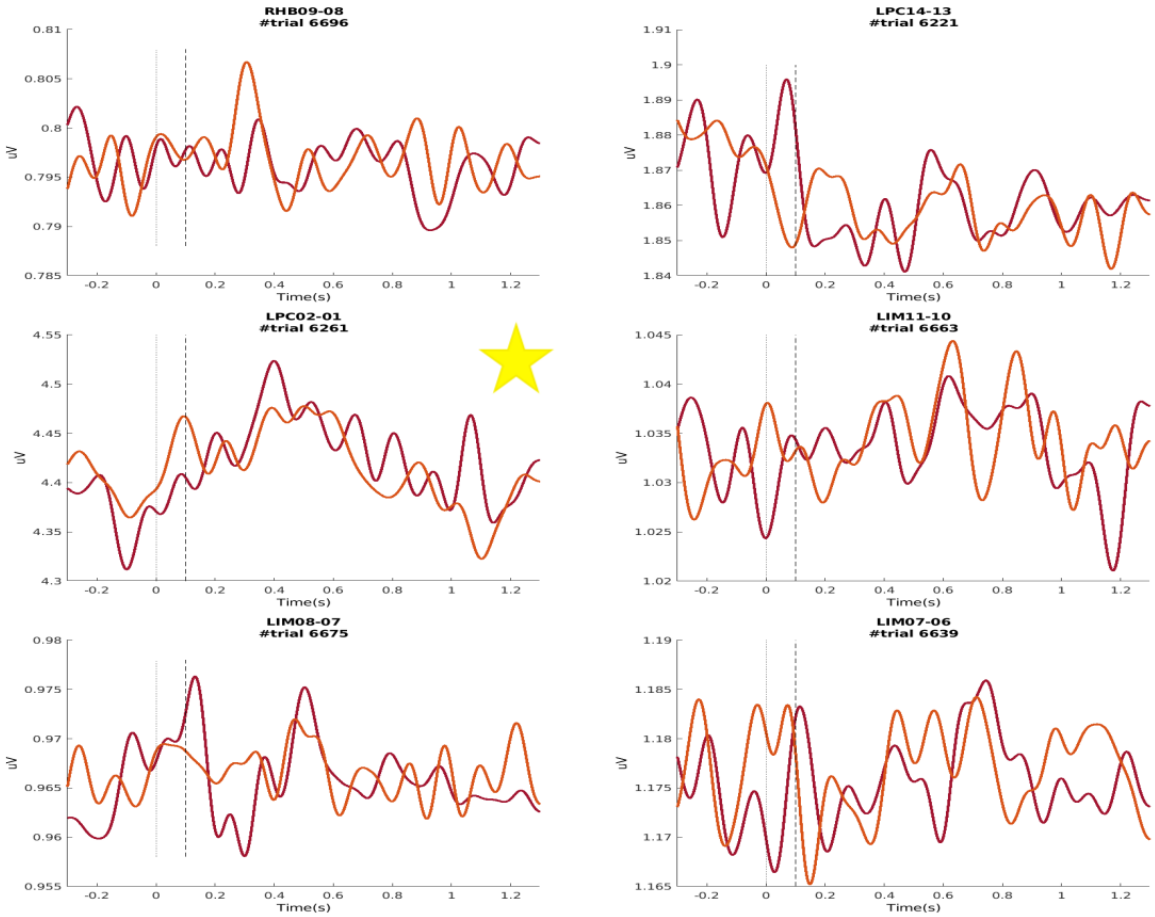

Figure 4.31: **Subject 19 HG Response Odd/ Even Validation Part II** Channel notations & anatomical locations: RHB 09-08: superior temporal sulcus, LPC 14-13: postcentral gyrus, LPC 02-01: posterior cingulate, LIM 11-10: fundus of superior frontal sulcus, LIM 08-07 & 07-06: insula

From Figure 4.30, only channel RHH 14-13, LIM 11-10 and LPC 2-1, have the response replicated in both odd & even trial averages. But the size of amplitude decrease in RHH 14-13 is not bigger than background variation, and LIM 11-10 has problematic waveform. There was also only channel LPC 2-1 passed Bomferroni correction for the number of tested channels in subject #19, therefore it was accepted for significant response. See channel LPC 2-1 electrodes in MRI image Figure 4.32, who are mainly located in comparing to cingulate cortex, which explains the minuscule response size.

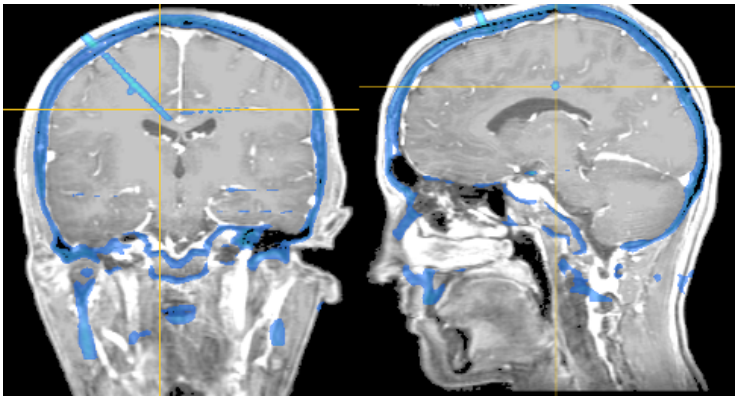

Figure 4.32: Starred channel LPC 2-1 electrodes localization

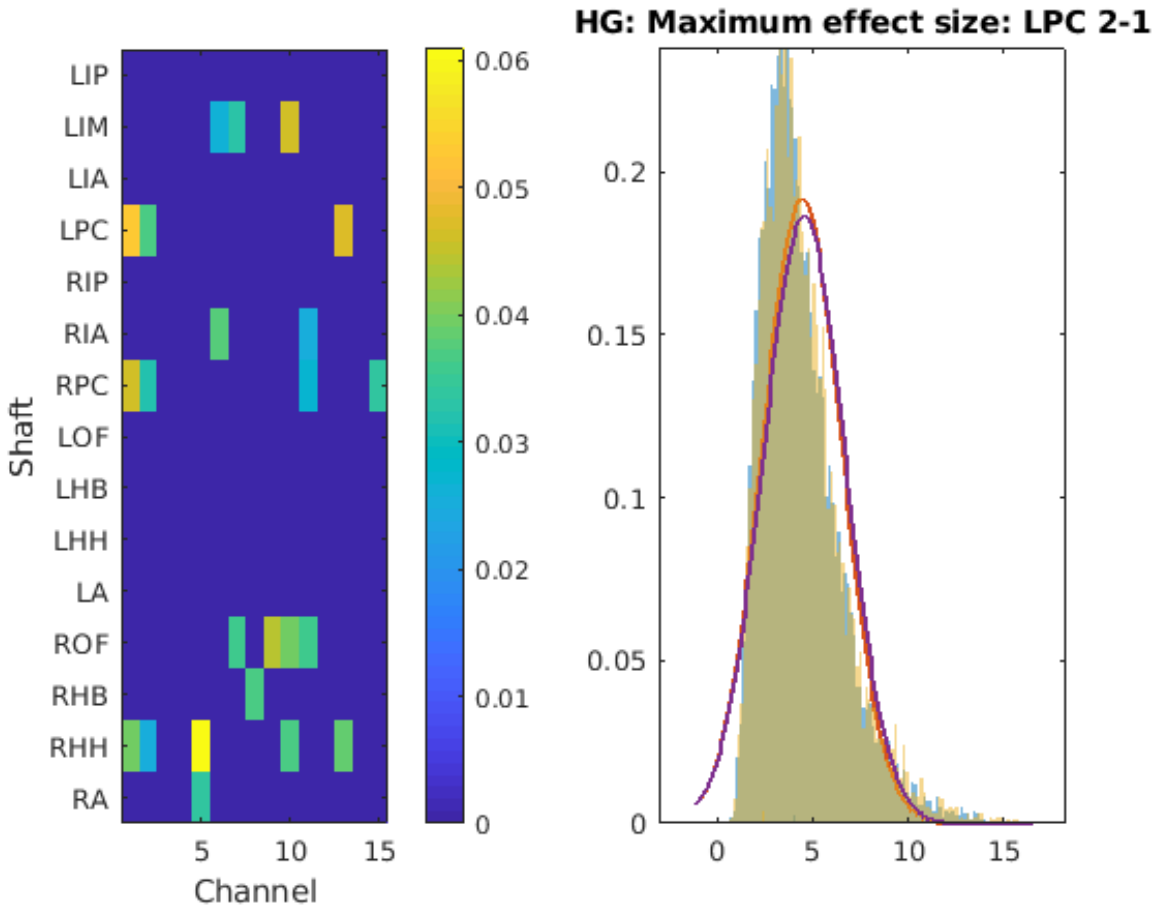

Figure 4.33: **Subject 19 Effect Size Map and Distribution Example of HG** The left panel of figure above shows biggest effect size in each channel across responsive time window. Right panel: distribution: x-axis unit micro-volts, y-axis probability density. the distribution of HG amplitude values during baseline window across all trials is plotted in blue bars, and the distribution of those during responsive window is plotted in yellow bars

Among all the channels, channel RHH 6-5 has the biggest effect size in the color-map at around 0.06 but its response is not replicated in odd & even trial averages. For the starred channel LPC 2-1, the analytical amplitude was upregulated for 0.114 microvolts, when the post stimulation variance is about 2.14, together the effect size is about 0.05.

Subject 21

The following figure is from subject 21. In subject 21, time domain responses are found in the following areas: prefrontal cortex, cingulate cortex, and precentral sulcus.

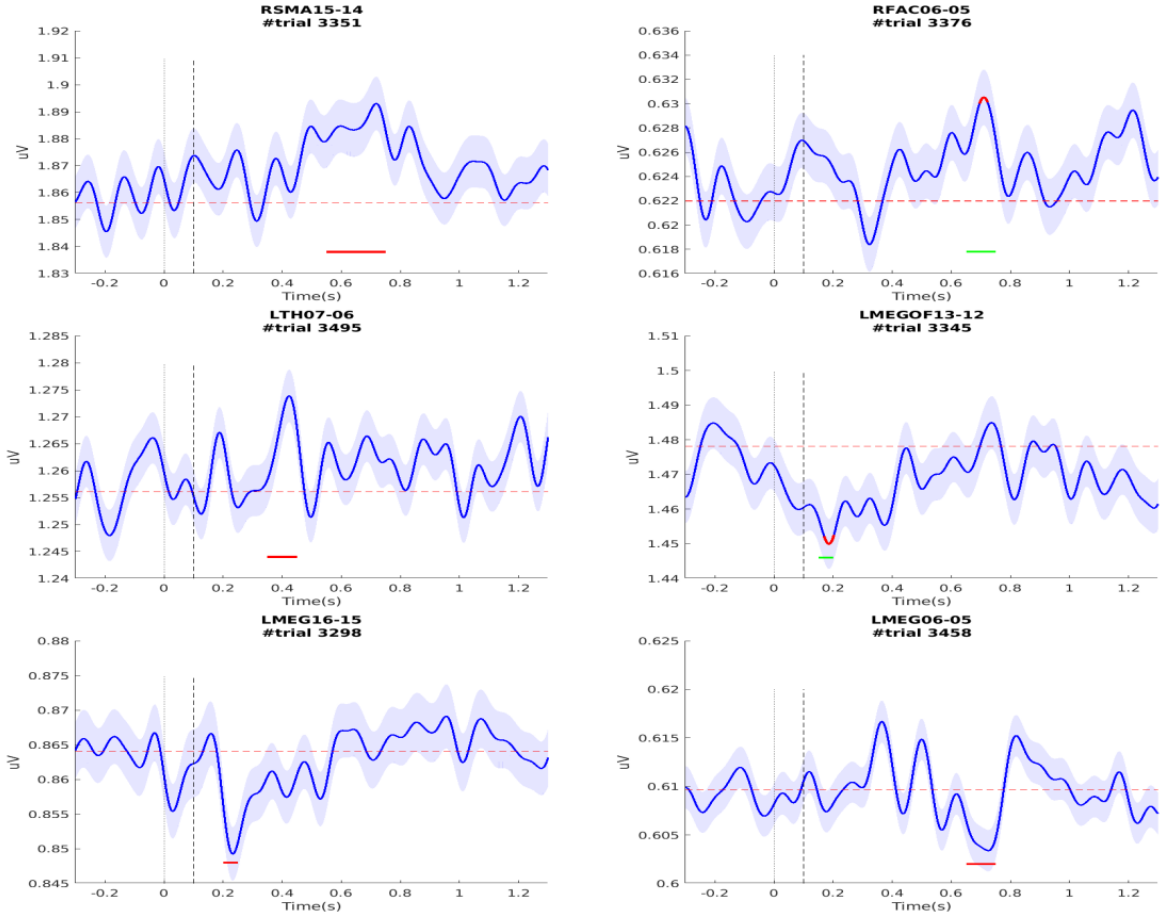

Figure 4.34: **Subject 21 HG responses** Channel notations & anatomical locations: RSMA 15-14: precentral sulcus, RFAC 06-05: orbital, LTH 07-06: putamen, LMEGOF 13-12: inferior frontal gyrus, LMEG 16-15: inferior frontal gyrus, LMEG 06-05: anterior cingulate cortex

Out of 109 clean channels in subject 21, 6 channels presented above are detected containing significant responses when expecting 5 channels by chance with $\alpha = .05$ Channel LMEGOF 13-12 and LMEGOF 16-15 located in inferior frontal gyrus have the earliest response occurring at around 200ms post-stimulation onset. Channel RSMA 15-14 contains response with amplitude of 0.03 microvolts, channel LMEGOF 13-12 contains response with amplitude of 0.03 microvolts,

the rest responses are all minuscule smaller than 0.01 microvolts.

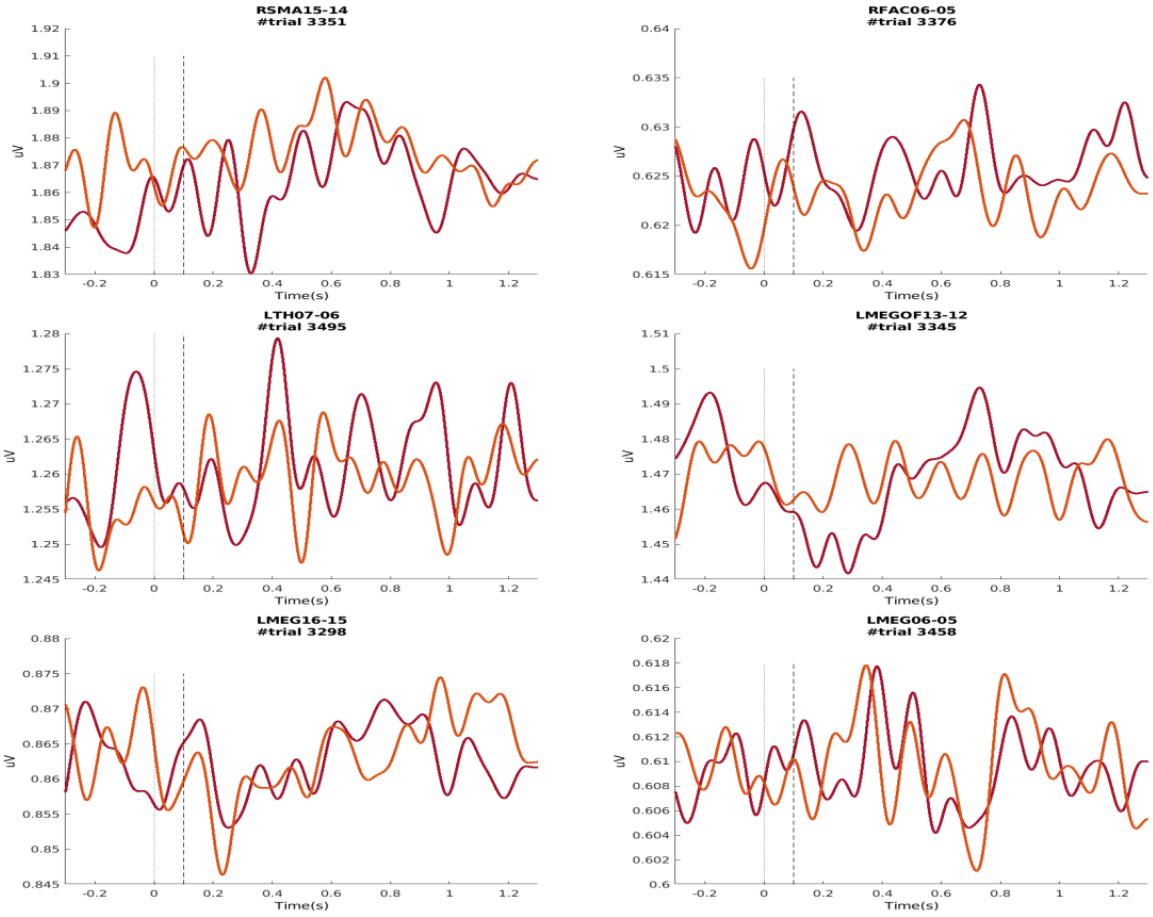

Figure 4.35: **Subject 21 HG Response Odd/ Even Validation** Channel notations & anatomical locations: RSMA 15-14: precentral sulcus, RFAC 06-05: orbital, LTH 07-06: putamen, LMEGOF 13-12: inferior frontal gyrus, LMEG 16-15: inferior frontal gyrus, LMEG 06-05: anterior cingulate cortex

In Figure 4.35, only channel LMEG 16-15 & 6-5 have the responses replicated in both odd & even trial averages during the statistically reported significant time.

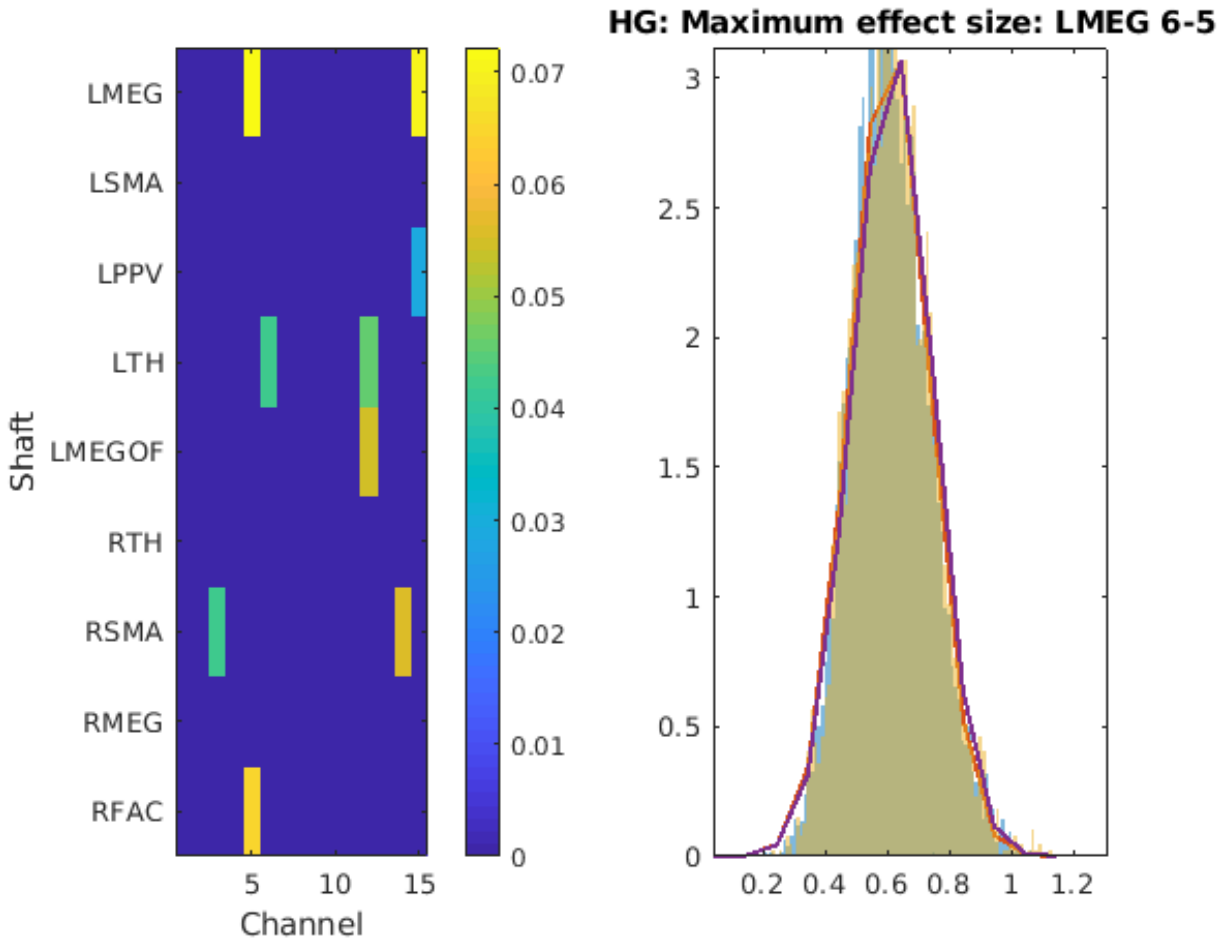

Figure 4.36: **Subject 21 Effect Size Map and Distribution Example of HG** The left panel of figure above shows biggest effect size in each channel across responsive time window. Right panel: distribution: x-axis unit micro-volts, y-axis probability density. the distribution of HG amplitude values during baseline window across all trials is plotted in blue bars, and the distribution of those during responsive window is plotted in yellow bars

Effect sizes of HG envelope in subject 21 are all small. The biggest effect size is about 0.07, which is in channel LMEG 6-5 located in anterior cingulate cortex. From the distribution on right panel, we can see stimulation downregulates the mean of LFP amplitude by 0.009 microvolts when post-stimulation LFP variance is around 0.127. Even though the effect size is comparable to accepted responses in other subjects, this channel didn't pass the Bonferroni correction for the number of tested channels in subject #21.

Table 4.1: **Summary of LFP and HG responses across all subjects** "Sig Epoch" represents for event-related LFP and HG responses that are reported through epochs-based t-test and FDR correction. "Stared" represents for yellowed stared channels in each subject that pass the Family-Wise Error Rate (FWER) controlling by Bonferroni correction for the number of channels tested. "Type I errors" represents for the number of truly null responses that have p-value below threshold .05 by chance among total number of channels been tested.

Anatomical Locations	LFP (sig epoch)	After FWER control by sub (starred)	HG (sig epoch)	After FWER control by sub (starred)	Total Channels	Type I errors
Prefrontal cortex	11	0	13	1	143	7
Cingulate cortex	5	0	5	1	45	2
Amygdala & Hippocampus	9	1	2	0	96	4
Insula operculum	3	2	3	0	44	2
Rolandic & Supramarginal gyrus	4	1	3	0	37	1
Temporal lobe	8	1	8	2	115	5
Total	40	5	34	4	487	24

4.1.3 Summary across all subjects

After adding up the number of channels containing responses across all 5 subjects, and clustering the channels by their anatomical locations into 6 brain regions, we got a responses counts summary table with comparison to the number only due to chance.

All potential significant responses of event-related LFP and HG analytical amplitude are addressed in details in the sections above. Table 4.1 mainly summarizes the counts of responses under each cortical regions, and demonstrates the evaluation of the statistical significance of the responses from another perspectives. Across five subjects, there are in total 40 channels containing significant LFP responses listed in Section 4.1.1, and in total 34 channels containing significant HG analytical amplitude response listed in Section 4.1.2, both numbers are larger than 24 the number of channels by chance with $\alpha = .05$ (Type I errors). When looking at the number of responses within each brain region, the number of significant LFP responses is larger than the number by chance in all regions, and the number of significant HG responses is larger

than the number by chance in all regions except Amygdala & Hippocampus region, suggesting that VNS effect is widely spread in cerebral cortex. But when looking at the total number of responses that passed Bonferroni correction within each subject for the number of tested channels, only event-related LFP activity in Insula and Rolandic two regions have just the same number of reported responses as the number by chance. Those responses are considered real effect induced by VNS also due to their amplitude modulations are replicated in odd and even trial averages as presented in sections above.

4.2 Time-frequency Exploration

The next set of figures are Event-Related Spectral Perturbation (ERSP) plots showing modulations on multiple signal frequency bands simultaneously during post-stimulation time. We ran ERSP analysis on channels that contain significant responses in either the LFP or HG envelope, and only chose the ones that have significant power modulation to present here.

Each subfigure consists of four parts: 1) the top-center panel shows mean event-related changes in spectral power relative to pre-stimulus baseline (dotted line represents stimulation onset) at each time during the epoch (in ms) and at each frequency (8Hz to 190Hz). 2) the left panel shows the baseline mean power spectrum in log scale. 3) the bottom center panel shows the ERSP envelope (low and high mean dB values, relative to baseline, at each time in the epoch). 4) the right panel shows a color bar with 0 dB in the center in green color representing no significant change in spectral power relative to baseline (masked out by setting). The minimum decrease in power is represented in blue, and the maximum increase in power is represented in red. The color bar range is scaled to each channel.

All power change responses shown in the ERSP plot have p-value < 0.0005 after the random shuffling significant test and BYFDR correction [5], which has more strict threshold compare to Bonferroni correction.

The following three figures show the ERSP response from subject 15, subject 17, and subject 19, in which we observed that modulation is mostly in the beta band (12Hz–30Hz) and alpha band (8Hz–15Hz). This phenomenon was observed in the following areas: insula, prefrontal cortex, cingulate gyrus, and a special case of power increase in basal temporal lobe.

Subject 15

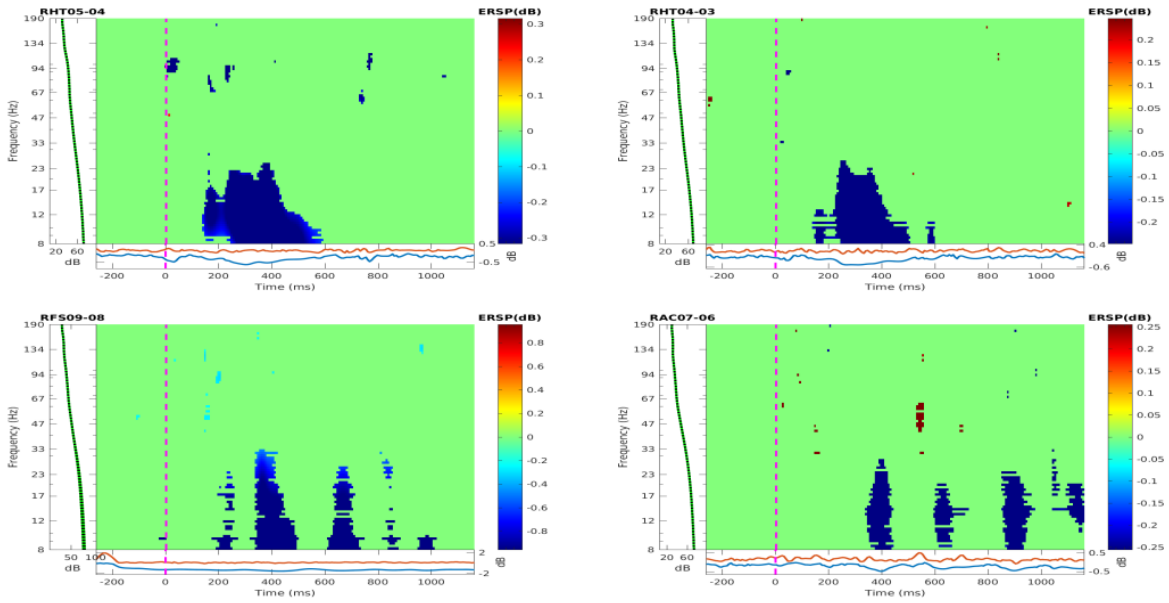

Figure 4.37: **Subject 15 ERSP** Channel notations & anatomical locations: RHT 05-04 & 04-03: insula; RFS 09-08: frontal pole/rostral middle frontal gyrus; RAC 07-06: middle frontal sulcus

The largest modulation is the reduction of beta and alpha band power in channel RHT 05-04 and 04-03 (located around insula), shown in Figure 4.37. The power reduction in both channels is about 0.3 dB, which starts from around 150ms post-stimulation onset and lasts for around 400ms. In channel RFS 09-08 (located in frontal pole/rostral middle frontal gyrus) and channel RAC 07-06 (located in middle frontal sulcus), both modulations seem coupled with the theta band (4-7Hz) compared to continuous modulation in insula channels, the power reduction of beta and alpha rhythm in RFS 9-8 frontal area is around 0.9dB which is larger than the two in insula and the one in middle frontal sulcus. In addition, modulation in channel RFS 09-08 starts

at 200ms and lasts until 1s post-stimulation onset, while modulation in channel RAC 07-06 starts about 200ms later and lasts until 1.2s post-stimulation onset.

Subject 17

The following Figure 4.38 is ERSP from Subject 17, where we observed the special case that modulation located in basal temporal lobe is power increase in beta band (12Hz–30Hz) and alpha band (8Hz–15Hz).

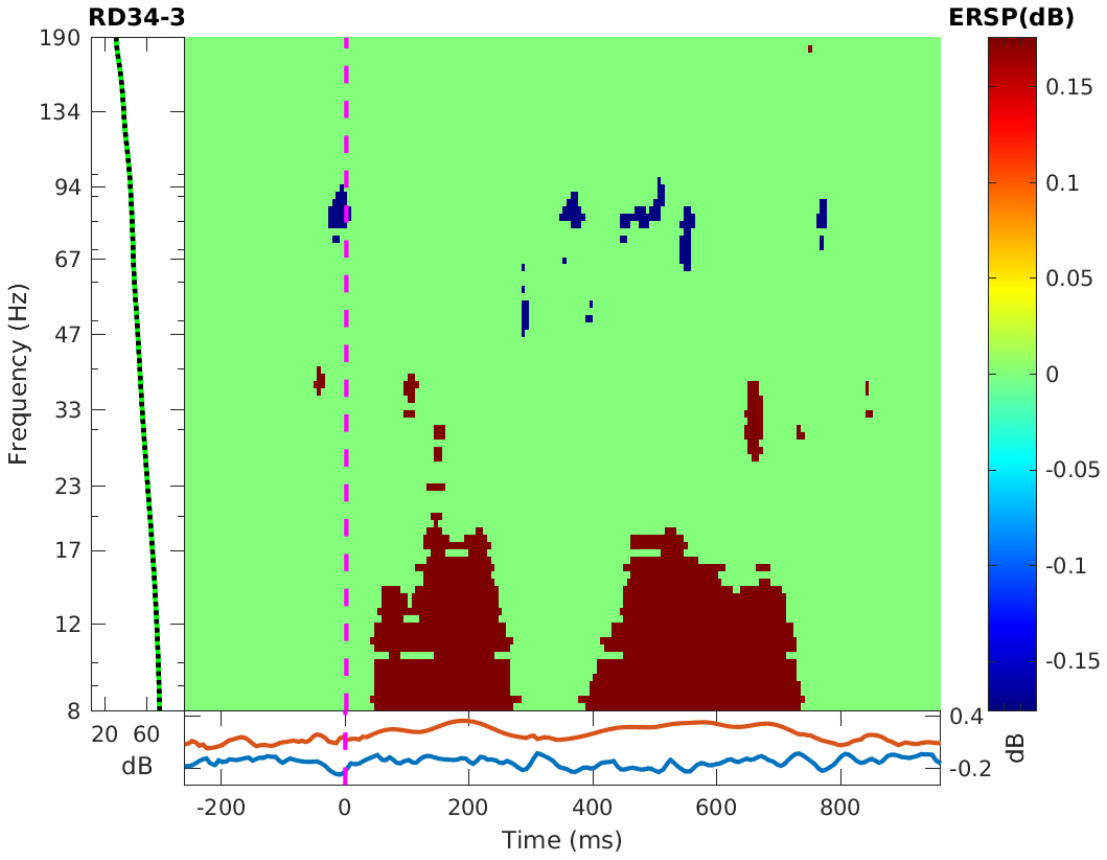

Figure 4.38: **Subject 17 ERSP** Channel notations & anatomical locations: RD3 4-3: fusiform gyrus/lingual gyrus

The modulation in channel RD3 4-3 (located between fusiform gyrus and lingual gyrus) is power increase of beta and alpha band, which starts shortly after 50ms stimulation onset and

stops at around 300ms, but starts again after 100ms and lasts till around 800 ms post-stimulation onset with size of 0.2 dB.

Subject 19

The following Figure 4.39a 4.39b is ERSP from Subject 19, where we observed that modulation is mostly in beta band (12Hz–30Hz) and alpha band (8Hz–15Hz).

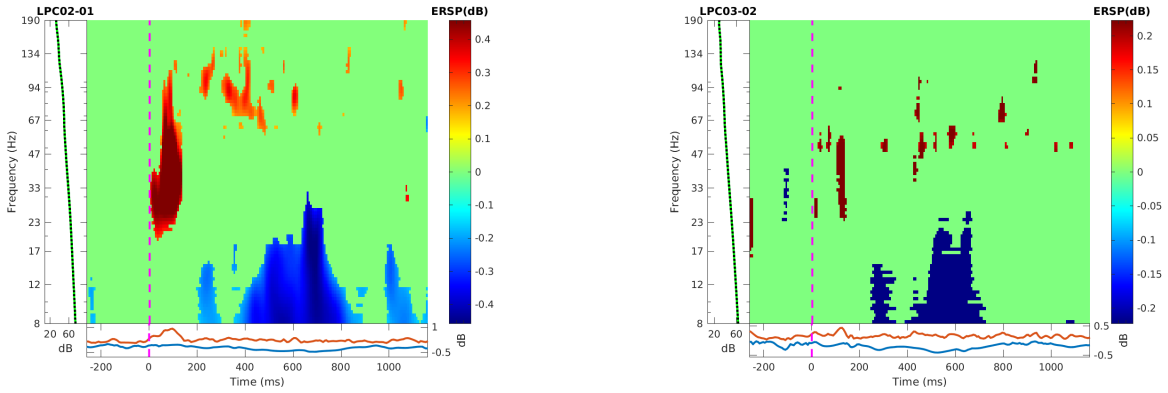

(a) Channel LPC 02-01

(b) Channel LPC 03-02

Figure 4.39: **Subject 19 ERSP** Channel notations & anatomical locations: LPC 03-02 & 02-01: posterior cingulate

Channel LPC 03-02 & 02-01 (located in posterior cingulate) have the power reduction with the size of 0.3 dB on average. The modulation started around 250ms stimulation onset, lasted for around 100ms and stopped for another 100ms, then started again and lasts till around 800ms poststimulation onset which is similar to what was observed in subject 17. In channel LPC 02-01, the red power increase around 0.4dB ranging from stimulation onset to offset is obviously from stimulation artifact, but the following small red clusters with size about 0.3dB is aligned with high gamma analytical amplitude increase observation in Section 4.1.2.

In summary, alpha and beta band power modulations were found in three out of five subjects with 71 channels tested in total. Six out of seven modulations found are power reduction by 0.3 dB on average, four channels located in insula and cingulate cortex share similar modulation

pattern, though the power reductions in insula started earlier than the ones in cingulate cortex at around 150ms post stimulation onset, and modulations in cingulate cortex contained a paused window time between 300ms to 400ms. While two channels located in prefrontal cortex have distinguished pattern which seems that the power reduction amplitude was modulated by theta band. The special power increase case was found in subject # 17 only, whose amplitude was around 0.2dB and located in basal temporal lobe. The modulation started earliest compared to other regions at around 50ms post stimulation onset, and lasted till around 700ms post stimulation onset, it also contained a paused window time between 300ms to 400ms post stimulation onset.

4.3 Sleep Grapho-elements exploration

The next set of figures are Peri-Stimulus Time Histograms (PSTH), which present the counts and the timing of sleep grapho-elements' occurrence in relation to stimulation. Figures are grouped by subject. For each figure, the x-axis is time in seconds, the height of each bar represents the total number of occurrences across all trials within a 100ms time window. Blue, yellow, and red colored bars represent Slow Oscillation (SO) upstate, SO downstate, and spindles, respectively. Solid and dotted vertical lines at 0s and 0.1s indicate stimulation onset and offset, respectively. The red horizontal lines indicate the average counts across 5 bars (equivalent to 500ms). The p1 & p2 values above each figure are p-values of the null hypothesis: there is no association between the average counts from the first or second 500ms time window post-stimulation and the average counts from the 500ms pre-stimulation, respectively.

Subject 16

The following figure includes PSTH of SO up state, SO down state, and spindles from subject 16, whose recording contains one sleep cycle. The modulations are found in the following brain regions: insula, prefrontal cortex, cingulate cortex and hippocampus formation.

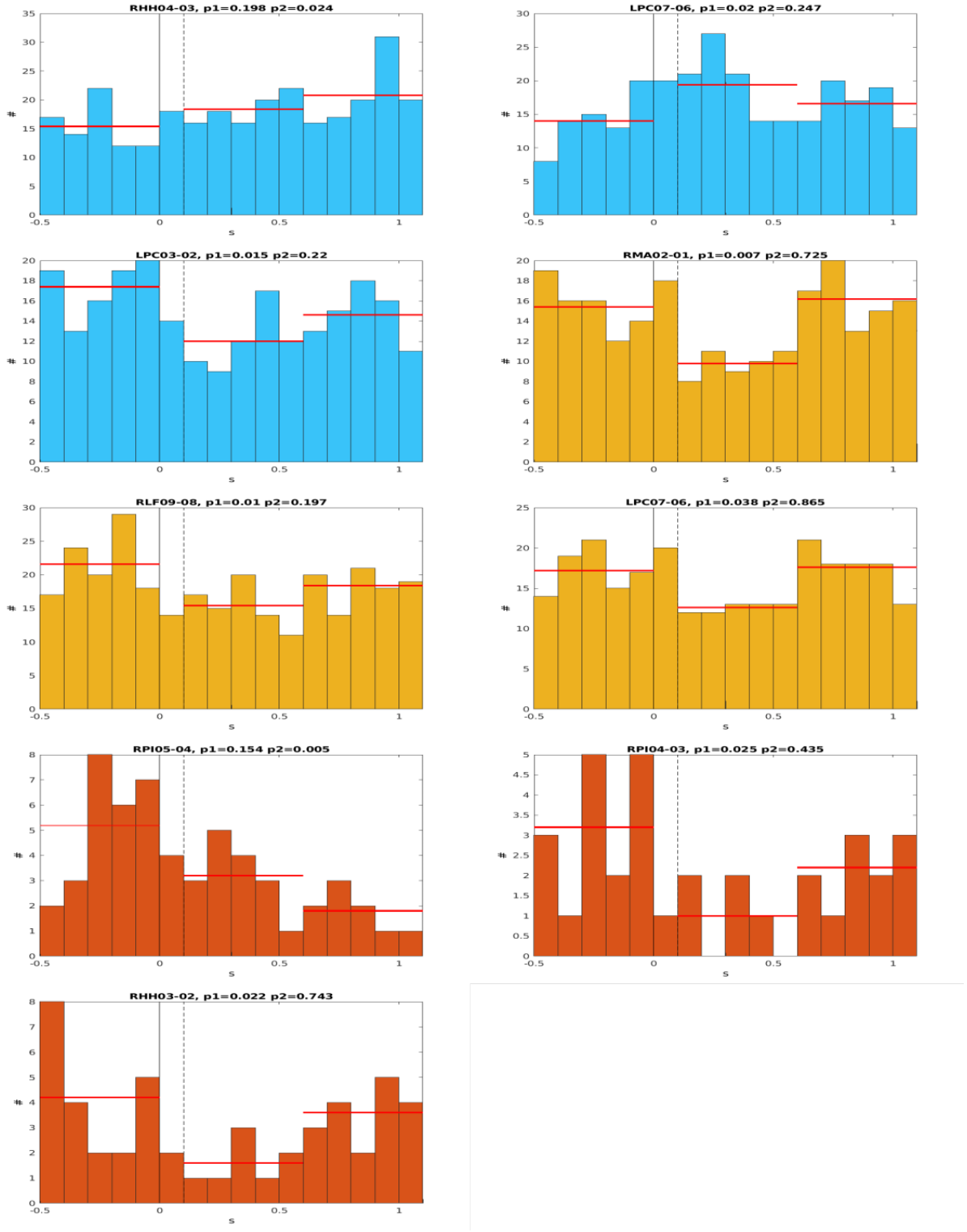

Figure 4.40: **Subject 16 PSTH** Channel notations & anatomical locations: RHH 04-03: hippocampal formation, LPC 03-02: posterior cingulate, RMA 02-01: cingulate, RLF 09-08: middle frontal gyrus, LPC 07-06: rolandic, RPI 05-04: parietal operculum, RPI 04-03: posterior insula, RHH 03-02: hippocampal formation

Table 4.2: Subject 16 Sleep Grapho-elements

Sleep Grapho-elements	**Latency post-stim (s)**	**# of sig ch (inc+dec)**	**total channel /# by chance only only**
SO up	0.1 - 0.6	2 (1+1)	51 / 2
	0.6 - 1.1	1 (1+0)	
SO down	0.1 - 0.6	3 (0+3)	27 / 1
	0.6 - 1.1	0	
Spindle	0.1 - 0.6	2 (0+2)	61 / 3
	0.6 - 1.1	1 (0+1)	

In this subject, most of the regulation occurred during the 1st 500 ms post-stimulation. The count of SO up states increases while SO down states decreases in channel LPC 07-06 (located in rolandic). The count of SO up states in channel LPC 03-02 and the count of SO down states in channel RMA 02-01 decreases, both of which are located in the cingulate. In channel RLF 09-08 (located in middle frontal gyrus), the count of SO down states decreases. As for spindles, stimulation only exhibits a downregulation effect on this subject. The count of spindles in channel RHH 03-02 (located in entorhinal/cisterna ambiens) decreases during the 1st 500 ms. The count of spindles from channel RPI 04-03 decreases first during 1st 500 ms, then decreases during the 2nd 500 ms in channel RPI 05-04, both of which are located in insula.

Subject 19

The first two figures below are PSTH of SO up state from subject 19, and the rest two figures are SO down state and spindles separately. The recording from subject 19 contains three sleep cycle. The modulations are found in the following brain regions: insula, prefrontal cortex, amygdala & hippocampus, cingulate cortex, temporal lobe and supramarginal gyrus.

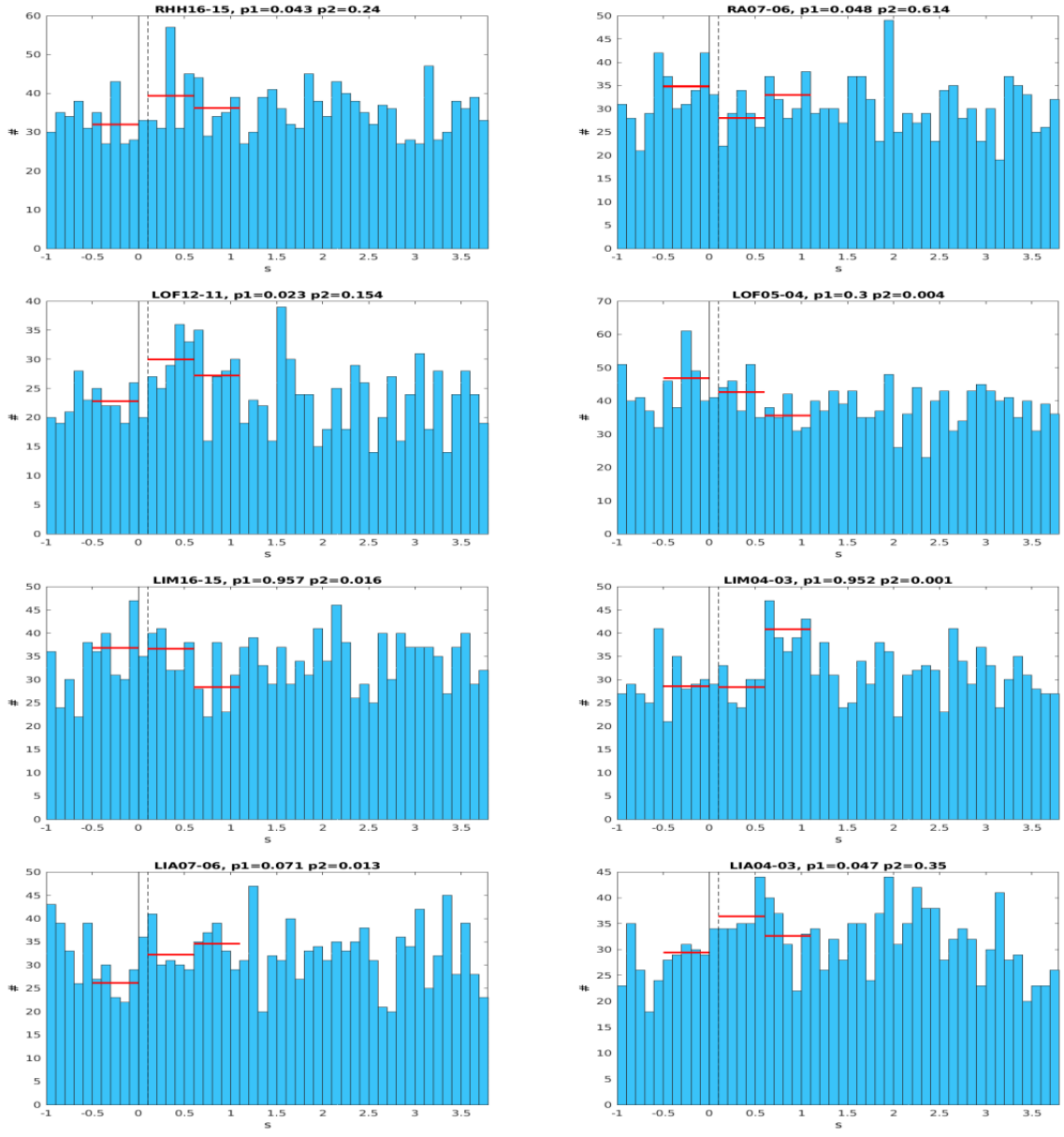

Figure 4.41: **Subject 19 PSTH-SO up state Part I** Channel notations & anatomical locations: RHH 16-15: inferior temporal sulcus, RA 07-06: amygdala, LOF 12-11 & 05-04: frontal pole, LIM 16-15: superior frontal gyrus, LIM 04-03: insula, LIA 07-06 & 04-03: insula

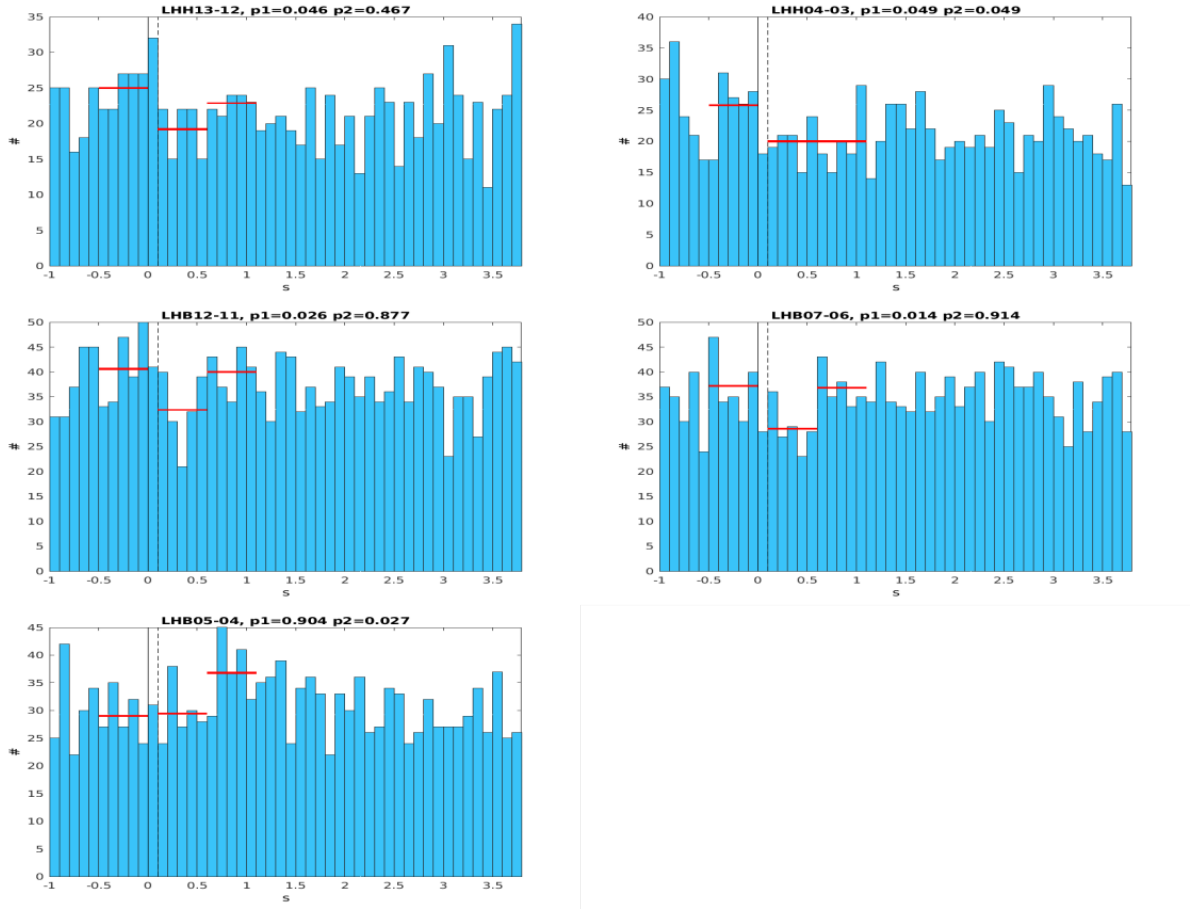

Figure 4.42: **Subject 19 PSTH-SO up state Part II**Channel notations & anatomical locations: LHH 13-12: middle temporal gyrus, LHH 04-03: hippocampus, LHB 12-11: middle temporal sulcus, LHB 07-06 & 05-04: hippocampus

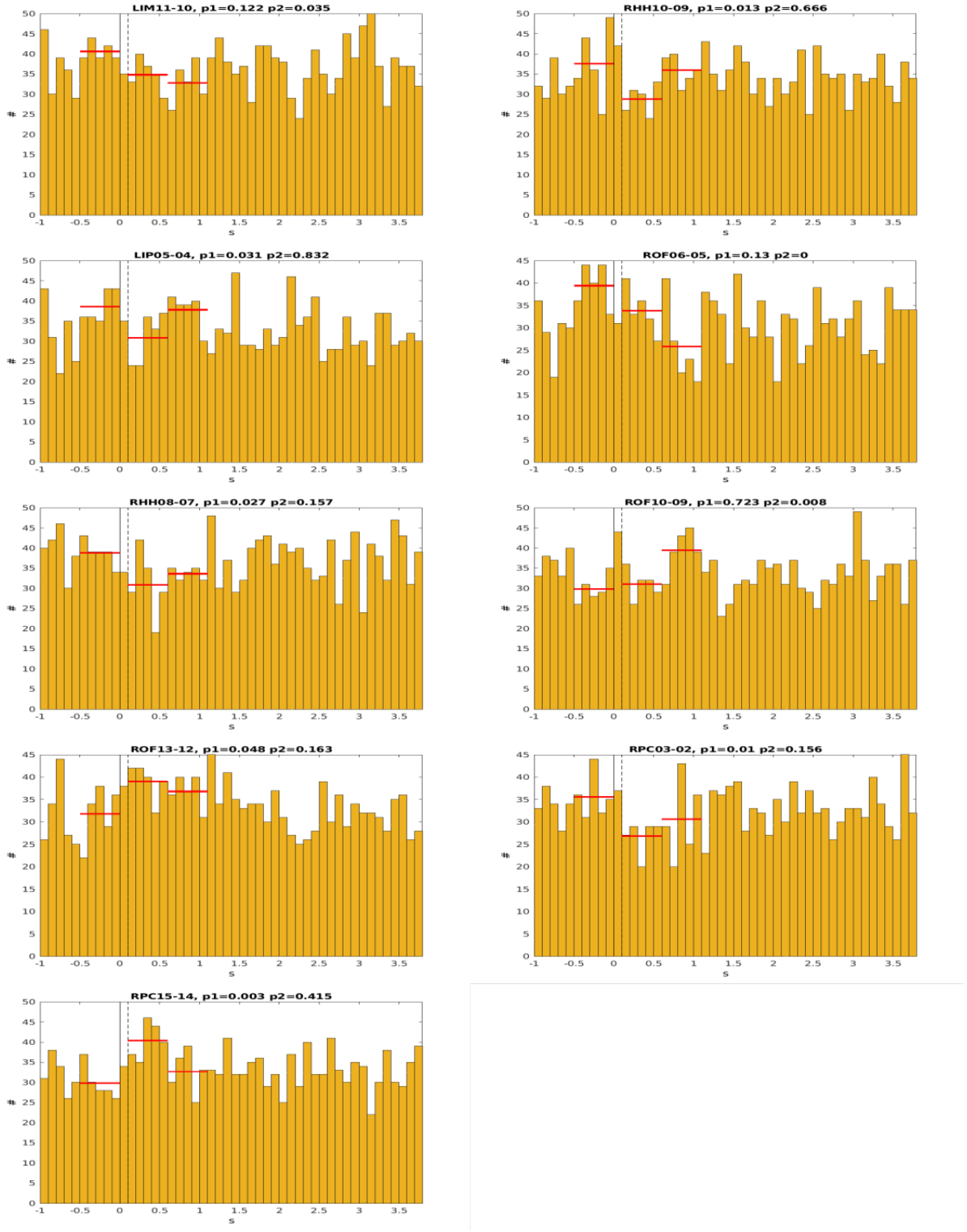

Figure 4.43: **Subject 19 PSTH-SO down state** Channel notations & anatomical locations: LIM 11-10: superior frontal sulcus, RHH 10-9: perirhinal, LIP 05-04: insula, ROF 06-05: inferior frontal gyrus, RHH 08-07: hippocampus, ROF 10-09 & 13-12: inferior frontal gyrus, RPC 03-02: cingulate gyrus, RPC 15-14: supramarginal gyrus

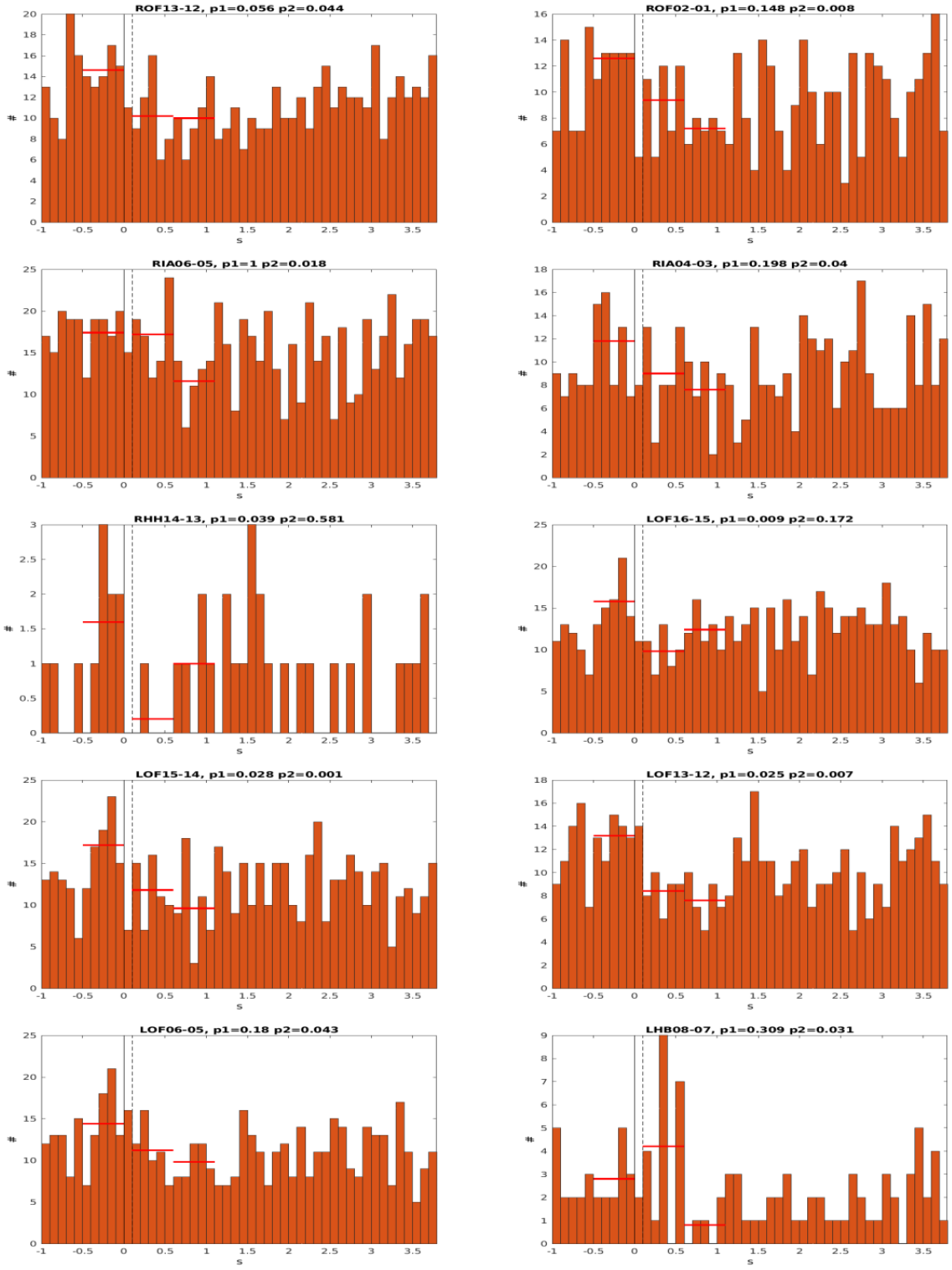

Figure 4.44: **Subject 19 PSTH-Spindle** Channel notations & anatomical locations: ROF 13-12: inferior frontal gyrus, ROF 02-01: orbital cortex, RIA 06-05 & 04-03: insula, RHH 14-13: inferior temporal sulcus, LOF 16-15 & 15-14 & 13-12 & 06-05:frontal pole, LHB 08-07: hippocampus

Table 4.3: Subject 19 Sleep Grapho-elements

Sleep Grapho-elements	Latency post-stim (s)	# of sig ch (inc+dec)	total channel /# by chance only
SO up	0.1 - 0.6	7 (3+4)	116 / 5
	0.6 - 1.1	6 (3+3)	
SO down	0.1 - 0.6	6 (2+4)	95 / 4
	0.6 - 1.1	3 (1+2)	
Spindle	0.1 - 0.6	4 (0+4)	132 / 6
	0.6 - 1.1	8 (0+8)	

Among 132 channels in total for sleep grapho-elements detection, there isn't a channel that contains both SO up and down state regulation. In addition, around 85% of regulation on SO up state is in left hemisphere, while around 78% of regulation on SO down state is in right hemisphere, under the experiment condition that stimulation was applied to left ear. Channels located in insula, hippocampus area, middle temporal sulcus, first response to stimulation and shows SO up state regulation during the 1st 500 ms post-stimulation. For SO down state regulation, channels that response to stimulation in the 1st 500 ms are mostly located in insula, hippocampus, supramarginal gyrus, and cingulate. Stimulation only shows downregulation effect on spindles of subject 19. In channel LOF 16-15 & 15-14 & 13-12 (located in frontal pole) and channel RHH 14-13 (located in inferior temporal sulcus), the count of spindles decrease during the 1st 500 ms post-stimulation. For rest channels located in prefrontal cortex, insula and hippocampus, downregulation occurs during the 2nd 500 ms.

Subject 21

The first figure below is PSTH of SO up and down state from subject 21, and the other figure is PSTH of spindles. The recording from subject 21 contains five sleep cycle. The

modulations are found in the following brain regions: prefrontal cortex and rolandic area.

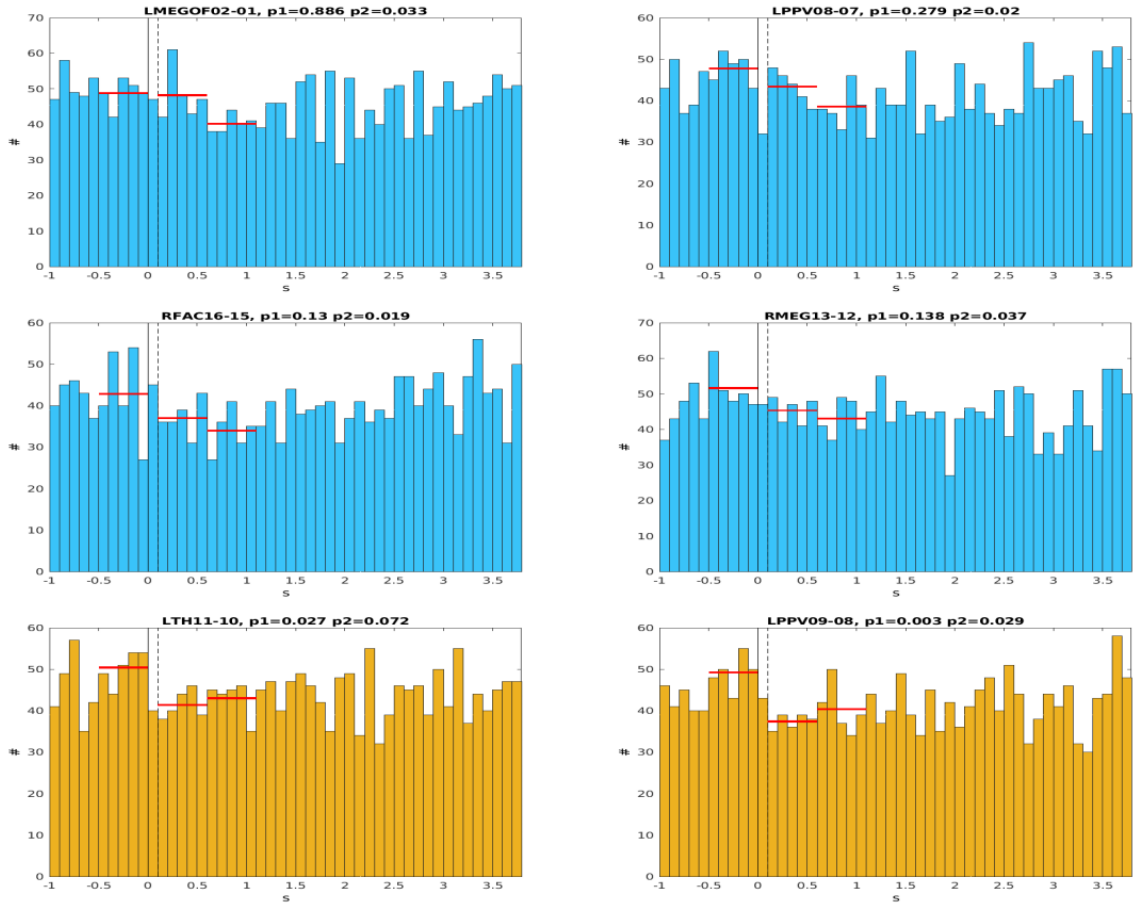

Figure 4.45: **Subject 21 PSTH-SO** Channel notations & anatomical locations: LMEGOF 02-01: gray matter of the frontal pole, LPPV 09-08: precentral gyrus, LPPV 08-07: frontal operculum, RFAC16-15 & 13-12: middle frontal gyrus, LTH 11-10: fundus of inferior frontal gyrus

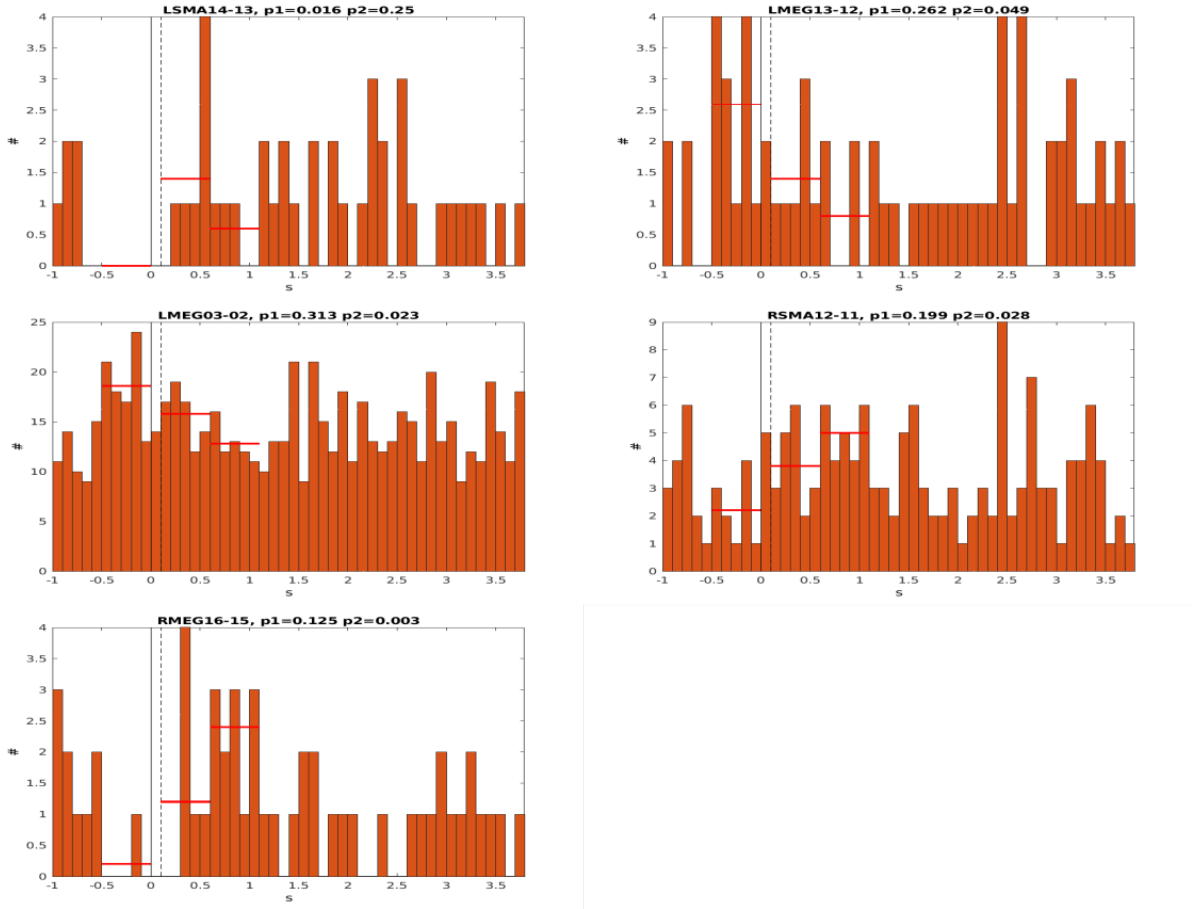

Figure 4.46: **Subject 19 PSTH-Spindle** Channel notations & anatomical locations: LSMA 14-13: middle frontal gyrus, LMEG 13-12: inferior frontal gyrus, LMEG 03-02: anterior cingulate, RSMA 12-11: precentral grey matter, RMEG 16-15: precentral sulcus

Table 4.4: Subject 21 Sleep Grapho-elements

Sleep Grapho-elements	**Latency post-stim (s)**	**# of sig ch (inc+dec)**	**total channel /# by chance only**
SO up	0.1 - 0.6	0	56 / 2
	0.6 - 1.1	4 (0+4)	
SO down	0.1 - 0.6	2 (0+2)	57 / 2
	0.6 - 1.1	1 (0+1)	
Spindle	0.1 - 0.6	1 (1+0)	70 / 3
	0.6 - 1.1	4 (2+2)	

For channels containing SO up and down state regulation, all significant responses in subject 21 are downregulation. All the channels that contains SO up state regulation are located in prefrontal cortex area, in which the responses occur in the 2nd 500 ms post-stimulation. In Channel LPPV 09-08 and channel LTH 11-10 (both located in precentral gyrus), the count of SO down state decrease during the 1st 500 ms post-stimulation. The first spindles regulation is upregulation which occurs in channel LSMA 14-13 (located in middle frontal gyrus) during the 1st 500 ms post-stimulation. Later during the 2nd 500 ms post-stimulation, spindles downregulation happens in two left hemisphere channels LMEG 13-12 (located in inferior frontal gyrus) & 03-02 (located in anterior cingulate) while upregulation happens in two right hemisphere channels RSMA 12-11(located in precentral gyrus) and channel RMEG 16-15 (located in middle frontal sulcus). Table 4.5, a combination of tables 4.2, 4.3 and 4.4, shows significant test results of VNS modulation effect on three types of sleep grapho-elements across subjects.

Table 4.5: Summary of Sleep Grapho-elements

Sleep Grapho-elements	**Latency post-stim (s)**	**# of sig ch (inc+dec)**	**total channel /# by chance only**
SO up	0.1 - 0.6	9	223 / 11
	0.6 - 1.1	11	
SO down	0.1 - 0.6	11	179 / 8
	0.6 - 1.1	4	
Spindle	0.1 - 0.6	7	263 / 13
	0.6 - 1.1	13	

SO down state is the only type of sleep grapho-element that shows significant responses across subjects. During 0.1s - 0.6s post-stimulation, the number of channels containing SO down state modulation is bigger than the number of possible false positive chance. Among 179 channels that contain SO down state, 9 channels show downregulation effect and 2 channels from subject 19 show upregulation. The two channels containing upregulation are ROF 13-12 (located in inferior frontal gyrus), and RPC 15-14 (located in supramarginal gyrus). The anatomical locations of the remaining channels are: 2 in cingulate cortex, 2 in rolandic area, 2 in prefrontal cortex, 1 in insula, 2 in hippocampus/perirhinal area.

Chapter 5

Discussion

The ascending modulation on cortical activity level from sub-perception stimulation of electrodes on external ear was studied in epileptic human subjects. In our investigation, non-invasive auricular VNS output current was set below the threshold of perception, 20kHz biphasic stimulation was applied for 100ms following by a random Inter-Stimulus Interval (ISI) ranging from 1050ms to 4300ms, and the entire trial was repeated for around 2h on awake subjects or throughout sleep cycles of asleep subjects. For measurement, we used depth electrodes and bi-polarized the recording of adjacent contacts to get activity of a local neuron population.

Our results provide limited support for the hypothesis that sub-perceptual external ear stimulation induces significant acute intracranial EEG changes in human studies. Statistical analysis (t-test versus baseline, and FDR correction[4]) was run separately on each of 487 channels, whose anatomical locations were distributed in six main regions: prefrontal cortex, cingulate cortex, amygdala & hippocampus, insula operculum, rolandic cortex & supra-marginal gyrus, and temporal lobe.4.1 We then compared the number of channels with a significant response with an alpha of .05 to that expected given the number of channels. Both the event-related Local Field Potential (LFP) and High Gamma activity (HG), and estimate of population firing, were examined. In four of five subjects, a minimum of 3k trials were obtained for each analyzed

channel, after artifact rejection. Ten epochs were examined in each waveform, from 50ms to 1050ms after stimulus offset.

In all grouped six regions, the number of channels with significant LFP responses was greater than expected by chance, suggesting that there may be widespread modulation. However, several considerations argue against this interpretation. First, with two exceptions, the size of the putative responses were extremely small, about 2 microvolts on average, whereas spontaneous waves and cognitive or sensory activity in the cortex typically ranges from 100 to 1000 microvolts. Second, there was no consistency in the waveform or latency of the responses, as would be expected if they represented a reliable and repeatable phenomenon. Certainly, well-validated responses in different locations can vary in their waveforms and latencies, but they always begin relatively soon after the stimulus and have components that repeat across structures, a pattern that was not observed in our study. Third, the effect size (Cohen's *d*) was minuscule; with three exceptions they were about 0.01 for significant channels (i.e., the difference between response and baseline was only about 1% of the standard deviation). Significance was only obtained because there were thousands of trials; typical event-related potential averages have 60 trials, and high gamma responses can sometimes be seen on single trials. Fourth, and most important, we constructed for each channel, separate averages of the odd and even trials, which should have been identical except for noise, and therefore, actual responses should have been visible in both. However, that was only rarely the case.

Overall, there are five channels passed Bonferroni correction and contained responses replicated in odd and even trial averages. (two channels share the same electrode located in insula due to bi-polarization) Two of those channels were the two exception channels mentioned above, where a recording was obtained that was greater than 3 microvolts in amplitude, with typical ERP waveforms, and effect size was larger than 0.10. Although these two responses were weak and small, they are probably reliable responses. The best response was about 5 microvolts in peak amplitude, with a typical waveform beginning about 50ms after stimulus onset, peaking

at 180ms, with an effect size of 0.24. This channel was in the insula, an area that is specialized for the autonomic system. The other channel was about 6 microvolts in peak amplitude, with a typical waveform beginning after stimulus offset, peaking at 210ms, with an effect size of 0.12. This channel was in the post-central gyrus, raising the possibility that it represents a weak somatosensory response, which is aligned with a study revealed that the amplitude of vagal somatosensory evoked potentials (vSEPs) increased with increasing cervical non-invasive VNS intensity.[43] The other two responses with small sizes are from electrodes located in temporal stem and amygdala. The response in amygdala was only about 1.2 microvolts in peak amplitude, without a typical ERP waveform beginning after stimulus offset , peaking at 210ms, ending abruptly at 310ms, with an effect size of 0.065. None of these channels generated a significant high gamma response. This would be consistent with the observation that the responsive insula electrode was probably in the white matter immediately adjacent to the gray matter of the insula. The same as the responsive post-central gyrus electrode, which was probably in the white matter next to the gray matter of the sensory receptive area for the sense of touch. As for the response in amygdala, it's possible that the LFP amplitude change was not big enough to trigger action potential in the neurons.

High gamma responses overall were also rare. A total of four channels produced responses that approximately replicated in split half averages and passed Bonferroni correction, with fluctuations which were larger than those in the baseline average. Three of these channels were in subject #15 and located in lateral temporal or frontal cortex. In all cases the response was a small (0.1 to 0.17uV) decrease beginning shortly before 200 ms and lasting about 50-400ms, effect size was 0.05-0.10. In all cases a stimulus artifact was present indicating that a technical issue could be responsible for the response. The other response was in subject #19 where a 0.07uV increase 350-600ms after stimulus onset, but no stimulus artifact, was recorded in an electrode in or near the corpus callosum adjacent to the posterior cingulate gyrus (effect size 0.05). The white matter does not generate high gamma responses. Overall, these responses are very small

and problematic. The other possible response was in subject #15, although it didn't pass strict Bonferroni correction its decrease is replicated in split half averages, it shows HG decrease of 0.03 microvolts beginning shortly after stim onset and lasting for 500ms. Note that high gamma activation is more often around 0.7 to 8 microvolts or 3 standard deviation in effective behavioral stimulation that produces a subjective precept and is often visible in single trials [10] [19][44]

In summary, a close examination of the data from 487 channels fails to reveal locations with evoked local field potential responses which pass minimal accepted criteria with the exception of one insula channel and one post central gyrus channel. These channels failed to record significant high gamma modulation, and the five which did were problematic but cannot be ruled out as genuine responses. We should note that other electrodes in the insula and post central gyrus failed to record responses, but this is reasonable given that autonomic responses have previously been found to be localized to only a portion of the insula. However, the responsive electrode was in posterior insula whereas it is the ventral anterior insula that is thought to be specialized for autonomic functions[11].

In order to identify possible LFP responses that were not phase-locked with the stimulus train, Event-Related Spectral Perturbation analysis was performed on the channels which had an LFP or HG reponse at the p¡.05 level, non-Bonferroni corrected for multiple channels (a total of 71 channels across all patients). We observed a significant change that passed Bonferroni correction in 7 channels. The change was mainly in the alpha and beta bands, and small in power (on average -0.3dB). In six channels, beta decreased and in one it increased. Four of those channels were found in subject #15, two out of these four channels are located in insula where we observed significant event revoked LFP responses, and the other two out of these four channels are located in prefrontal cortex. The other two channels containing beta band power reduction were found in subject #19, near the cingulate cortex area where we observed significant HG envelop modulation. Those power reduction effects can start from 200ms post stim onset in insula or start from 400ms post stim onset in cingulate areas and last continuously for roughly 400ms, while

the power reduction effect is more phasic in prefrontal cortex area. In addition, increased beta was observed in the basal temporal lobe of subject #17. we noticed one study from gammaCore device has beta-band power extracted from cap EEG Cz location, and observed power increase under non-invasive neck VNS [33]. The trial consists of 120sec stimulation (5kHz sine-wave stimulus) following a 1-2 min rest and the second round of stimulation. EEG was collected at four time points: baseline, 15min, 120min, 240min post stimulation on each day. Comparing to our observation in beta decrease also exist in non-motor cortex, the beta power increase at Cz location in gammaCore study may just movement-related modulation within sensorimotor cortex of the subject [57].

Finally, we tested whether upstates, downstates or spindles changed in frequency of occurrence after stimulus trains in 3 patients. The number of channels with sleep slow oscillation down-states reduction is slightly larger than the number expected by chance among all three sleep recordings. For three channels located in cingulate, MFG, and rolandic in subject#16, the average count of SO down-state during 500ms post stimulation always decreases about 30% comparing to baseline through 1k trials in N2 sleep stage. For four channels located in cingulate, insula, hippocampus, and supramarginal gyrus in subject#19, the average count of SO down-state during 500ms post stimulation always decreases about 24% comparing to baseline through 3.5k trials in N2 sleep stage. For two channels located in fundus of inferior frontal gyrus and precentral gyrus in subject#21, the average count of SO down-state during 500ms post stimulation always decreases about 20% comparing to baseline through 2.5k trials in N2 sleep stage. However, with Bonferroni correction there is only one channel located in inferior frontal gyrus still shows SO down-state reduction during 500-1000ms post stim onset, which seems result from elevated baseline. Therefore, our study failed to provide sufficient evidence of VNS modulation on sleep grapho-elements.

In conclusion, we have shown that VNS is able to induce statistically rare but significant small modifications on intracranial EEG: 1) event-related average of LFP (0.1-40Hz) activity

changes in insula and post-central gyrus; 2) High gamma (70-190Hz) analytic amplitude decrease in lateral temporal or frontal cortex, as well as increase in cingulate gyrus; 3) α & β (8-30Hz) band power reduction in posterior insula, prefrontal cortex and cingulate gyrus, as well as power increase in basal temporal lobe. Although those modifications are rare statistically and not consistent across our five subjects, they are still reliable responses individually and more concentrated in the VNS afferent network out of 487 channels distributed around the cerebrum. Therefore, our study supports the hypothesis of sub-perception VNS on external ear modulates the level of cortical activity in human, which provides a promising direction to modulate various cognitive and affective functions.

It has been well studied that within the brain, ascending pathways of noradrenergic fibers from the Locus Coeruleus (LC) and cholinergic fibers from the Nucleus Basalis (NB) widely project to the cortex and modulate the level of cortical activity [50] [1]. VNS's facilitation effect on attention, emotion recognition [51], learning and memory consolidation [37] in many studies, may be via activation on the cholinergic and noradrenergic systems. ERP component P3b amplitude was found increase during tVNS via LC-Norepinephrine system activation[54], in which LC receives direct inputs from the Nucleus Tractus Solitarius (NTS) where vagal afferents primarily project to. Besides low frequency LFP, our observation in HG frequency band directly reflected modification on local neuronal firing, whose location may be explained by that the cholinergic innervation is highest in temporal and frontal lobes in human cortex [28], especially Ch4 complex of NB provides the major cholinergic innervation to medial cortical areas, including the cingulate gyrus. With emerging studies showing that the early involvement of Ch4 has a magnifying effect on Alzheimer's pathology [40], VNS provides the potential of regulating corresponding cholinergic circuitry for Alzheimer's disease treatment. Beta-band reduction is generally seen in motor cortex stimulation studies, which supports hypothesis of a structurally connected functional network between frontal cortex and Subthalamic Nucleus (STN) that operates in the beta-band. [53] Currently STN Deep Brain Stimulation is commonly used to

treat Parkinson Disease in which there is pathologically high resting beta activity, its behavioral benefit may be improving the fidelity of information transfer in cortico-basal-ganglia circuits. Therefore, reducing beta-band power through VNS also has the potential benefit for Parkinson Disease. In addition, studies suggested low amplitude beta response were often associated with active, busy or anxious thinking and active concentration [2], which aligns with the clinical depression treatment with VNS[46].

Finally, some limitations of the our study should be mentioned. First, due to complicated situation for hospitalized epilepsy patients and we needed to collect enough number of trials in a limited time, we were not able to study long-term effect that only appear after several VNS treatment sessions. We looked at acute effect on EEG rhythms in post-stimulation period versus pre-stimulation at 2s trial base, comparing to most studies on clinical chronic VNS treatment which showed increased synchronization and power of gamma frequency band (F. Marrosu et al.,2005; Betty Koo,2001). Second, five subjects is a small sample size. Due to the exploratory property of this investigation, we had different stimulus parameters (including duration, ISI, amplitude) applied on each subject with either awake or asleep status which could affect the consistency of response. Another consideration is the heterogeneous composition of the vagus nerve across human subjects, which increases the difficulty to verify each type of response especially when VNS non-responders could potentially mix in the group. Ibrahim GM et al. found that thalamic connections to the anterior cingulate and insular cortices are stronger in VNS responders. Third, the VNS output current we applied on external ear is lower than the threshold of perception comparing to most VNS treatments deliver current above the perception level. Traditional analysis of trial-by-trial signal averaging may not be suitable for extracting weak response signal from the low Signal-Noise Ratio EEG recordings. Therefore, a larger scale of this study could help to provide further information on the mechanisms of VNS-induced cerebral cortical activity modification and the optimum stimulus parameters for human subjects.

Bibliography

[1] E. Ballinger, M. Ananth, D. Talmage, and L. Role. Basal forebrain cholinergic circuits and signaling in cognition and cognitive decline. Neuron, 91(6):1199 – 1218, 2016. ISSN 0896-6273. doi: https://doi.org/10.1016/j.neuron.2016.09.006. URL http://www.sciencedirect.com/science/article/pii/S0896627316305657.

[2] J. Baumeister, T. Barthel, K. Geiss, and M. Weiss. Influence of phosphatidylserine on cognitive performance and cortical activity after induced stress. Nutritional Neuroscience, 11(3):103–110, 2008. doi: 10.1179/147683008X301478. URL https://doi.org/10.1179/147683008X301478. PMID: 18616866.

[3] F. Beissner, K. Meissner, K.-J. Bär, and V. Napadow. The autonomic brain: An activation likelihood estimation meta-analysis for central processing of autonomic function. Journal of Neuroscience, 33(25):10503–10511, 2013. ISSN 0270-6474. doi: 10.1523/JNEUROSCI.1103-13.2013. URL https://www.jneurosci.org/content/33/25/10503.

[4] Y. Benjamini and Y. Hochberg. Controlling the false discovery rate: A practical and powerful approach to multiple testing. Journal of the Royal Statistical Society: Series B (Methodological), 57(1):289–300, 1995. doi: 10.1111/j.2517-6161.1995.tb02031.x. URL https://rss.onlinelibrary.wiley.com/doi/abs/10.1111/j.2517-6161.1995.tb02031.x.

[5] Y. Benjamini and D. Yekutieli. The control of the false discovery rate in multiple testing under dependency. Ann. Statist., 29(4):1165–1188, 08 . doi: 10.1214/aos/1013699998. URL https://doi.org/10.1214/aos/1013699998.

[6] B. Bonaz, V. Sinniger, and S. Pellissier. Vagus nerve stimulation: a new promising therapeutic tool in inflammatory bowel disease. Journal of internal medicine, 282(1):46–63, 2017.

[7] L. Borovikova, S. Ivanova, M. Zhang, H. Yang, I. Botchkina, L. Watkins, H. Wang, N. Abumrad, J. Eaton, and K. Tracey. Borovikova lv, ivanova s, zhang m, yang h, botchkina gi, watkins lr, wang h, abumrad n, eaton jw, tracey kjvagus nerve stimulation attenuates the systemic inflammatory response to endotoxin. nature 405:458-462. Nature, 405:458–62, 06 2000. doi: 10.1038/35013070.

[8] M. Brázdil, P. Chadim, P. Daniel, R. Kuba, I. Rektor, Z. Novák, and J. Chrastina. Effect of vagal nerve stimulation on auditory and visual event-related potentials. European Journal of Neurology, 8(5):457–461, 2001.

[9] F. Bremer and V. Bonnet. * convergence et interaction des influx afferents dans lecorce cerebelleuse, principe fonctionnel du cervelet, 1951.

[10] R. T. Canolty, E. Edwards, S. S. Dalal, M. Soltani, S. S. Nagarajan, H. E. Kirsch, M. S. Berger, N. M. Barbaro, and R. T. Knight. High gamma power is phase-locked to theta oscillations in human neocortex. Science, 313(5793):1626–1628, 2006. ISSN 0036-8075. doi: 10.1126/science.1128115. URL https://science.sciencemag.org/content/313/5793/1626.

[11] L. J. Chang, T. Yarkoni, M. W. Khaw, and A. G. Sanfey. Decoding the Role of the Insula in Human Cognition: Functional Parcellation and Large-Scale Reverse Inference. Cerebral Cortex, 23(3):739–749, 03 2012. ISSN 1047-3211. doi: 10.1093/cercor/bhs065. URL https://doi.org/10.1093/cercor/bhs065.

[12] M. H. Chase, Y. Nakamura, C. D. Clemente, and M. B. Sterman. Afferent vagal stimulation: neurographic correlates of induced eeg synchronization and desynchronization. Brain research, 5(2):236–249, 1967.

[13] J. E. Childs, A. C. Alvarez-Dieppa, C. K. McIntyre, and S. Kroener. Vagus nerve stimulation as a tool to induce plasticity in pathways relevant for extinction learning. JoVE (Journal of Visualized Experiments), (102):e53032, 2015.

[14] K. B. Clark, D. K. Naritoku, D. C. Smith, R. A. Browning, and R. A. Jensen. Enhanced recognition memory following vagus nerve stimulation in human subjects. Nature neuroscience, 2(1):94–98, 1999.

[15] L. S. Colzato, R. Sellaro, and C. Beste. Darwin revisited: The vagus nerve is a causal element in controlling recognition of other's emotions. Cortex, 92:95 – 102, 2017. ISSN 0010-9452. doi: https://doi.org/10.1016/j.cortex.2017.03.017. URL http://www.sciencedirect.com/science/article/pii/S0010945217300977.

[16] V. Constantinescu, D. Matei, D. Cuciureanu, C. Corciova, B. Ignat, and C. D. Popescu. Cortical modulation of cardiac autonomic activity in ischemic stroke patients. Acta Neurologica Belgica, 116(4):473–480, 2016.

[17] A. Diedrich, L. Okamoto, B. Black, M. D. Hale, and I. Biaggioni. Abstract p387: Subperception transdermal vagal stimulation in postural tachycardia syndrome. Hypertension, 72(Suppl_1):AP387–AP387, 2018.

[18] H. Duvernoy. The human brain: surface, blood supply, and three-dimensional anatomy. Wien NY: Springer Verlag, 1999.

[19] W. J. Freeman. Origin, structure, and role of background eeg activity. part 1. analytic amplitude. Clinical Neurophysiology, 115(9):2077 – 2088, 2004. ISSN 1388-2457. doi: https://doi.org/10.1016/j.clinph.2004.02.029. URL http://www.sciencedirect.com/science/article/pii/S1388245704001695.

[20] R. Galli, E. Bonanni, C. Pizzanelli, M. Maestri, L. Lutzemberger, F. S. Giorgi, A. Iudice, and L. Murri. Daytime vigilance and quality of life in epileptic patients treated with vagus nerve stimulation. Epilepsy & Behavior, 4(2):185–191, 2003.

[21] A. Geerts. Detection of interictal epileptiform discharge in eeg, September 2012. URL http://essay.utwente.nl/62290/.

[22] L. D. Hachem, S. M. Wong, and G. M. Ibrahim. The vagus afferent network: emerging role in translational connectomics. Neurosurgical focus, 45(3):E2, 2018.

[23] D. J. Hagler, I. Ulbert, L. Wittner, L. Erőss, J. R. Madsen, O. Devinsky, W. Doyle, D. Fabó, S. S. Cash, and E. Halgren. Heterogeneous origins of human sleep spindles in different cortical layers. Journal of Neuroscience, 38(12):3013–3025, 2018. ISSN 0270-6474. doi: 10.1523/JNEUROSCI.2241-17.2018. URL https://www.jneurosci.org/content/38/12/3013.

[24] E. J. Hammond, B. M. Uthman, S. A. Reid, and B. Wilder. Electrophysiologic studies of cervical vagus nerve stimulation in humans: Ii. evoked potentials. Epilepsia, 33(6):1021–1028, 1992.

[25] S. Iversen, L. Iversen, and C. B. Saper. The autonomic nervous system and the hypothalamus. Principles of neural science, 4:960–680, 2000.

[26] W. Janig. Autonomic Nervous System. Springer Berlin Heidelberg, Berlin, Heidelberg, 1989. ISBN 978-3-642-73831-9. doi: 10.1007/978-3-642-73831-9_16. URL https://doi.org/10.1007/978-3-642-73831-9_16.

[27] H. Jaseja. Eeg-desynchronization as the major mechanism of anti-epileptic action of vagal nerve stimulation in patients with intractable seizures: clinical neurophysiological evidence. Medical hypotheses, 74(5):855–856, 2010.

[28] F. Javoy-Agid, B. Scatton, M. Ruberg, R. L'heureux, P. Cervera, R. Raisman, J.-M. Maloteaux, H. Beck, and Y. Agid. Distribution of monoaminergic, cholinergic, and gabaergic markers in the human cerebral cortex. Neuroscience, 29(2):251 – 259, 1989. ISSN 0306-4522. doi: https://doi.org/10.1016/0306-4522(89)90055-9. URL http://www.sciencedirect.com/science/article/pii/0306452289900559.

[29] K. Kim, J. Ladenbauer, M. Babo-Rebelo, A. Buot, K. Lehongre, C. Adam, D. Hasboun, V. Lambrecq, V. Navarro, S. Ostojic, and C. Tallon-Baudry. Resting-state neural firing rate is linked to cardiac-cycle duration in the human cingulate and parahippocampal cortices. Journal of Neuroscience, 39(19):3676–3686, 2019. ISSN 0270-6474. doi:

10.1523/JNEUROSCI.2291-18.2019. URL https://www.jneurosci.org/content/39/19/3676.

[30] M. A. Kramer, A. B. Tort, and N. J. Kopell. Sharp edge artifacts and spurious coupling in eeg frequency comodulation measures. Journal of Neuroscience Methods, 170(2):352 – 357, 2008. ISSN 0165-0270. doi: https://doi.org/10.1016/j.jneumeth.2008.01.020. URL http://www.sciencedirect.com/science/article/pii/S0165027008000538.

[31] Y. Kubota, W. Sato, M. Toichi, T. Murai, T. Okada, A. Hayashi, and A. Sengoku. Frontal midline theta rhythm is correlated with cardiac autonomic activities during the performance of an attention demanding meditation procedure. Cognitive brain research, 11(2):281–287, 2001.

[32] R. Köhling and K. Staley. Network mechanisms for fast ripple activity in epileptic tissue. Epilepsy Research, 97(3):318 – 323, 2011. ISSN 0920-1211. doi: https://doi.org/10.1016/j.eplepsyres.2011.03.006. URL http://www.sciencedirect.com/science/article/pii/S092012111100074X. Special Issue on Epilepsy Research UK Workshop 2010 on "Preictal Phenomena".

[33] J. D. Lewine, K. Paulson, N. Bangera, and B. J. Simon. Exploration of the impact of brief noninvasive vagal nerve stimulation on eeg and event-related potentials. Neuromodulation: Technology at the Neural Interface, 22(5):564–572, 2019. doi: 10.1111/ner.12864. URL https://onlinelibrary.wiley.com/doi/abs/10.1111/ner.12864.

[34] B. A. Malow, J. Edwards, M. Marzec, O. Sagher, D. Ross, and G. Fromes. Vagus nerve stimulation reduces daytime sleepiness in epilepsy patients. Neurology, 57(5):879–884, 2001.

[35] F. Marrosu, F. Santoni, M. Puligheddu, L. Barberini, A. Maleci, F. Ennas, M. Mascia, G. Zanetti, A. Tuveri, and G. Biggio. Increase in 20–50 hz (gamma frequencies) power spectrum and synchronization after chronic vagal nerve stimulation. Clinical neurophysiology, 116(9):2026–2036, 2005.

[36] M. Massimini, R. Huber, F. Ferrarelli, S. Hill, and G. Tononi. The sleep slow oscillation as a traveling wave. Journal of Neuroscience, 24(31):6862–6870, 2004. ISSN 0270-6474. doi: 10.1523/JNEUROSCI.1318-04.2004. URL https://www.jneurosci.org/content/24/31/6862.

[37] M. Mather, D. Clewett, M. Sakaki, and C. W. Harley. Norepinephrine ignites local hotspots of neuronal excitation: How arousal amplifies selectivity in perception and memory. Behavioral and Brain Sciences, 39:e200, 2016. doi: 10.1017/S0140525X15000667.

[38] S. C. Matthews, M. P. Paulus, A. N. Simmons, R. A. Nelesen, and J. E. Dimsdale. Functional subdivisions within anterior cingulate cortex and their relationship to autonomic nervous system function. Neuroimage, 22(3):1151–1156, 2004.

[39] L. K. McCorry. Physiology of the autonomic nervous system. American journal of pharmaceutical education, 71(4):78, 08 2007. doi: 10.5688/aj710478.

[40] M.-M. Mesulam. Cholinergic circuitry of the human nucleus basalis and its fate in alzheimer's disease. Journal of Comparative Neurology, 521(18):4124–4144, 2013. doi: 10.1002/cne.23415. URL https://onlinelibrary.wiley.com/doi/abs/10.1002/cne.23415.

[41] Z. Nahas, C. Teneback, J.-H. Chae, Q. Mu, C. Molnar, F. A. Kozel, J. Walker, B. Anderson, J. Koola, S. Kose, M. Lomarev, D. E. Bohning, and M. S. George. Serial vagus nerve stimulation functional mri in treatment-resistant depression. Neuropsychopharmacology, 32(8):1649–1660, 2007.

[42] A. Neuhaus, A. Luborzewski, J. Rentzsch, E.-L. Brakemeier, C. Opgen-Rhein, J. Gallinat, and M. Bajbouj. P300 is enhanced in responders to vagus nerve stimulation for treatment of major depressive disorder. Journal of affective disorders, 100:123–8, 07 2007. doi: 10.1016/j.jad.2006.10.005.

[43] R. Nonis, K. D'Ostilio, J. Schoenen, and D. Magis. Evidence of activation of vagal afferents by non-invasive vagus nerve stimulation: An electrophysiological study in healthy volunteers. Cephalalgia, 37(13):1285–1293, 2017. doi: 10.1177/0333102417717470. URL https://doi.org/10.1177/0333102417717470. PMID: 28648089.

[44] Y. Oganian and E. F. Chang. A speech envelope landmark for syllable encoding in human superior temporal gyrus. Science Advances, 5(11), 2019. doi: 10.1126/sciadv.aay6279. URL https://advances.sciencemag.org/content/5/11/eaay6279.

[45] OpenStax. Anatomy and Physiology. OpenStax CNX, 02 2016. URL http://cnx.org/contents/14fb4ad7-39a1-4eee-ab6e-3ef2482e3e22@8.24.

[46] A. Rush, M. S. George, H. A. Sackeim, L. B. Marangell, M. M. Husain, C. Giller, Z. Nahas, S. Haines, R. K. Simpson, and R. Goodman. Vagus nerve stimulation (vns) for treatment-resistant depressions: a multicenter studysee accompanying editorial, in this issue. Biological Psychiatry, 47(4):276 – 286, 2000. ISSN 0006-3223. doi: https://doi.org/10.1016/S0006-3223(99)00304-2. URL http://www.sciencedirect.com/science/article/pii/S0006322399003042.

[47] M. C. Salinsky and K. J. Burchiel. Vagus nerve stimulation has no effect on awake eeg rhythms in humans. Epilepsia, 34(2):299–304, 1993.

[48] D. Santesso, L. Schmidt, and L. Trainor. Frontal brain electrical activity (eeg) and heart rate in response to affective infant-directed (id) speech in 9-month-old infants. Brain and cognition, 65:14–21, 11 2007. doi: 10.1016/j.bandc.2007.02.008.

[49] P. J. Schwartz, G. M. De Ferrari, A. Sanzo, M. Landolina, R. Rordorf, C. Raineri, C. Campana, M. Revera, N. Ajmone-Marsan, L. Tavazzi, and A. Odero. Long term vagal stimulation

in patients with advanced heart failure first experience in man. European journal of heart failure, 10(9):884–891, 2008.

[50] L. A. Schwarz and L. Luo. Organization of the locus coeruleus-norepinephrine system. Current Biology, 25(21):R1051 – R1056, 2015. ISSN 0960-9822. doi: https://doi.org/10.1016/j.cub.2015.09.039. URL http://www.sciencedirect.com/science/article/pii/S0960982215011501.

[51] R. Sellaro, B. de Gelder, A. Finisguerra, and L. S. Colzato. Transcutaneous vagus nerve stimulation (tvns) enhances recognition of emotions in faces but not bodies. Cortex, 99: 213 – 223, 2018. ISSN 0010-9452. doi: https://doi.org/10.1016/j.cortex.2017.11.007. URL http://www.sciencedirect.com/science/article/pii/S001094521730388X.

[52] V. Sharma, K. Alataris, G. Heit, J. Sutor, and P. Sunkeri. Auricular nerve stimulation to address patient disorders, and associated systems and methods, Mar. 26 2020. US Patent App. 16/581,139.

[53] N. Swann, H. Poizner, M. Houser, S. Gould, I. Greenhouse, W. Cai, J. Strunk, J. George, and A. R. Aron. Deep brain stimulation of the subthalamic nucleus alters the cortical profile of response inhibition in the beta frequency band: A scalp eeg study in parkinson's disease. Journal of Neuroscience, 31(15):5721–5729, 2011. ISSN 0270-6474. doi: 10.1523/JNEUROSCI.6135-10.2011. URL https://www.jneurosci.org/content/31/15/5721.

[54] C. Ventura Bort, J. Wirkner, H. Genheimer, J. Wendt, A. Hamm, and M. Weymar. Effects of transcutaneous vagus nerve stimulation (tvns) on the p300 and alpha-amylase level: A pilot study. Frontiers in Human Neuroscience, 12, 06 2018. doi: 10.3389/fnhum.2018.00202.

[55] S. R. Waldstein, W. J. Kop, L. A. Schmidt, A. J. Haufler, D. S. Krantz, and N. A. Fox. Frontal electrocortical and cardiovascular reactivity during happiness and anger. Biological psychology, 55(1):3–23, 2000.

[56] J. Y. Y. Yap, C. Keatch, E. Lambert, W. Woods, P. R. Stoddart, and T. Kameneva. Critical review of transcutaneous vagus nerve stimulation: Challenges for translation to clinical practice. Frontiers in Neuroscience, 14:284, 2020. ISSN 1662-453X. doi: 10.3389/fnins.2020.00284. URL https://www.frontiersin.org/article/10.3389/fnins.2020.00284.

[57] M. Zaepffel, R. Trachel, B. E. Kilavik, and T. Brochier. Modulations of eeg beta power during planning and execution of grasping movements. PLOS ONE, 8(3):1–10, 03 2013. doi: 10.1371/journal.pone.0060060. URL https://doi.org/10.1371/journal.pone.0060060.

[58] A. Zanchetti, S. Wang, and G. Moruzzi. The effect of vagal afferent stimulation on the eeg pattern of the cat. Electroencephalography and clinical neurophysiology, 4(3):357–361, 1952.

[59] Y. Zhang, Z. B. Popovic, S. Bibevski, I. Fakhry, D. A. Sica, D. R. Van Wagoner, and T. N. Mazgalev. Chronic vagus nerve stimulation improves autonomic control and attenuates systemic inflammation and heart failure progression in a canine high-rate pacing model. Circulation: Heart Failure, 2(6):692–699, 2009.